The redox potential of human Protein Disulphide Isomerase' a' domain, and further characterisation of hPDI's ligand binding behaviour

By Jonathan Holbrook

School of Biosciences, University of Kent at Canterbury

August 2016

Supervisors – Dr Richard Williamson and Dr Mark Howard

Research Masters in Biochemistry

University of Kent

Declaration

No part of this thesis has been submitted in support of an application for any degree or qualification of the University of Kent or any other university or institute of learning.

Jonathan Holbrook

Acknowledgements

Firstly I would like to express my sincere gratitude to both my supervisors, Dr Richard Williamson and Dr Mark Howard for providing me with the opportunity to undertake this research as well as for their endless guidance and encouragement throughout my project.

I would also like to thank Dr Haris Panagos for his willingness to share his knowledge and continuous help with the NMR issues I encountered.

I would like to thank Joe Perkins, the other member of our small lab group, for his help throughout the project.

I would also like to thank Nadin Fathallah and my family for being a constant source of support and encouragement throughout my project; I dedicate my thesis to them.

Contents

Chapter 1

Chapter 2

Chapter 3

Abbreviations

^{1}H – Proton (magnetic nuclei - 100% natural abundance)

^{15}N – Nitrogen isotope-15 (magnetic nuclei – 0.36% natural abundance)

2D – Two dimensional

3D – Three dimensional

Amp – Ampicillin

AMPS – Ammonium perulphate

Chloramp – Chloramphenicol

D_2O – Deuterium oxide

Da – Dalton

DTT – Dithiothreitol

E. coli – Escherichia coli

EDTA - ethylenediaminetetraacetic acid

ER – Endoplasmic Reticulum

ERo1 – Endoplasmic reticulum protein oxidoreductin-1

GB1 – B1 domain of the *Streptococcus* protein GB1

hPDI – human Protein Disulphide Isomerase

HSQC – Heteronuclear Single Quantum Coherence

IPTG - Isopropyl β-D-1-thiogalactopyranoside

LB – Lysogeny Broth

NMR – Nuclear Magnetic Resonance

PDI – Protein Disulphide Isomerase

Ppm – Parts per million

P+ – Precision plus marker (Bio-rad)

Rpm – Revolutions per minute

SDS – Sodium dodecyl sulfate

SDS-PAGE – Sodium dodecyl sulfate polyacrylamide gel electrophoresis

TEMED - Tetramethylethylenediamine

TGS – Tris-glycine SDS buffer

UPR – Unfolded Protein Response

Δ-som – Δ-somatostatin

Abstract

Protein Disulphide Isomerase (PDI) is a 57 kDa multi-domain protein found within the endoplasmic reticulum. PDI consists of four thioredoxin-like domains (named **a** and **b**) each containing five β-sheets and four α-helices in the conformation $\beta\alpha\beta\alpha\beta\alpha\beta\beta\alpha$. The four domains are ordered in the sequence **abb'xa'c**; with a 19 amino acid **x** linker between the **b'** and **a'** domains, and an acidic tail, **c**, after the **a'** domain. PDI acts as an oxidoreductase and chaperone to help fold newly synthesized proteins into their native state through the formation of disulphide bonds via the oxidation of sulfhydryl groups of cysteines, as well as the rearrangement of mispaired disulphides in an isomerisation reaction. The catalytic domains responsible for the thiol/disulphide reactions are **a** and **a'**, and one of the aims of this work is to determine the redox potential of the **a'** domain and how it is influenced by the adjacent **b'**, **x** and **c** regions. Fragments of human PDI containing the **a'** domain were expressed in *E.coli* and their redox potential measured by $^{15}N/^{1}H$ NMR using mixtures of reduced and oxidised glutathione. The **b'** domain of PDI which is known to contain the primary binding site for unfolded substrates was also investigated. The interaction of the **b'xa'c** fragment to the PDI ligand Δ-somatostatin fused to the carrier protein GB1 was used to investigate its binding behaviour by NMR in a range of different redox conditions.

CHAPTER 1

1.0 Introduction

1.1 Overview

The endoplasmic reticulum (ER), located in all eukaryotic cells, has a vast array of functions; one of its key functions being; acting as the cells centre for protein folding and quality control [1]. This is essential; as even though the proteins final conformation is determined by its amino acid sequence the ER plays a large part in increasing the efficiency of folding the proteins into their final structure [2].

As proteins are folded into their final form, post-translational modifications such as disulphide bonds are formed as part of the folding process, these bonds are produced via reduction-oxidation (redox) reactions. This bond is formed when two side chain cysteine residues are oxidised to form a covalent sulphur-sulphur bond, this reaction is catalysed by one of the many resident molecular chaperone and protein folding catalysts located in the ER such as Protein Disulphide Isomerase (PDI) [3]; a protein expressed in nearly all mammalian tissues [4].

The discovery of this protein was made in 1963 by two independent research groups, first by Venetianer and Straub by extracting PDI from chicken and pigeon pancreas [5], and secondly by Goldberger, Epstein and Anfinsen from purified rat liver samples [6]. This makes PDI the founding member of the PDI family of thiol-disulphide oxidoreductases.

This introduction focuses on the structure and function of the human PDI (hPDI) family, and goes into detail on the structure-function relationship in relation to redox reactions and chaperone activity.

1.2 Introduction to PDI

PDI is one of a family of 21 structurally related proteins (shown in Figure 1.1); grouped together due to their thioredoxin-like domain structure and although the family name of PDI implies that all the proteins within the family possess isomerase activity (redox reaction with no net change in charge) this has not been demonstrated experimentally for all of them. PDILT also lacks any obvious oxidoreductase activity [7], which is probably true of the PDI family members ERp44, AGR2 and AGR3 as well; as they also only have one cysteine in the active site [8]. ERp27 and ERp29 are also non-catalytic members of the PDI family [9]; showing that the grouping of these proteins into the PDI family is based largely on sequence, ER localisation and structural similarity as opposed to common function and enzymatic properties.

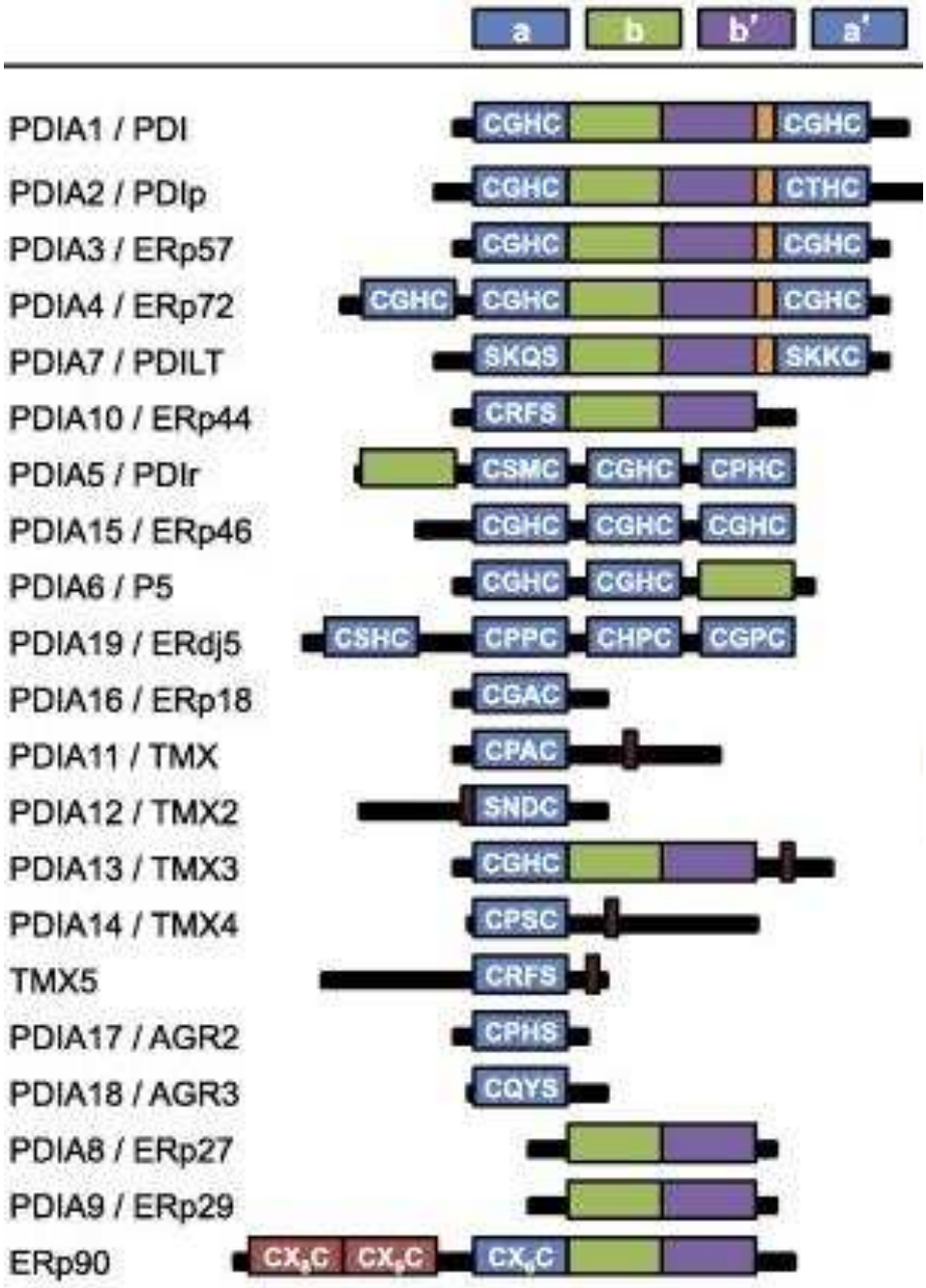

Figure 1.1 The 21 members of the PDI family of proteins

The catalytic domains of **a** and **a'** being shown in blue, the non-catalytic domains **b** and **b'** shown in green and purple respectively, the **x** linker between **b'** and **a'** shown in orange and the transmembrane domains shown in red.

Adapted from Andreu et al 2012 [36].

PDI is a 491 amino acid, 57kDa protein, the full amino acid sequence of which is shown in Figure 1.2. As well as acting as an independent entity PDI also forms the β-subunit of prolyl 4-hydroxylase [10], involved in synthesis of collagen [11], and the 58 kDa subunit of microsomal triglyceride transfer protein complex involved in lipoprotein assembly [12].

```
        10         20         30         40         50         60
DAPEEEDHVL VLRKSNFAEA LAAHKYLLVE FYAPWCGHCK ALAPEYAKAA GKLKAEGSEI

        70         80         90        100        110        120
RLAKVDATEE SDLAQQYGVR GYPTIKFFRN GDTASPKEYT AGREADDIVN WLKKRTGPAA

       130        140        150        160        170        180
TTLPDGAAAE SLVESSEVAV IGFFKDVESD SAKQFLQAAE AIDDIPFGIT SNSDVFSKYQ

       190        200        210        220        230        240
LDKDGVVLFK KFDEGRNNFE GEVTKENLLD FIKHNQLPLV IEFTEQTAPK IFGGEIKTHI

       250        260        270        280        290        300
LLFLPKSVSD YDGKLSNFKT AAESFKGKIL FIFIDSDHTD NQRILEFFGL KKEECPAVRL

       310        320        330        340        350        360
ITLEEEMTKY KPESEELTAE RITEFCHRFL EGKIKPHLMS QELPEDWDKQ PV KVLVGKNF

       370        380        390        400        410        420
EDVAFDEKKN VFVEFYAPWC GHCKQLAPIW DKLGETYKDH ENIVIAKMDS TANEVEAVKV

       430        440        450        460        470        480
HSFPTLKFFP ASADRTVIDY NGERTLDGFK KFLESGGQDG AGDDDDLEDL EEAEEPDMEE

       490
DDDQKAVKDE L
```

Figure 1.2 Full amino acid sequence of hPDI
a domain is shown in red, **b** domain in orange, **b'** domain in green, the **x** linker in purple, the **a'** domain in blue and the c-terminal tail in black, both CGHC catalytic sites are highlighted in yellow.
Domain boundaries defined by Alanen et al 2003 [27].

As well as catalysing the formation of disulphide bonds; PDI can also form a PDI-substrate complex [13], can interact with polypeptides which are prone to aggregation [14], in addition to facilitating the targeting of proteins which need to be degraded [15].

When PDI has a peptide bound to it; it can help to stabilise the major histocompatibility complex (MHC) class I within the ER by regulating disassociation of tapasin-ERp57 disulphide conjugate by binding to both tapasin and ERp57 causing them to dissociate from one another. On the other hand when PDI does not have a peptide bound to it, it cannot dissociate the tapasin-ERp57 conjugate, resulting in MHC class 1 being retained in the ER [16].

Another function was suggested for PDI relatively recently, the ability for it to act as a reservoir for hormones, this is due to the observation that hormone 17β-estradiol was able to bind to the hydrophobic region between the **b** and **b'** domains. It was shown that the amino acid residue H256 was the key residue for the interaction between PDI and 17β-estradiol, and it is believed that the nitrogen of H256 is linked via a hydrogen bond to the 3-hydroxyl group of the hormone [17].

PDI's chaperone activity and the efficient folding of newly translated proteins into their native state in the ER is essential, as potential disease states can occur due to aggregation of these proteins, disease states such as, diabetes, Alzheimer's disease, Parkinson's disease and both non-alcoholic and alcoholic liver disease [18].

Although PDI is mainly located within the ER; it has also been found in other places such as the cell membrane [19], where it has been shown to aid in the fusion of the HIV envelope (Env) glycoprotein (gp) 120 to the lymphocyte receptors CD4 and CXCR4 of the CD4(+) lymphocytes. PDI aids in the fusion of HIV to the cell membrane by catalysing thiol-

disulphide interchange reactions on the cell membrane; altering gp120 via the reduction of two disulphide bonds and allowing the HIV to fuse [20], [21].

On the cell surface; PDI is also thought to play a regulatory role in the proliferation, adhesion, aggregation and secretion of platelets by reducing the disulphide bonds on fibrinogen receptors in platelets, this exposes them and activates the glycoprotein IIbIIIa receptor [22].

PDI can be transported into the cytosol where it can eventually be presented on the cell surface exhibiting immunogenic characteristics, as they can appear as damage associated molecular patterns which the immune system targets to induce apoptosis [23].

All of this coupled with the fact that over a third of all human proteins that are secreted contain disulphide bonds [24] and that PDI (the most abundant member of its family) makes up roughly 0.8% of total cell protein within the ER lumen [25]; makes PDI a very interesting target for research.

1.3 Structure of hPDI

PDI's structure consists of four thioredoxin-like domains each containing five β-sheets and four α-helices in the conformation $\beta\alpha\beta\alpha\beta\alpha\beta\beta\alpha$ [26]. The four domains are thioredoxin-like as they are similar in structure to the protein thioredoxin as they share the same thioredoxin-like structural fold of $\beta\alpha\beta\alpha\beta\alpha\beta\beta\alpha$ [26].

The four domains are ordered in the sequence **abb'a'**; with a 19 amino acid **x** linker between the **b'** and **a'** domains, and an acidic tail, **c**, after the **a'** domain, this makes the final sequence **abb'xa'c**, demonstrated in Figure 1.3 below. The acidic tail **c** contains a KDEL retention sequence which keeps PDI within the ER. The **b** and **b'** domains do not contain a catalytic active site whereas the **a** and **a'** domains both contain CXXC active site motifs [27], [28]. These 4 domains are arranged in a U shape with both catalytic domains **a** and **a'** at the top and the non-catalytic domains **b** and **b'** at the bottom (see Figure 1.4) [29].

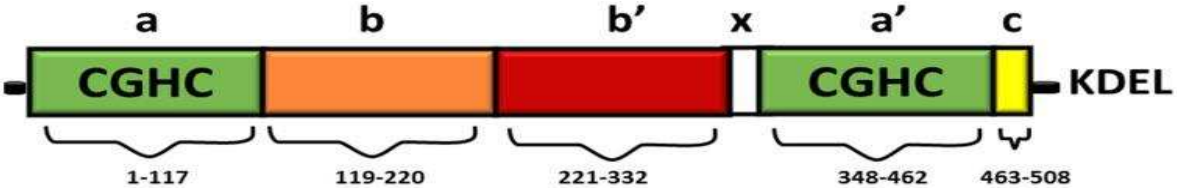

Figure 1.3 Full PDI domain structure.
Catalytically active domains shown in green, the catalytically inactive domains **b** and **b'** represented in orange and red respectively, the **x** linker responsible for the U shape structure of PDI in white, acidic tail **c** in yellow and the KDEL endoplasmic reticulum retention sequence after the C-terminal.
Adapted from Parakh, S. and Atkin, J.D. (2015) [116].

The structure of PDI (Figure 1.4) has been developed relatively recently through the study of several PDI family members leading to insights into the structure and mechanisms by which the proteins function. Although the biggest advancement in the understanding of PDI's structure came when yeast PDI1p's full-length crystal structure was solved, implying the position of substrates relative to the two catalytic domains [29]. The first near full length crystal structures of hPDI **abb'xa'** in both the oxidised and reduced states was recently published in 2013 [30] along with the **bb'xa'** hPDI in 2012, both studies suggested that the removal of the acidic **c** tail of PDI helps the crystallisation process [31].

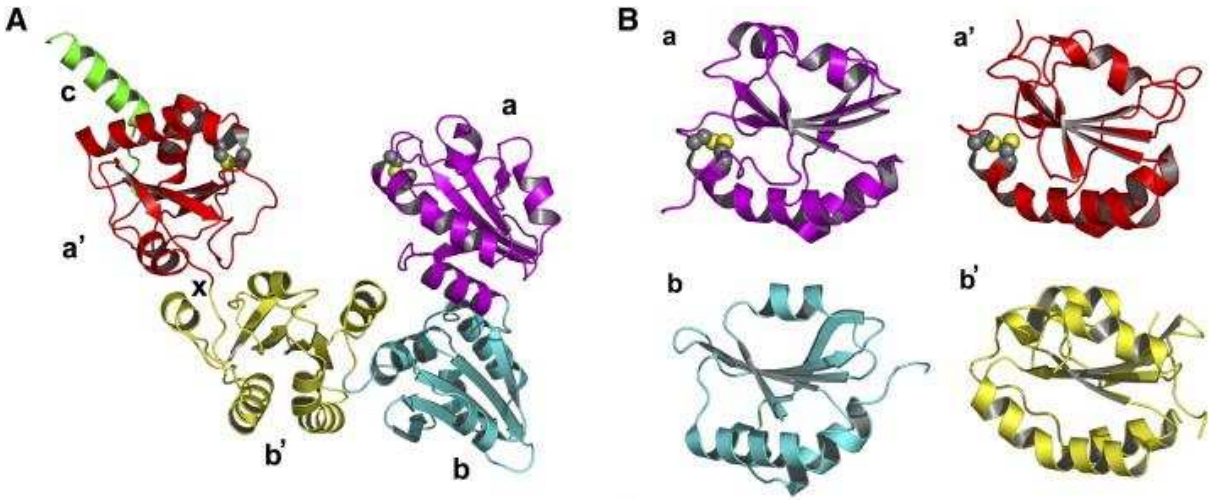

Figure 1.4 Full structure of PDI

Section A - The ribbon structure of PDI with the **a** domain in purple, **b** domain in turquoise, the **b'** domain in yellow, the **x** linker indicated by the letter x, the **a'** domain in red and the **c**-terminal tail in green. The catalytic active sites in the **a** and **a'** domains are represented by the grey and yellow balls, the sulphur atoms being represented in yellow. Section B – A structural comparison of the four main domains of PDI. All four domains are shown in the same orientation with the alpha helices above and below the beta sheets in the middle

Adapted from Tian, G., et al 2006 [29].

The **b'** domain has been shown to act as the ligand binding domain to aid in the folding of peptide ligands as well as misfolded proteins whereas the **a** and **a'** domains facilitate the catalytic oxidase and reductase activity due to their CXXC active site motifs or to be specific WCGHC [32]. The **b'** domain is essential for the isomerase activity of PDI to take place as the minimum PDI fragment for the isomerase activity is **b'xa'**, whereas for the redox reaction to take place the catalytic domains **a** and **a'** can work in isolation [31].

The non-catalytic domains **b** and **b'** contain lower sequence homology to thioredoxin than the catalytic domains **a** and **a'**; this is true across all the PDI family; they also present an increased structural variability, such as the PDI family member ERp44 (ER protein, 44kDa), whose non-catalytic domains secondary structure is in the unusual conformation of $\beta\beta\alpha\beta\beta\beta\alpha$ [33].

The **b** domain is thought to play a part in protein solubility due to its overall hydrophilic properties [34], the **b** domain also has a higher than usual number of hydrophobic regions which assists in increasing the binding cleft between the catalytic domains therefore allowing larger peptides and misfolded peptides to bind [35].

1.4 Catalytic Activity

The catalytic activity of PDI involves the formation of disulphide bonds via the reduction, oxidation and isomerisation of disulphide bonds. The catalytic motif CXXC is essential for activity and found in all catalytically active domains. Other variants of the motif can also be found, but these domains are thought to be catalytically inactive [36]. PDI acts as a good oxidant due to its redox potential being -180mV, this shows that PDI's disulphide bond is unstable, making it easier for it to become reduced as it is more ready to accept electrons [37].

PDI catalyses the formation of disulphide bonds through the oxidation of sulfhydryl groups of cysteines, as well as the rearrangement of some mispaired disulphide bonds in an isomerisation reaction where there is no net change in charge [1] (shown in Figure 1.5). PDI catalyses the formation of these disulphide bonds as its oxidised **a** domain is able to catalyse the oxidation of a reduced substrate, therefore causing itself to become reduced. PDI substrates predominantly contain cysteine residues which are in the reduced dithiol state (R-S-H) but are then oxidised to form disulphide bonds (R-S-S-R). In PDI, the cysteine residue on the N-terminus (C53) forms an intermediary disulphide bond with the substrate while the substrate is released by the C-terminus cysteine, C56 [38]. The **a** domain is then re-oxidised by the **a'** domain via an intramolecular reaction which allows the **a** domain to reform its disulphide bond [39]. The **a'** domain is then re-oxidised itself by the ER

oxidoreductin protein ERo1 which involves the reduction of O_2 to H_2O_2 [39], [40] (demonstrated in Figure 1.6). ERo1 is present in two isoforms α and β this is discussed in the next section [17].

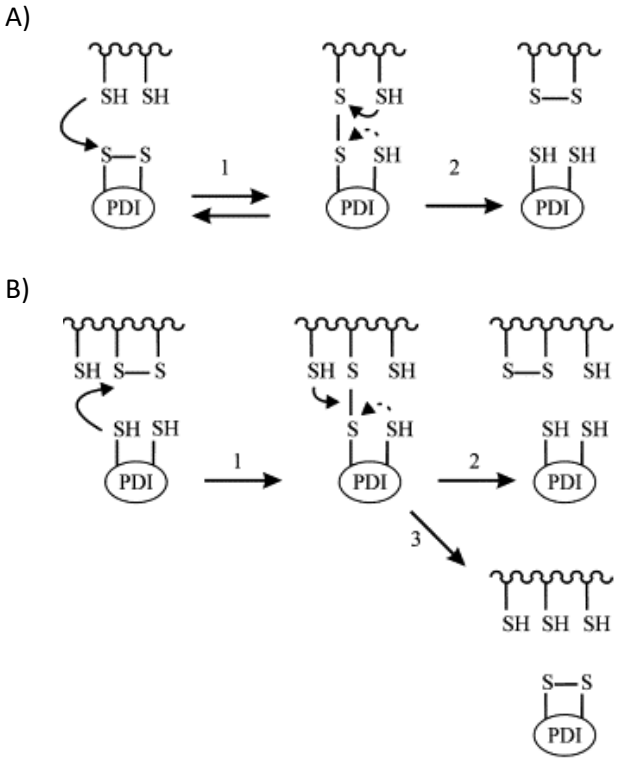

Figure 1.5 Oxidoreductase and isomerisation activity of PDI

For both figures, nucleophilic attack is shown by a solid curved arrow and the reverse reaction is shown by a dotted curved arrow

Panel A – The formation of a disulphide bond on a substrate via the oxidisation of the substrate and the reduction of the N-terminal cysteine C53. In the intermediate step, the C-terminal cysteine of PDI must have a higher than average pKa value than the protein substrate, otherwise the reverse reaction will be kinetically more favourable.

Panel B – The rearrangement of a mispaired disulphide bond on a protein substrate via an isomerisation reaction, again the intermediate step is shown. For reaction 1 to occur the N-terminal active site cysteine must have a low pKa value. In the intermediate reaction the C-terminal cysteine, C56, must have a higher than average pKa value, leading to direct isomerisation. If direct isomerisation does not occur, cycles of oxidation and reduction take place until the correct conformation is achieved. Reactions 1 and 3 show reduction of a substrate disulphide bond by PDI.

Adapted from Karala AR et al 2010 [42].

It has been reported that the catalytic activity of PDI family members is regulated by the arginine residue located close to the CXXC motif [41], [42]. The pKa value of the cysteine residues in the active site plays a large role in determining the physiological function of PDI. Increasing the pKa value of the C-terminal cysteine prompts the oxidation of substrates, whereas it causes an inhibitory effect to occur on the re-oxidation of PDI. However, a low pKa is required for PDI to become re-oxidised and complete the catalytic cycle. This situation is solved by the arginine residues, arginine 120, found in the loop between β5 and α4 of the catalytic site of the **a** domain and arginine 461 in the **a'** domain. This residues side chain moves in and out of the active site locale, which has an indirect regulatory effect on the pKa value of the C-terminal cysteine of the active sites [41], [42].

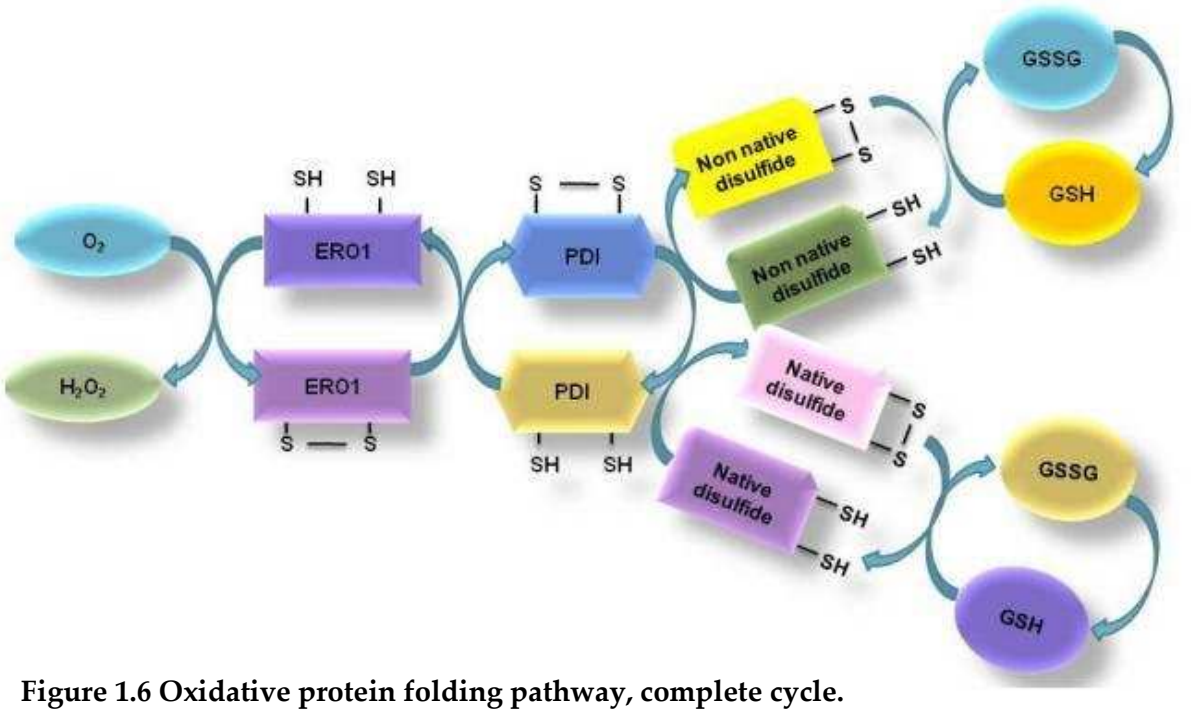

Figure 1.6 Oxidative protein folding pathway, complete cycle.
The transfer of electrons within the endoplasmic reticulum protein folding pathway which results in the formation of disulphide bonds to help fold newly synthesised proteins into their native state. When non-native disulphides are formed, reduced glutathione assists in reducing them so that they can form a native disulphide bond. This decreases the GSH to GSSG ratio, altering the redox environment in the ER.
Adapted from Bhandary, B., et al. 2013 [66].

1.5 Re-oxidation of PDI

Once PDI has oxidised its substrate, it must be re-oxidised itself to complete the catalytic cycle. This can be achieved in a number of ways, GSSG present in the cell can re-oxidise PDI, as well as, hydrogen peroxide, Ero1α and β, peroxidases or peroxiredoxins [43].

Although both Ero1α and β can re-oxidise PDI, the α isoform is the most prominent in most human cells [44], whereas Ero1β is located in a smaller subset of cells[45].

The **b'** domain of reduced PDI is bound to by the β hairpin in Ero1α aided by the co-factor FAD [46] (shown in Figure 1.7). This interaction is between the aromatic residues W272 of

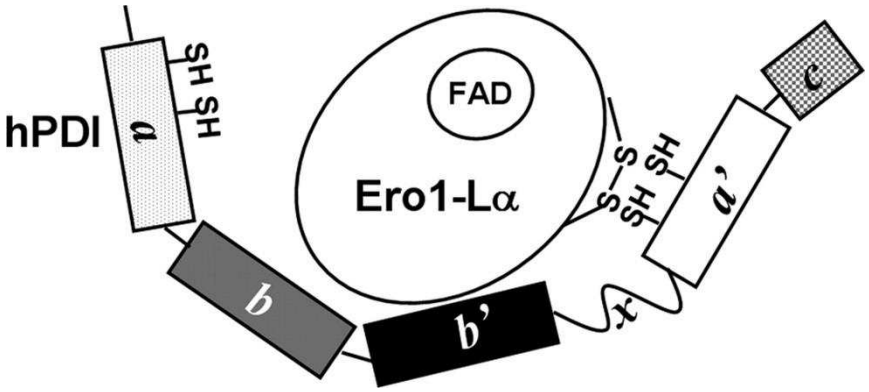

Figure 1.7. Binding of Ero1α to PDI
Diagram showing the binding of Ero1α to the **b'** domain of PDI via the β hairpin in ERo1α as well as the Ero1α active site binding to the catalytic active site of the **a'** domain **Adapted from Wang, L., et al. 2009 [117].**

Ero1α and F240, F249 and F304 of PDI, the bond formed was non-covalent [46]. This means that Ero1α is orientated so that the **a'** domain of PDI is oxidised but the **a** domain was left alone [39], [46]. After Ero1α has re-oxidised the **a'** domain of PDI, Ero1α's own active site is re-oxidised, ultimately leading to the production of H_2O_2 as the electrons are passed to O_2, Ero1α's inner active site disulphides are used to achieve this [44]. Both α and β isoforms of Ero1 preferentially bind to the **a'** domain of PDI and oxidise it [47], [48].

Ero1α catalytic activity and binding affinity to PDI was shown to be pH dependent, with improved catalytic activity and binding affinity at pH 7 and depleted activity at pH 7.5 and 8 [39].

Obviously the **a'** domain wouldn't need re-oxidising if it hadn't aided in the re-oxidation of the **a** domain of PDI by accepting electrons from it [39]. The re-oxidation of the **a** domain is modulated by three other proteins present in the ER, they are, glutathione peroxidase 7 (GPx7), glutathione peroxidase 8 (GPx8) and peroxiredoxin 4 (Prx IV) [49], [50]. H_2O_2 is a by-product produced when Ero1α is re-oxidised, a build-up in hydrogen peroxide could result in damage to the cell, therefore GPx7 and GPx8 help to remove the hydrogen peroxide by converting it back to oxygen. In doing so C57 and C86 of GPx7 are converted into sulfenic acid and disulphide respectively [49], [50].

1.6 Chaperone activity

PDI was first proposed to act as a chaperone, as well as a protein folding catalyst in 1993 [51]. It was suggested that PDI plays a role in preventing protein aggregation by binding to unfolded proteins [52]–[55], as well as interacting with proteins that have been newly synthesised [56], [57].

All PDI domains contribute to its ability to bind to specific proteins for its chaperone activity [58], although when PDI is in its oxidised form it has greater chaperone activity than when it is reduced. This is due to the conformational changes that occur when the **a'** domain is oxidised, causing it to move out of its compact conformation exposing the hydrophobic areas [31], [59]. This shows that the chaperone activity of PDI is redox regulated, where being in its oxidised state results in an open conformation allowing itself to bind to larger non-native proteins and closed in its reduced state [31], [59]. This was discovered only

relatively recently due to issues in obtaining the crystal structure of human PDI in both the reduced and oxidised forms. The crystal structure obtained allowed us to observe that in its reduced form the **a** and **a′** domains were 27.6 Å's apart where as in the oxidised form they are 40.3 Å apart as the **a′** domain is twisted 45 degrees around the **x** linker and away from the **b′** domain. Therefore in the oxidised state there are more open hydrophobic areas and a larger cleft for substrates to bind to at the **b′** domain [30]. This adds to the evidence that the chaperone activity of PDI is regulated by its redox status.

The **b′** domain acts as the primary hydrophobic binding site for peptides and is the site at which the **x** linker binds, meaning peptides have to compete with the **x** linker to bind to the site [60], [61]. This discovery added further evidence to the hypothesis that the **x** linker aids in modulating the **b′** binding site.

In 2014 it was shown that PDI can distinguish between fully folded, partially folded and unfolded substrates This was shown as the dissociation constant (Kd) for fully unfolded basic pancreatic trypsin inhibitor (BPTI) was shown to be 1.5 μM, whereas in its partially unfolded state the Kd was about three times higher, and in the fully folded state; ten times higher. This led to the conclusion that PDI can distinguish between fully folded, partially folded and unfolded substrates, with a preference to binding to unfolded substrates more strongly [62].

PDI's chaperone activity has also been demonstrated *in vivo* by the study of folding, modification and assembly of type X collagen in semi-permeable cells. This role is related to PDI's ability to function as the β subunit of prolyl 4-hydroxylase as it interacts transiently with type X collagen during helix formation, this reaction is not thiol dependent as a type X

polypeptide was shown to be able to fold into its native state and interact with PDI despite the polypeptide not containing any cysteine residues [63].

1.7 Disease states and potential drug targets

Even though the ER retains a large reservoir of chaperones and folding proteins, both misfolded and unfolded proteins can still build up leading to a range of disease states such as Alzheimer's, Parkinson's, Motor Neurone as well as Huntington's Disease. In these cases the unfolded protein response (UPR) is activated, this involves, up regulating expression of chaperone proteins, targeting misfolded as well as unfolded proteins to be degraded by the proteasome, and also reducing the rate at which new proteins are synthesised [64].

PDI is upregulated in the UPR leading to a reduction in misfolded and unfolded proteins within the ER. However extensive activation of the UPR can lead to disease states itself, such as multiple metabolic diseases such as, obesity, diabetes, renal disease, macular degeneration, liver disease and atherosclerosis [65], [66]. This makes PDI a potential drug target so to inhibit chronic activation of the UPR.

A number of PDI inhibitors have been discovered in recent years such as Bacitracin which consists of a mixture of polypeptides. The analogs of bacitracin have been shown to be more inhibitory than bacitracin itself, they bind to the **b'** domain but do not appear to inhibit the oxidative and isomerase activity [67], [68].

A derivative of propynoic acid carbamoyl methyl amids (PACMA), named PACMA31 has been shown to be an irreversible inhibitor of PDI as it forms a covalent bond with the active site cysteine. PACMA31 can potentially be used to target ovarian tumours, this was shown

in 2012 as it bound to the overexpressed PDI in the ovarian tumour cells inhibiting their growth and yet caused no harm to normal cells in the process [69].

There are many peptides which can inhibit the chaperone activity of PDI, such as ribostamycin, which inhibits the chaperone activity [70]. Qurcetin-1-rutinoside is an inhibitor of PDI's reductase activity as well as being able to inhibit PDI mediated platelet aggregation, leading to the idea that it can be used as an antithrombic agent [71].

1.8 Project Aims

The aim of this project is to characterise the redox potential of human PDI's **a'** domain by expressing and purifying **xa'c**, **b'xa'c** and **a'c** in ^{15}N isotopically enriched media. This is to elucidate how the addition of neighbouring domains influences its redox potential. To elucidate the redox potential of the **a'** domain, the various fragments of PDI will be put into a range of redox conditions using oxidised glutathione (GSH) and reduced glutathione (GSSG) and analysed by NMR spectroscopy.

Another aim of the project is to further characterise ligand binding behaviour of hPDI using the **b'xa'c** fragment and the ligand Δ-somatostatin. Both GB1 and GB1-Δ-somatostatin were expressed and purified in ^{15}N isotopically enriched media, whereas **b'xa'c** was expressed in unlabelled minimal media. The binding behaviour of **b'xa'c** to the GB1-Δ-somatostatin fusion was characterised by NMR spectroscopy together with the effect of the oxidation state of the PDI fragment on binding affinity.

2.0 Materials and Methods

Fragments were expressed from pET-23b vectors transformed into *E. coli* strain BL21 DE3 pLysS [72]. The fragments were expressed and purified first on a small scale in 100 ml of lysogeny broth (LB) media and minimal media (MM), and then scaled up for large scale production. GB1 and GB1-Δ-somatostatin fusion were also expressed from pET23a in BL21 DE3 pLysS cells and the proteins purified from cultures grown both in LB and minimal medium.

2.1 Growth on agar plates

Agar plates were made using 10 g/L tryptone, 5 g/L yeast extract, 10 g/L NaCl and 15 g/L agar. Ampicillin and chloramphenicol added to a concentration of 100 μg/ml and 34 μg/ml respectively. Agar plates were streaked with appropriate *E. coli* glycerol stock (PDI fragments **xa'c**, **b'xa'c** or **a'c**, or PDI ligand GB1-Δ-somatostatin as well as the control GB1) and left to incubate overnight at 37 °C.

2.2 Growth in LB media

LB media was prepared containing 10 g/L tryptone, 5 g/L yeast extract and 10 g/L NaCl, and the same antibiotic concentration as used for growth on agar plates (see above). LB media was then inoculated with a colony from an agar plate and incubated at 200 rpm, 37 °C until the absorbance at 600nm = 0.6

2.3 Growth in ^{15}N labelled minimal media

Minimal medium was prepared using the components shown in Table 1.1 and cultures grown in flasks 5x the culture volume.

Stock Component	Stock Solution		Volume
1 - ($^{15}NH_4$)$_2SO_4$ (x50)	-	30 g/L	20 ml
2 - PO_4/NaCl (x10)	Na_2HPO_4 KH_2PO_4 NaCl	68 g/L 30 g/L 5 g/L	100 ml
3 - Na_2SO_4 (x1000)	-	42.6g/L	1 ml
4 - EDTA Trace Elements (x100)	EDTA $MnCl_2$ $FeCl_3$ $ZnCl_2$ $CuCl_2$ $CoCl_2$ H_3BO_3	10 g/L 3.2 g/L 1 g/L 0.1 g/L 20 mg/L 20 mg/L 20 mg/L	10 ml
5 - $MgSO_4$ (x1000)	-	246 g/L	1 ml
6 - $CaCl_2$ (x1000)	-	44.1 g/L	1 ml
7 - Biotin (x1000)	-	1 g/L	1 ml
8 - Thiamine (x1000)	-	1 g/L	1 ml
9 - $^{13}C_6H_{12}O_6$ (x50)	-	150 g/L	20 ml
10 - MilliQ® water	-	-	845 ml
11- Ampicillin (x100)	-	100 g/L	1 ml
12 - Chloramphenicol (x100)	-	34 g/L	1 ml

Table 1.1 MM stock solutions and appropriate concentrations.

2, 3 and 4 were all autoclaved whereas all other stock solutions were filter sterilised using a 0.2 μm single use syringe (Sartorius, Epsom, UK) and then added aseptically once autoclaved solutions had cooled.

2.4 Recombinant expression in *E. coli*

Starting with a 50 ml starter culture of MM. The culture was grown at 37 °C, shaken at 200 rpm until the A_{600} is 1.0. Cells were spun down at 4000 rpm, 4 °C for 15 minutes, supernatant poured off and the pellet re-suspended in 3 ml of MM. The re-suspended pellet was used to inoculate 3 x 400 ml MM cultures, 1 ml in each. The large cultures were incubated at 37 °C, 200 rpm until A_{600} = 0.6.

The cultures were then induced using IPTG at 0.5 mM overnight for the PDI fragments, but just 3 hours for the PDI ligands, both sets of cultures incubated at 30°C. The cultures were spun down at 10,000 rpm, 4 °C for 10 minutes using a JA-10 rotor, the supernatant poured off and each 400 ml culture equivalent pellet re-suspended in 10 ml lysis buffer (50 mM

NaCl, 20 mM NaH_2PO_4, pH 7.3, 4 °C). The 3 x 10 ml re-suspended pellets were split into 2 x 15 ml (2 x 600 ml equivalent cell pellet) and frozen at -20 °C.

0.5 ml pre and post IPTG samples taken for SDS-PAGE analysis, spun down in a centrifuge for 1 minute at 13,000 rpm, supernatant poured off and the pellet frozen at -20 °C.

2.5 Cell Lysis

PDI Fragments:

600 ml equivalent cell pellet was defrosted at room temperature, 300 µl Triton X-100 (5% v/v stock in lysis buffer) added and the solution incubated for 20 min at room temperature. 75 µl $MgCl_2$ (2 M) and 150 µl DNase (2 mg/ml) were then added and the solution incubated at room temperature for a further 20 min. The mixture was then centrifuged at 12,000 rpm, 4 °C for 10 min (JA-20 rotor) and the supernatant collected for further protein purification.

PDI Ligand:

600 ml equivalent cell pellet defrosted at room temperature, lysis buffer added to a total volume of 20 ml and then 400 µl Triton X-100 (5% v/v stock in lysis buffer) added. The mixture was sonicated in an ice bath for 3 min (10 s on / 10 s off); and the lysate then centrifuged at 4,000 rpm, 4 °C for 10 min (JA-20 rotor). The supernatant was collected for further protein purification.

2.6 Nickel Affinity Chromatography

A 2 ml and 5 ml bed volume column was used for the small and large preps respectively. Each column was packed with chelating sepharose fast flow (GE Healthcare).

The column washed using 10 column volumes (CV) of MilliQ® water, charged using 1 CV of $NiSO_4$ (0.2 M) in water, then washed with 5 CV sodium acetate (20mM sodium acetate, 0.5

M NaCl, pH 4) followed by 10 CV of binding buffer (20mM phosphate, 0.5 M NaCl, pH 7.3) to equilibrate it.

The supernatant from the lysis was then loaded after it had been filter sterilised through a 0.2 μm single use syringe (Sartorius, Epsom, UK), added to the column and 2 ml fractions of the flow through collected there on after. 10 CV of binding buffer was added to the column, then 10 CV of wash buffer (20 mM phosphate, 0.5 M NaCl, 50 mM Imidazole, pH 7.3), after which 15 CV of elution buffer (20 mM phosphate, 0.5 M NaCl, 20 mM EDTA, pH 7.3) was added to ensure elution of the protein. Ice cold binding, wash and elution buffer is used for PDI ligand purification.

The fractions collected were kept for SDS-PAGE analysis and to measure their absorbance at 280 nm to track the protein as it comes off the column. The column was stored in 20% ethanol at 4 °C.

2.7 Dialysis

Fractions were pooled and dialysed overnight at 4 °C against 2 l of 20 mM phosphate buffer, pH 7.3 (MWCO 12-14 kDa).

2.8 Ion Exchange Chromatography

Ion exchange chromatography was used to further purify the PDI fragments. An AKTA FPLC analyser (GE Healthcare) was used with a Source 30Q column (5 ml bed volume), with Buffers A and B (20 mM phosphate, pH 7.3 and 20 mM phosphate, 0.5 M NaCl, pH 7.3 respectively). The buffers were filtered and degassed before use.

The column was first washed using 10 CV of buffer A, followed by 10 CV of buffer B and then equilibrated using 10 CV buffer A. A blank gradient of buffer B (0 to 100% over 10 CV) was run to elute any contaminants on the column before use.

The dialysed protein was loaded onto the column using a 10 ml superloop and the separation of bound protein achieved using 0 to 100% of buffer B over 20 CV at a flow rate of 5 ml/min. 2 ml fractions were collected and their absorbance measured at 280 nm. Fractions were analysed by SDS-PAGE.

2.9 Gel Filtration

For the PDI fragment b'xa'c, gel filtration was required after ion exchange chromatography to separate the monomer and dimer forms. Superdex 200 matrix (300 ml; GE Healthcare) in a XK 26 column (2.6 cm diameter) was used with 20 mM phosphate buffer containing 0.15 M NaCl (pH 7.3) as running buffer. The pooled ion exchange samples were spin concentrated to 2 ml using a 10,000 MWCO Vivaspin 20 concentrator before loading. The column was run at a flow rate of 2 ml/min and 5 ml fractions were collected. The absorbance of each fraction was measured at 280 nm.

2.10 SDS-PAGE

The protein was analysed at each purification step using sodium dodecyl sulphate gel electrophoresis (SDS-PAGE). Table 1.2 below shows solutions for both the resolving and stacking gels. The protein standard used was Precision Plus from Bio-Rad. TGS buffer 5 x stock was made using glycine 0.95 M (pH 8.3), 0.125 M Tris and 0.5% SDS. 4 x non-reducing loading was prepared with 0.33 M Tris-HCl, 8% SDS, 0.4% bromophenol blue and glycerol, final concentration was 40% in Sambrook & Russell 2001. For the reducing buffer 200 mM DTT was used and then stored at -20 °C.

Reagent	15% Resolving Gel	17.5% Resolving Gel	5% Stacking Gel
40 % Acrylamide	7.5 ml	8.75 ml	1.25ml
1.5 M Tris pH 8.8	5 ml	5 ml	-
0.5 M Tris pH 6.8	-	-	1.25ml
10% SDS	200µl	200µl	100µl
MilliQ® water	7.1 ml	6.85 ml	7.3ml
10% AMPS	50 µl	50 µl	50µl
TEMED	14 µl	14 µl	10µl

Table 1.2 Components of 15% and 17.5% SDS-PAGE resolving gel and 5% stacking gel PDI fragments analysed using 15% resolving and PDI ligands analysed using 17.5% resolving gels.

10 µl of the 4x reducing buffer was added to 30 µl of sample to make a total volume of 40 µl with a 1x reducing buffer, SDS-PAGE samples were then placed in boiling water for 3 minutes. 10 µl samples were placed in each well. Gels were run at 100 V through the stacking gel and 125 V through the resolving gel. Gels were stained using Coommassie stain containing 1 mg/ml Coommassie Brilliant Blue Bio-Rad, 10% acetic acid, 40% methanol and 50% MilliQ® water. Gels were stained for 3 hours and then de-stained with a solution containing 10% acetic acid, 10% methanol and 80% water.

2.11 Mass Spectrometry

Electrospray mass spectrometry was used to elucidate the molecular mass of purified proteins. All analyses were carried out by Kevin Howland (biomolecular science facility, Kent) using a Waters Synapt G2-Si mass spectrometer. The samples were desalted on-line by reverse-phase HPLC on Phenomonex Jupiter C4 column (5 µm, 300Å, 2.0 mm x 50 mm) running on a Waters H Class Acquity UPLC system at a flow rate of 0.2 ml/min using a short water, acetonitrile, 0.1% formic acid gradient. The eluent was monitored at 280 nm and then directed into the electrospray source, operating in positive ion mode and mass spectra

recorded from 500-5000 m/z. Data was analysed and deconvoluted to give uncharged protein masses with Waters UNIFI software and the MaxEnt 1 algorithm.

2.12 Determination of protein concentration

Absorbance of the pooled PDI fragment samples were measured at 280 nm after ion exchange chromatography using an Ultropsec 2000 UV/Visible Spectrophotometer (Pharmacia Biotech). For the PDI ligand the A_{280} was measured after nickel column chromatography**.** The extinction coefficients were calculated from the amino acid sequence using ProtParam on the EXPASy website (http://web.expasy.org/protparam/).

2.13 Concentrating the protein

Pooled protein samples were concentrated using ultrafiltration. 10,000 Da MWCO Vivaspin® 20 spin concentrators were used for the PDI fragments and 5,0000 Da MWCO Vivaspin® 4 spin concentrators used for the PDI ligand. The concentrators were operated at 2000 rcf (bench centrifuge), 4 °C. Proteins were typically concentrated to 0.5 mM, aliquoted and frozen at -80 °C until needed. However, **b'xa'c** was kept at 4 °C and used as soon as possible.

2.14 NMR Sample Preparation

3 mm NMR tubes were used with a sample volume of 250 μl. 10 % D_2O (25 μl), 0.15 mM of protein (75 μl) and a total concentration of 5 mM GSH/GSSG was used for **xa'c** and **b'xa'c**, and rDTT/oxDTT was also used for **a'c** but to a total concentration of 1.5 mM.

2.15 NMR Data acquisition and processing

Heteronuclear single quantum coherence (HSQC) was the NMR experiment utilised throughout the study, all experiments were run at 298 K. ^{15}N HSQC spectra were obtained with 256 points in the F1 dimension (^{15}N) and 2048 points in the F2 dimension (^{1}H). The

NMR data was acquired and processed with the assistance of Dr Mark Howard and Dr Haris Panagos using NMRpipe. The spectrometer used to acquire the data was a Bruker AV3 (Avance III) 600 MHz operating a 5 mm QCI-F cryoprobe.

For the ligand binding experiments, minimal chemical shift mapping was used. The data was analysed throughout the study using either Topspin 3.2 or Analysis v2.2 [73].

CHAPTER 2

1.0 Protein Expression and Purification of the PDI fragments and ligands

1.1 Introduction

To produce large quantities of ^{15}N labelled PDI fragments and ligands for NMR experiments; recombinant expression in *E. coli* was used. This technique can produce large quantities of protein quickly and cheaply, as well as allowing for easy isotopic enrichment of over 95% with ^{15}N. The T7 polymerase-based pET system was used to express the proteins using the *E. coli* strain BL21 (DE3) pLysS. This recombinant expression system utilises the *lac*UV5 promoter regulated T7 RNA polymerase gene [74], [75].

This system is one of the most popular and effective expression systems to use due to the T7 RNA polymerases high level of activity leading to more than 50% of the total cell protein being the desired recombinant protein after the *lac*UV5 promoter is induced with isopropyl-β-D-thiogalactopyranoside (IPTG) [74]. IPTG is an effective inducer as it is not degraded by components of the cell and it imitates the natural inducer of the lac operon, lactose, the only down side is that it is both expensive and toxic [75].

IPTG works by binding to the inhibitor of the lac operator, LacI, this prevents LacI from inhibiting the lac operator which regulates the *lac*UV5 promoter as well as the T7-lac hybrid promoter (shown in Figure 2.1). LacI is bound to by a water molecule coupled with IPTG via hydrogen bonds and a IPTG hydroxyl group at S193 and D149, this prompts the lac operator inhibitor to undergo a conformational change where it moves away from the lac operator, allowing transcription to occur [76]–[78].

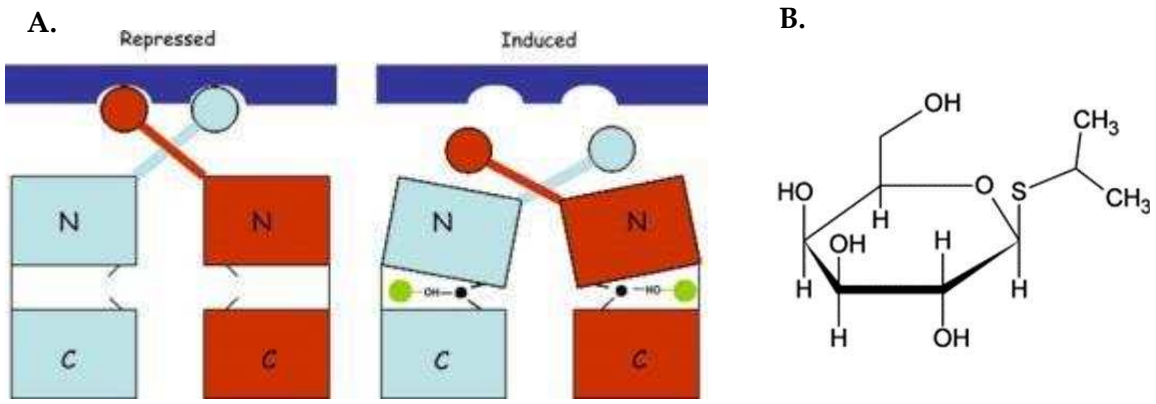

Figure 2.1
Binding mechanism **(A)** and structure **(B)** of IPTG. IPTG shown in green, water molecule in black, LacI as red and turquoise and the lac operator as blue.
Adapted from Daber R. et al 2007 [76]**.**

BL21 cells contain the pLysS plasmid which provides chloramphenicol resistance as well as coding for the T7 lysoszyme which aids in reducing background expression and improving the stability of the plasmid. BL21 cells are lacking the proteases *OmpT* and *Lon* which helps to reduce contamination of purified recombinant proteins by preventing the heat shock protein Hsp70 from being produced. As Hsp70 accounts for 1% of the total protein found in *E. coli*, this helps in producing the highest purity of the recombinant protein with the fewest number of purification steps [79], [80].

The pET-23a(+) vector shown in Figure 2.2 was used for the GB1 and GB1-Δ-somatostatin constructs, whereas for the PDI fragments the vector pET-23b(+) was used [74].

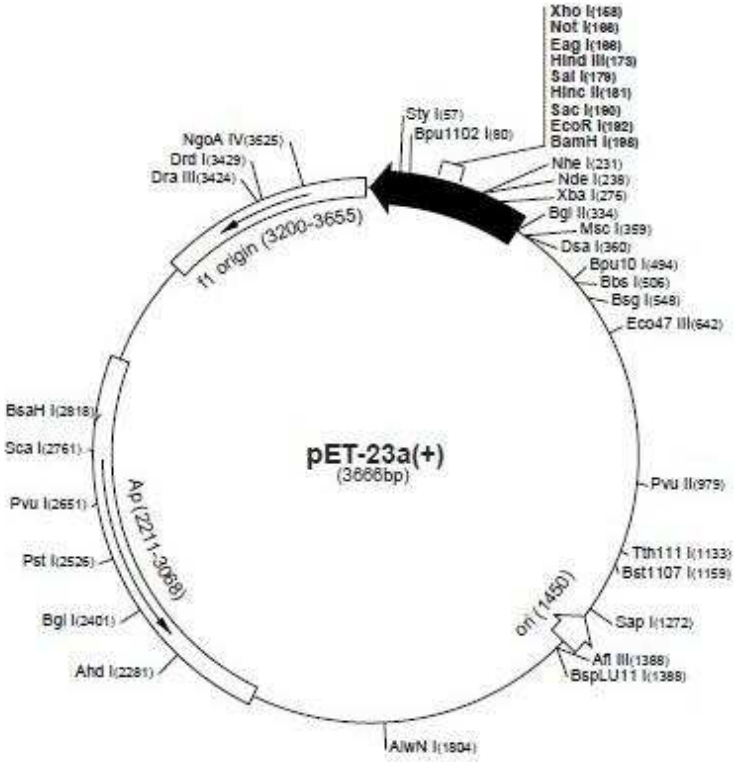

Figure 2.2 pET23a(+)
Adapted from Novagen pET-23a-d(+) Vectors [74].

The amino acid sequences of both PDI fragments and ligands are shown below.

Sequences of PDI fragments:

xa'c:

MHHHHHHMGKIKPHLMSQELPEDWDKQPVKVLVGKNFEDVAFDEKKNVFVEFYAPWCGHCKQLAPIWDKLGETYKDHE
NIVIAKMDSTANEVEAVKVHSFPTLKFFPASADRTVIDYNGERTLDGFKKFLESGGQDGAGDDDDLEDLEEAEEPDMEEDDD
QKAVKDEL

b'xa'c:

MHHHHHHMPLVIEFTEQTAPKIFGGEIKTHILLFLPKSVSDYDGKLSNFKTAAESFKGKILFIFIDSDHTDNQRILEFFGLKKEEC
PAVRLITLEEEMTKYKPESEELTAERITEFCHRFLEGKIKPHLMSQELPEDWDKQPVKVLVGKNFEDVAFDEKKNVFVEFYAP
WCGHCKQLAPIWDKLGETYKDHENIVIAKMDSTANEVEAVKVHSFPTLKFFPASADRTVIDYNGERTLDGFKKFLESGGQDG
AGDDDDLEDLEEAEEPDMEEDDDQKAVKDEL

a'c:

MHHHHHHMDKVLVGKNFEDVAFDEKKNVFVEFYAPWCGHCKQLAPIWDKLGETYKDHENIVIAKMDSTANEVEAVKVH
SFPTLKFFPASADRTVIDYNGERTLDGFKKFLESGGQDGAGDDDDLEDLEEAEEPDMEEDDDQKAVKDEL

His-tag shown in green, **b'** domain in red, **x** linker in grey, **a'** domain in blue and the tail **c** in black, the **a'** active site is highlighted in yellow.
PDI domains defined by Alanen et al. 2003 [27].

Sequences of PDI ligands:

GB1:

MHHHHHHMHHHHHHQYKLALNGKTLKGETTTEAVDAATAEKVFKQYANDNGVDGEWTYDDATKTFTVTE

GB1-FXa-Δ-som:

MHHHHHHMHHHHHHQYKLALNGKTLKGETTTEAVDAATAEKVFKQYANDNGVDGEWTYDDATKTFTVTEGSIEGRAG
SKNFFWKTFTSS

GB1 and GB1-Δ-som. with the FXa cleavage site between GB1 and Δ-som.
Double His-tag shown in blue, GB1 in black, FXa cleavage site in green and Δ-som. in red

1.2 Protein expression and purification

NMR experiments require the protein samples to have a high percentage of ^{15}N to produce high quality data however naturally occurring ^{15}N is only present in very low quantities at 0.23%. Therefore both the PDI fragments and ligands were grown in minimal media containing ^{15}N ammonium sulphate; this meant that the only nitrogen source was the ammonium sulphate allowing for a high percentage of the protein to be isotopically labelled.

For the PDI ligand experiments, unlabelled **b'xa'c** is required, the PDI construct was still grown in MM though. This was to try and prevent dimerization, as it has been previously reported that more dimerization occurs when **b'xa'c** is recombinantly expressed in LB media [81]. This could be due to it being expressed at a faster rate in LB media leading to a closer proximity of unfolded protein meaning greater dimerization occurs.

Throughout the purification process SDS-PAGE analysis was carried out to help ensure that the protein was being purified and was still present. Mass spectrometry was also utilised to make sure that the final product was the desired protein.

Firstly to release the proteins from the induced *E. coli* cells, the cells had to be lysed. The *E. coli* cells contained the cell wall disrupting protein T7 lysozyme due to the pLysS plasmid, therefore the freeze thaw process was utilised to lyse the cells.

Nickel affinity chromatography was used due to the His-tag located at the N-terminus on each of the PDI fragments and ligands. This allowed the protein to bind tightly to the nickel in the column as the unwanted protein was washed off. Firstly nickel was added to the column so it could bind to the chelating sepharose beads. After which the impure protein was added and then washed, first with binding buffer to wash off any very loosely bound protein, followed by a wash buffer containing imidazole. The imidazole washes off the weakly bound protein, leaving the His-tagged protein still bound to the nickel. Finally elution buffer was used to elute the protein from the column, this contained EDTA which strips the nickel off the column meaning the protein is washed out too. After dialysis to remove the nickel from the protein, the PDI fragments were further purified using ion exchange chromatography; this used the theoretical isoelectric point (pI) of the protein to separate out the impurities. Theoretical pI values are shown below in Figure 2.3 and were acquired by entering the amino acid sequences into ProtParam on the ExPASy website (http://web.expasy.org/protparam/). The negatively charged protein binds to the positively charged column and is eluted as the NaCl concentration increases through the column.

PDI Fragment:	Theoretical pI
xa'c	4.66
b'xa'c	4.80
a'c	4.61

Figure 2.3 Theoretical pI for PDI fragments

As previously mentioned **b'xa'c** requires a further purification step to separate out the monomer from the dimer, gel filtration chromatography was used for this. The **b'xa'c** monomer form was used for NMR experiments.

2.0 Results

2.1 PDI Fragments

2.1.1 Expression

To show that the induction of the cells to produce the desired protein was successful, SDS-PAGE analysis was carried out on culture samples before and after induction. Figure 2.4 shows SDS-PAGE analysis of **b'xa'c** expression for two separate culture growths. The **bxa'c** band is seen at expected molecular mass of 32 kDa.

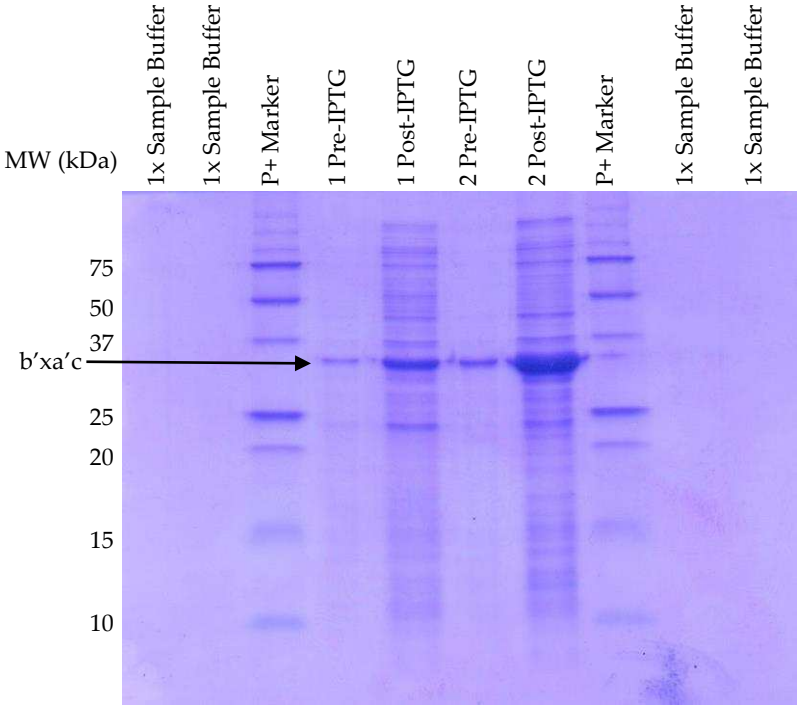

Figure 2.4 SDS-PAGE analysis of b'xa'c expression
Precision plus marker is shown on the left and right hand sides of the pre and post IPTG sample lanes. **b'xa'c** is indicated by the arrow. All lanes were in reducing conditions using DTT. Lanes 1, 2, 9 and 10 contain 1x Sample Buffer, lanes 3 and 8 contain precision plus marker, lanes 4 and 6 contain pre-IPTG samples from two different cultures and lanes 5 and 7 contain post-IPTG samples from two different cultures.

This shows a typical stage of analysis for pre and post IPTG used for the PDI fragments.

Fragments **b'xa'c**, **xa'c** and **a'c** were expected to have molecular weights of about 32, 19 and

16 kDa respectively. This made SDS-PAGE analysis at each stage of the purification procedure an invaluable tool.

2.1.2 Purification

2.1.2.1 Nickel Affinity Chromatography

Nickel affinity chromatography was utilised for all the PDI fragments and proved to be effective in removing the vast majority of the unwanted protein present in the supernatant. SDS-PAGE analysis of **b'xa'c** during cell lysis, loading and running of the nickel affinity column is shown in Figure 2.6. The total lysis sample was taken just before the lysate was spun down, the supernatant sample was taken post centrifugation, the pellet sample was taken after the pellet was re-suspended in an equivalent amount of lysis buffer, and the flow through was taken after the supernatant had gone through the column. The fractions shown after the flow through were samples taken once the elution buffer had been added, across the elution buffer peak as shown below. **xa'c** and **a'c** were purified and analysed in the same way.

Figure 2.5 shows the buffers used and the run off from the column. Binding buffer was used to wash off the protein that was not bound to the column; the wash buffer (50 mM imidazole) was then added to wash off any protein which is weakly bound to the column. The desired protein should remain bound to the nickel column due to the His-tag which binds to the nickel, the protein is only washed out once elution buffer (20 mM EDTA) is added, this contains EDTA which strips the nickel off the column and thus the protein with it.

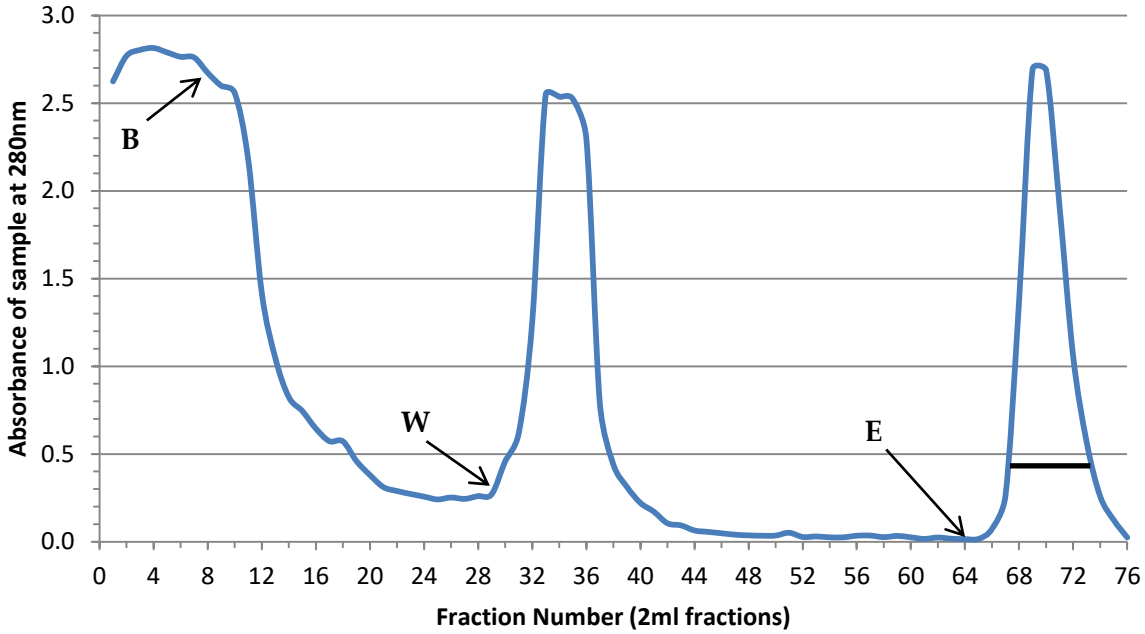

Figure 2.5 Nickel affinity chromatography of b'xa'c

The absorbance at 280nm of the samples is shown, **B** is when the binding buffer is added, **W** is when the wash buffer was added and **E** is when the elution buffer was added. The black line represents the fractions that were pooled for dialysis for the next stage of purification.

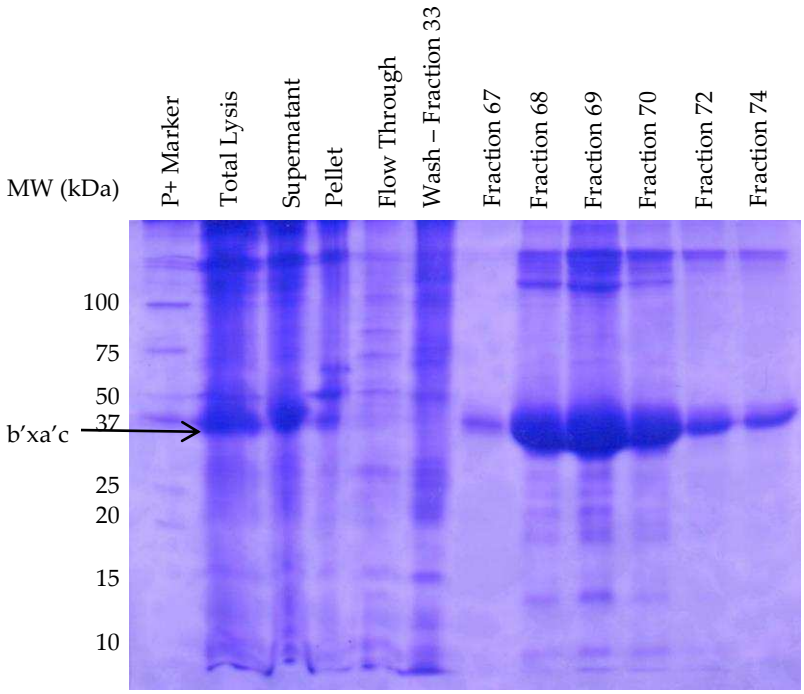

Figure 2.6 SDS-PAGE analysis of nickel affinity chromatography

The elution samples are labelled with fraction number as shown in Figure 2.5. **b'xa'c** is indicated by the arrow. All lanes were in reducing conditions using DTT. Lane 1 contains precision plus marker, lane 2 contains a sample of total lysate, lane 3 supernatant, lane 4 cell pellet, lane 5 flow through, lane 6 fraction 33, lanes 7 – 10 fractions 67 – 70, lane 11 fraction 72 and lane 12 fraction 74.

The lysis of the cells may not have been complete due to the presence of some **b'xa'c** in the pellet sample, this was also seen for both **xa'c** and **a'c**.

For all three PDI fragments; the vast majority of the impurities were removed through the use of nickel column chromatography, but some impurities still remained. Ion exchange chromatography was used to further purify the protein once the peak fractions were pooled and dialysed to remove the high salt concentration. This made it necessary to utilise another purification step once the fractions containing the protein had been pooled and dialysed to remove the nickel.

2.1.2.2. Ion Exchange Chromatography

As this is the final purification step for **xa'c** and **a'c**, their SDS-PAGE's are also shown. Figure 2.7 below shows the peak of **b'xa'c** with contaminants eluting after the main **b'xa'c** peak. It has been previously reported [81]; that even when the ion exchange peak appears symmetrical, implying only the presence of one species of the protein being present, native PAGE analysis showed this to be wrong, as at least two forms of the protein were present. This is possibly only true for **b'xa'c** due to its high level of dimerisation.

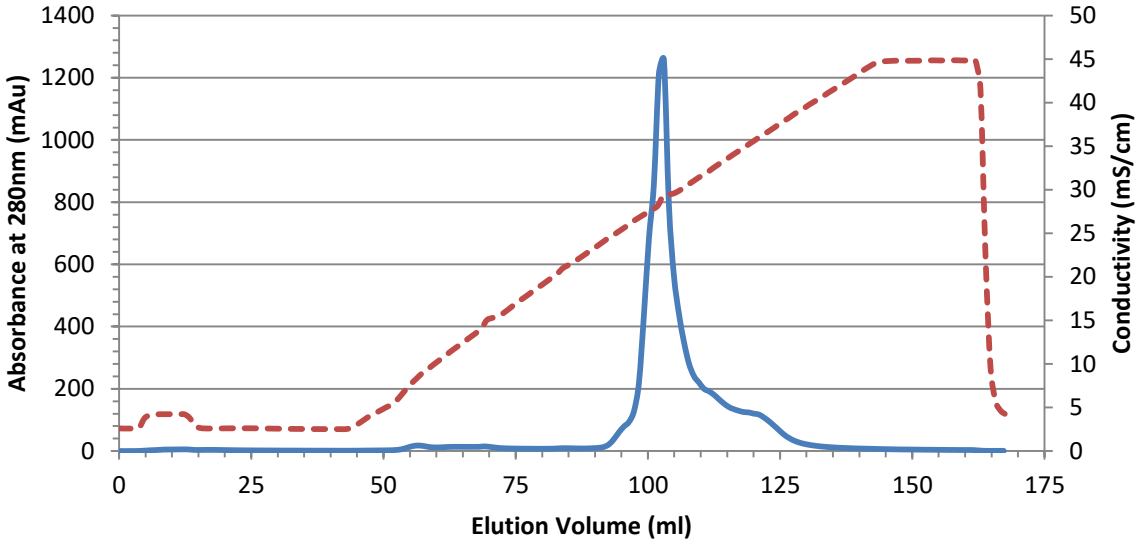

Figure 2.7 Ion Exchange Chromatography of b'xa'c using a 5ml Source30Q column
The absorbance at 280nm is shown by the blue line, while the conductivity is shown by the dotted red line.

The SDS-PAGE analysis (Figure 2.8) showed the high level of purity achieved for **b'xa'c** from ion exchange chromatography. A minor contaminating band at 250 kDa could be seen, but this was subsequently removed by gel filtration.

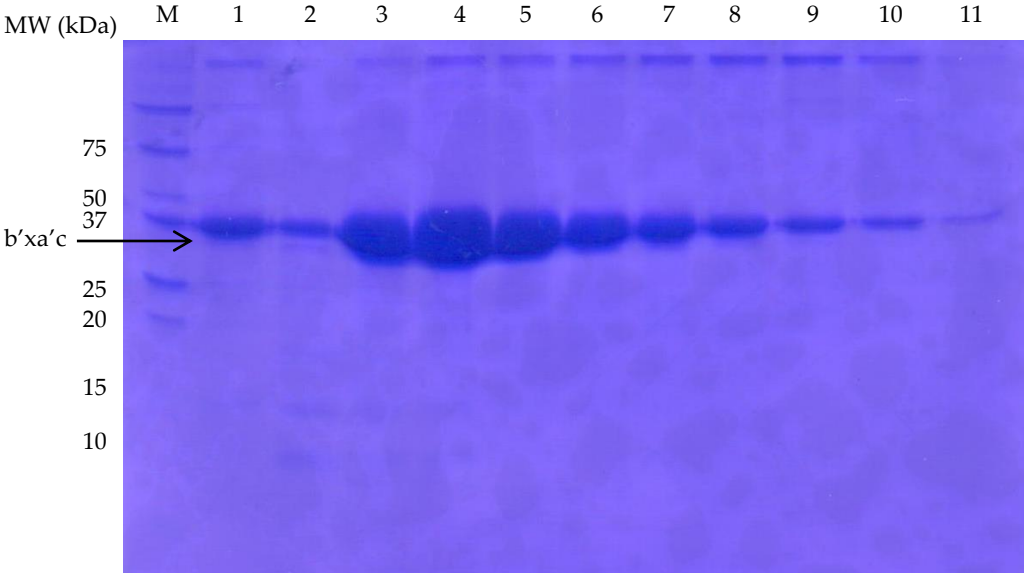

Figure 2.8 SDS-PAGE analysis of b'xa'c from ion exchange chromatography
M is the precision plus marker, Lanes 1 – 11 contain ion exchange fractions taken across the peak. **b'xa'c** is indicated by the arrow.

Figure 2.9 shows two peaks for the elution of **xa'c,** the first peak appearing asymmetrical, suggesting the presence of other **xa'c** species**.** SDS-PAGE analysis was carried out across both peaks (Figure 2.10), both peaks protein fractions were then pooled and their A_{280} measured before being spin concentrated.

Some impurities still remain as the band above **xa'c** in lane 3 shows (Figure 2.10), as well as the band below **xa'c** in lanes 1 – 3. The band below **xa'c** in lanes 1 – 3 is possibly cleaved **c** region of **xa'c**; this is because the **c** region is about 4 kDa in size and **xa'c** is about 19 kDa and the band below **xa'c** is very close to the 15 kDa marker on the gel. However the protein is still in a highly pure form after ion exchange chromatography.

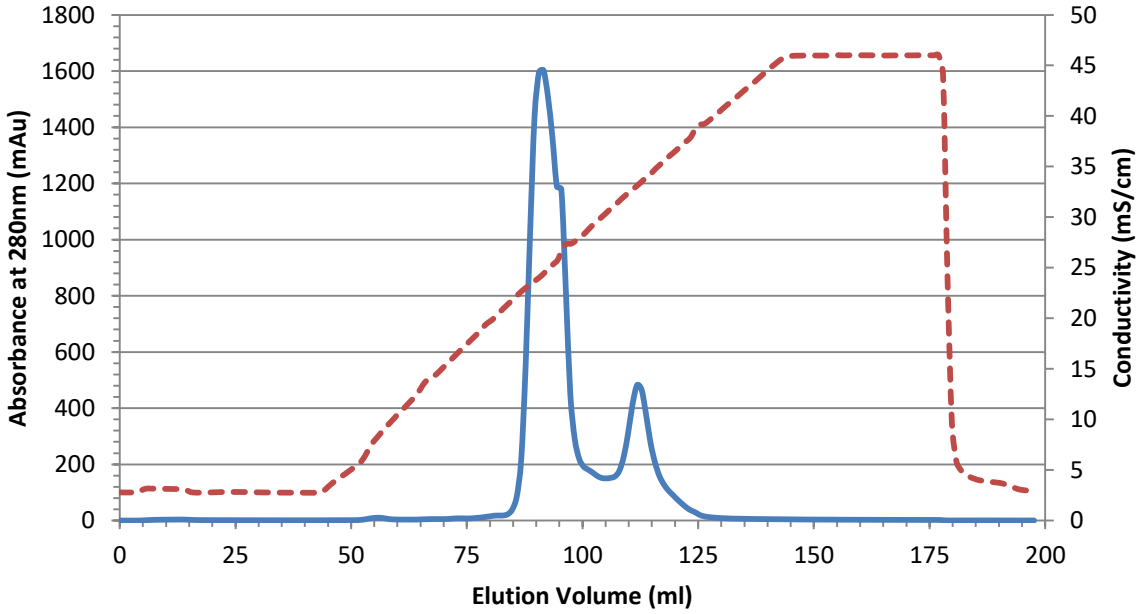

Figure 2.9 Ion Exchange Chromatography of xa'c using a 5ml Source30Q column
The absorbance at 280nm is shown by the blue line, while the conductivity is shown by the dotted red line.

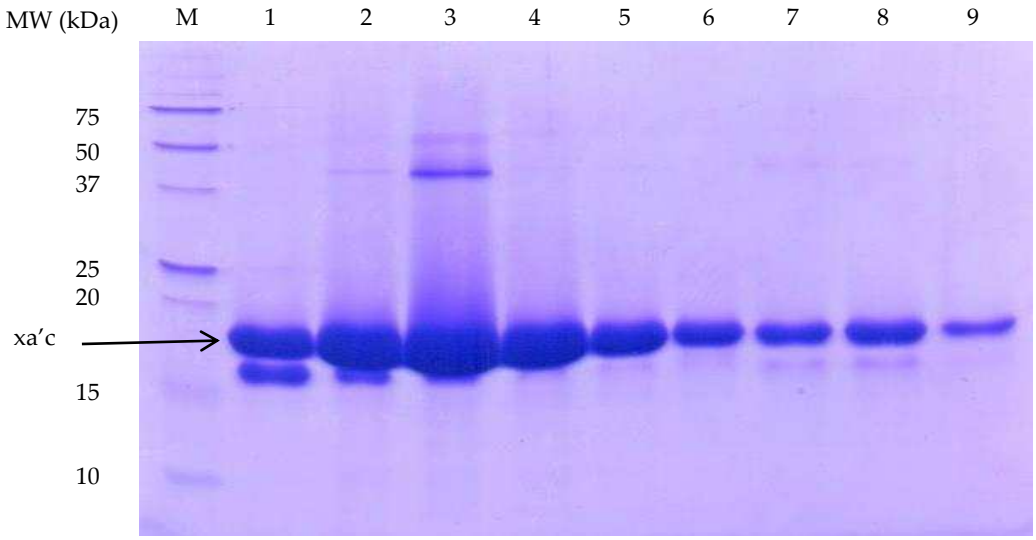

Figure 2.10 SDS-PAGE analysis of ion exchange fractions of xa'c
M is the marker, Lanes 1 – 9 contain ion exchange samples taken across both peaks. **xa'c** is indicated by the arrow.

The **a'c** ion exchange peak however also presented as two peaks, the first being asymmetrical (Figure 2.11), meaning there are most likely other **a'c** species present in the samples as well, the other species that are possibly present in each of the PDI fragments will most likely show up with mass spectrometry.

SDS-PAGE analysis of fractions taken across the ion exchange peaks is shown in Figure 2.12. **a'c** appears to be more pure than both **b'xa'c** and **xa'c** due to the lack of other bands on the gel, although there are faint bands beneath **a'c**.

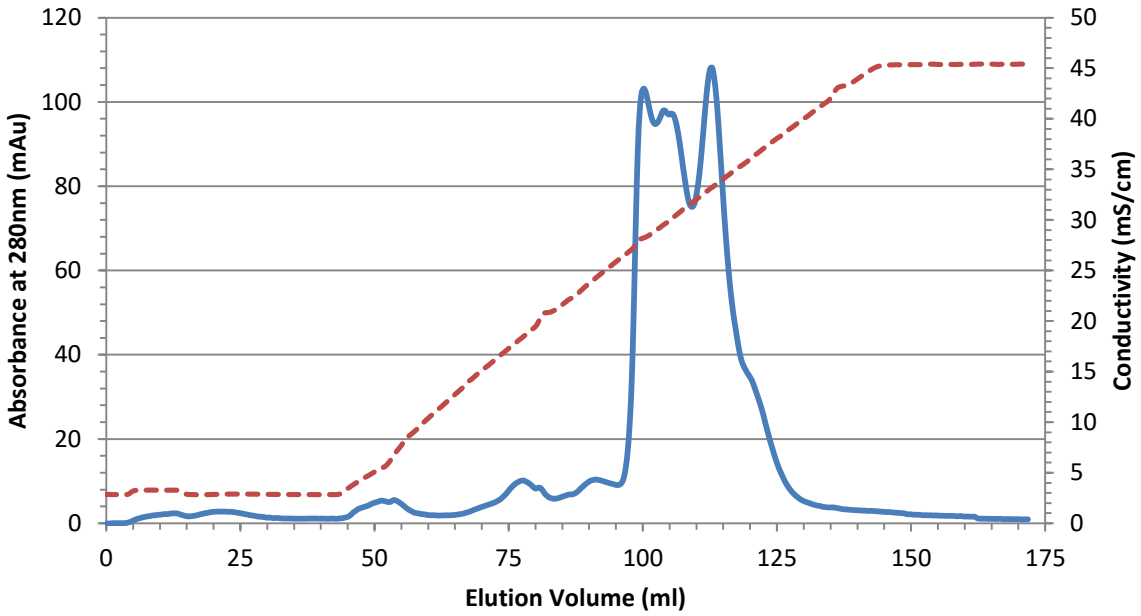

Figure 2.11 Ion exchange chromatography of a'c using a 5ml Source30Q column
The absorbance at 280nm is shown by the blue line, while the conductivity is shown by the dotted red line.

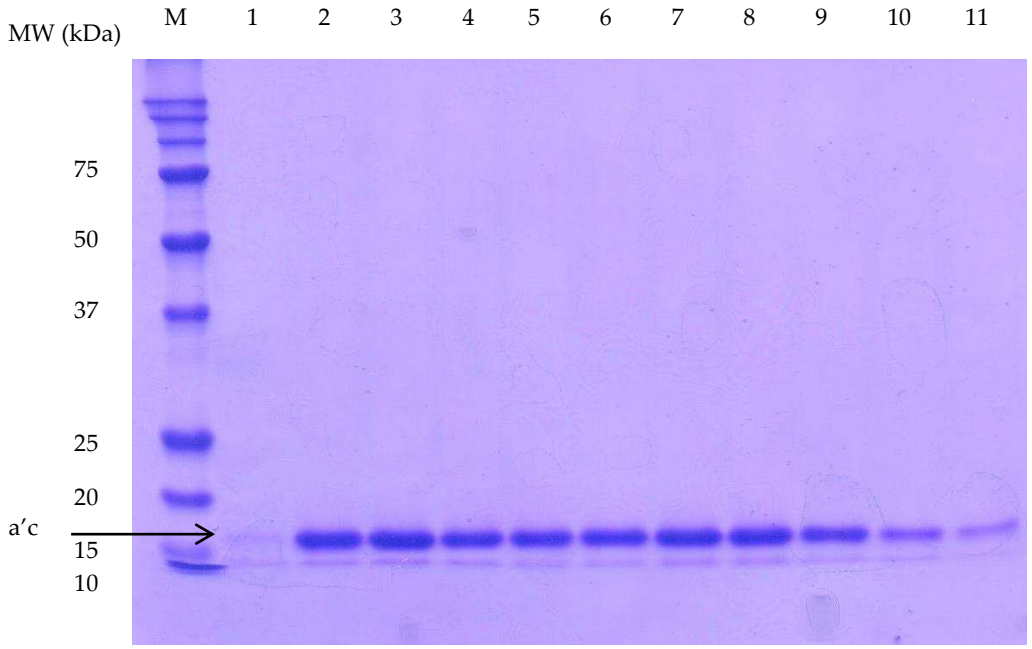

Figure 2.12 SDS-PAGE analysis of ion exchange fractions of a'c
M is the marker, Lanes 1 – 9 contain ion exchange samples taken across both peaks. **a'c** is indicated by the arrow.

After ion exchange chromatography both **a'c** and **xa'c** had their protein fractions pooled, they were then spin concentrated ready for use in the NMR experiments. **b'xa'c** went on to another purification step.

2.1.2.3 Gel Filtration

This purification step was only utilised for the PDI fragment **b'xa'c**, this was due to it previously being reported that a large proportion of the protein dimerises [81], the monomer form was required for NMR experiments, so gel filtration chromatography was used to separate the monomer from the dimer.

Figure 2.13 below shows the dimer and the monomer forms coming off the column, the second blue peak being the monomer form and the first peak the dimer. As **b'xa'c** was expressed in MM the monomer peak was a lot larger than it would have been if it had been expressed in LB media. This was obviously preferential as this means a higher yield of useful protein was obtained. Figure 2.14 shows the SDS-PAGE with samples taken across both peaks. This demonstrates that both the dimer and monomer samples appear as the same molecular weight on a reducing gel. This was the final purification step for **b'xa'c** before spin concentration, ready for use in the NMR experiments.

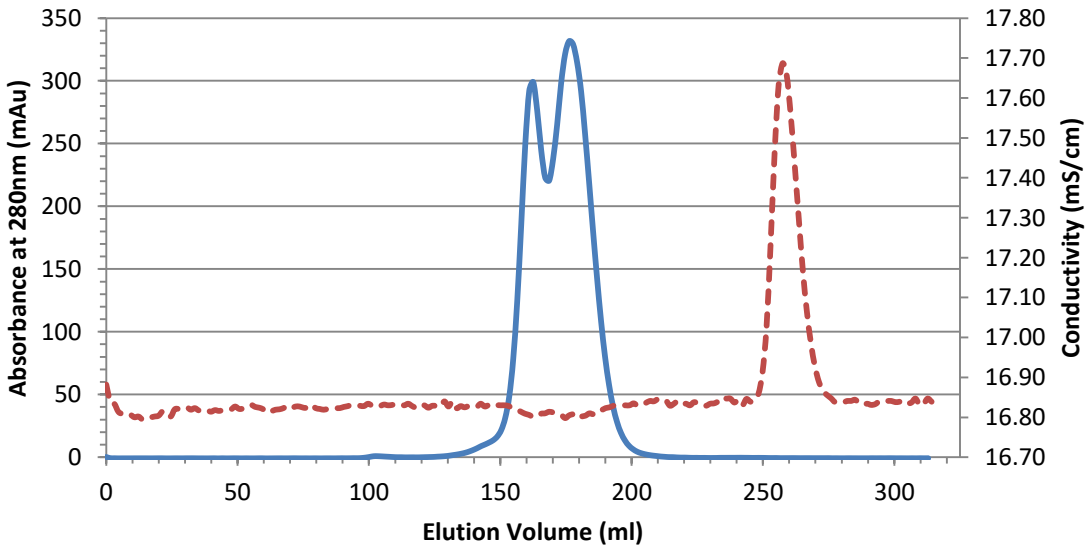

Figure 2.13 Gel Filtration Chromatography of b'xa'c using a 300ml column
The absorbance at 280nm is shown by the blue line and the conductivity shown by the dotted red line.

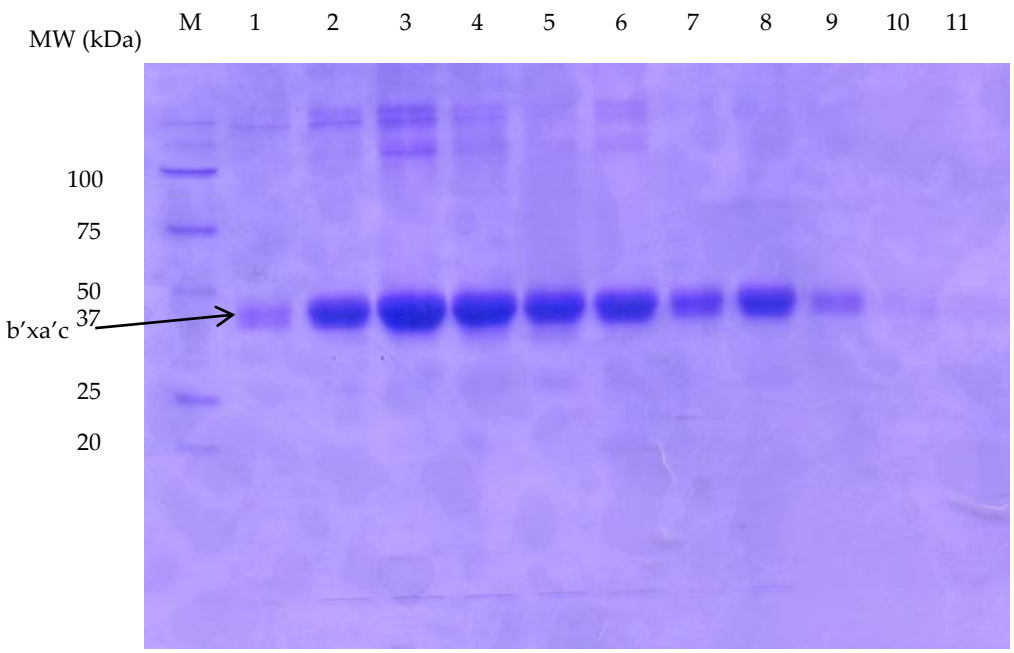

Figure 2.14 SDS-PAGE analysis of gel filtration fractions
M is the marker, Lanes 1 – 6 across the monomer peak and lanes 6 – 11 across the dimer peak

2.1.2.4. Molecular weight and protein yield

Mass spectrometry was carried out on the purified proteins in both the reduced and non-reduced states to elucidate their molecular weights. The results are shown below. The mass data for **b'xa'c** is shown as an example (Figure 2.17); both **xa'c** and **a'c** were analysed in the same manner and are shown in the Appendix Figures 1 and 2 respectively.

b'xa'c in the non-reduced state presented with a molecular weight of 32466 Da, with four other minor peaks at 31693, 32513, 32645 and 32724 Da, one which is 773 Da lighter and three which are 47, 179 and 258 Da higher in mass. The reduced protein however showed a molecular weight of 32467 Da, with four other peaks as well, one which is 832 Da lighter, and three which are 46, 178 and 258 Da higher in mass.

b'xa'c non-reduced and reduced had three higher molecular weighted species of about the same MW the reduced species being 1 Da smaller than the non-reduced. Both non-reduced and reduced presented with degradation products.

Non- reduced **xa'c** has a molecular weight of 19266 Da, with four other peaks, one which is lighter at 18472 Da and three which have a higher molecular weight at 19283, 19314 and 19444 Da, the lighter one being 794 Da less than **xa'c**, and the three heavier ones being 17, 48 and 176 Da higher in mass. Whereas reduced **xa'c** has a molecular weight of 19267 Da and only two extra peaks at 19314 and 19445 Da, making them 47 and 178 Da higher in mass.

Both non-reduced and reduced **xa'c** showed two higher MW species of about the same size, 48 and 176 non-reduced, 47 and 178 reduced. The non-reduced **xa'c** was the only one to have a degradation product, which was at 18472 Da.

a'c in the non-reduced state has a molecular weight of 17376 Da with an extra peak at 17555 Da, making it 179 Da higher in mass than **a'c**. Reduced **a'c** has the same molecular weight of 17376 Da and two extra peaks, at 17422 and 17555 Da, which makes them 46 and 179 Da higher in mass respectively.

The non-reduced and reduced **a'c** both presented with one species 179 Da higher in MW.
All three PDI fragments showed two extra species with MW from 46 to 48 Da higher and 176 to 179 Da higher than **a'c**.

The expected MW was taken from was taken from the ExPASy website (http://web.expasy.org/protparam/) through entering the amino acid sequence into ProtParam.

All PDI fragments expected and actual MW's from the mass spec. data were almost identical (Figure 2.15).

PDI Fragment	Expected MW (Da)	Mass Spec. Data (Da) Non-Reduced	Mass Spec. Data (Da) Reduced
xa′c	19267.3	19266.0	19267.0
b′xa′c	32467.5	32466.0	32467.0
a′c	17377.1	17376.0	17376.0

Figure 2.15 Expected and actual MW of the PDI fragments in Daltons (Da)

xa′c proved to have the highest yield as it had a yield of 73.5 mg/L protein purified, in comparison only 24.5 mg/L of **b′xa′c** and 17.7 mg/L of **a′c** was obtained. These quantities were calculated from the absorbance at 280 nm of the pooled protein fractions after ion exchange chromatography.

PDI Fragment	Total Quantity Purified (mg)	Concentration of protein produced (mg/L)
xa′c	44.1	73.5
b′xa′c	14.7	24.5
a′c	10.6	17.7

Figure 2.16 Quantity of protein produced from 600ml cell culture as well as its concentration

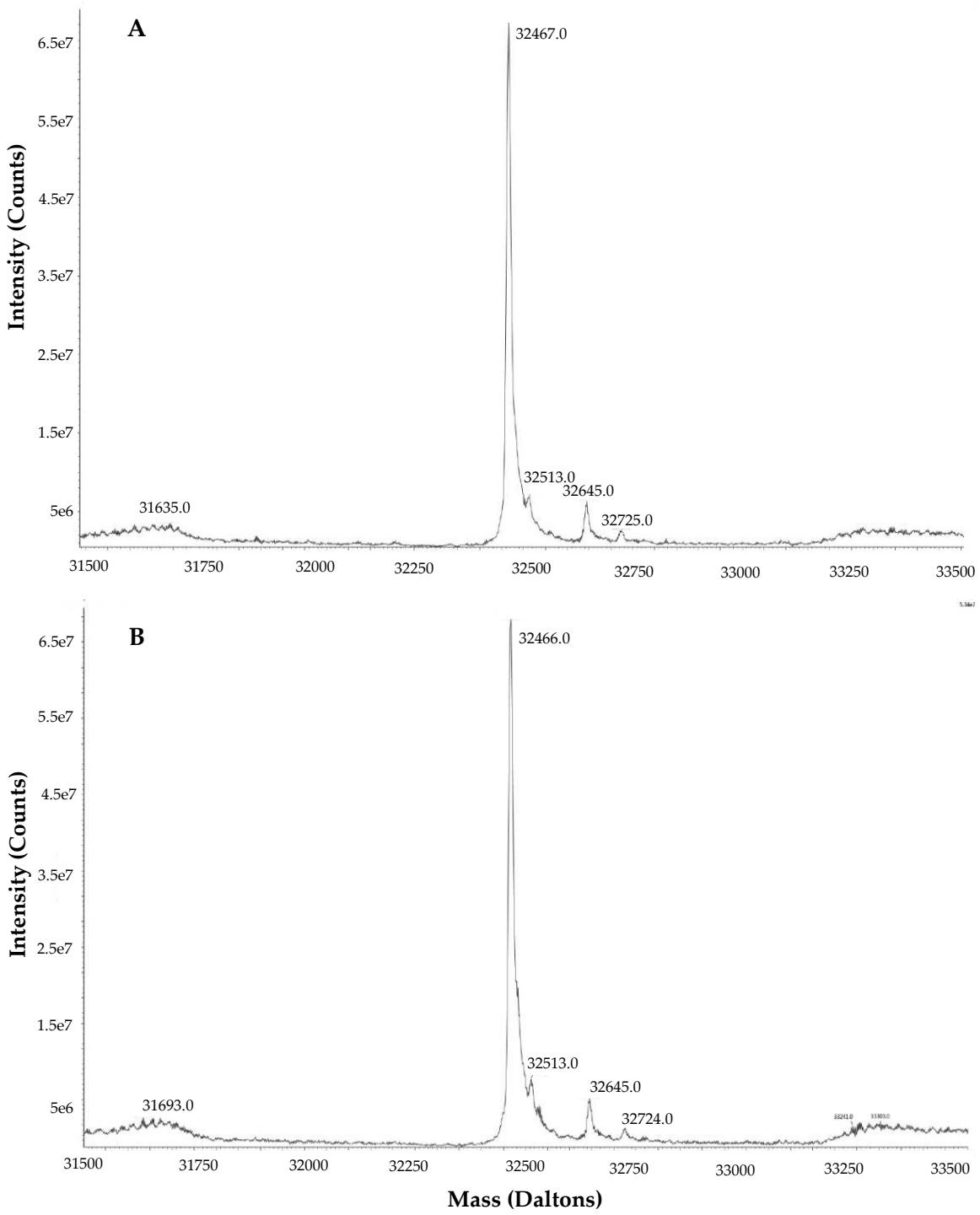

Figure 2.17 Mass spectrometry analysis of b′xa′c in the reduced (A) and non-reduced (B) forms.

The molecular weight of **b′xa′c** in daltons, in its reduced form is 32467 Da and in its non-reduced form is 32466 Da. Four additional peaks are shown in both the reduced and non-reduced forms.

2.2. PDI Ligand

2.2.1. Expression

Again, SDS-PAGE analysis was used at each stage of the purification process to aid in characterising the protein and to act as another way of making sure the protein made it through the purification step in high enough quantities.

Figure 2.18 below shows the expression of a small prep. and 3 large growth cultures. Pre and post IPTG induction of GB1-Δ-somatostatin is shown with an expected molecular weight of 10 kDa. The control GB1 was analysed in the same manner for its pre and post IPTG induction and had an expected molecular weight of 8 kDa.

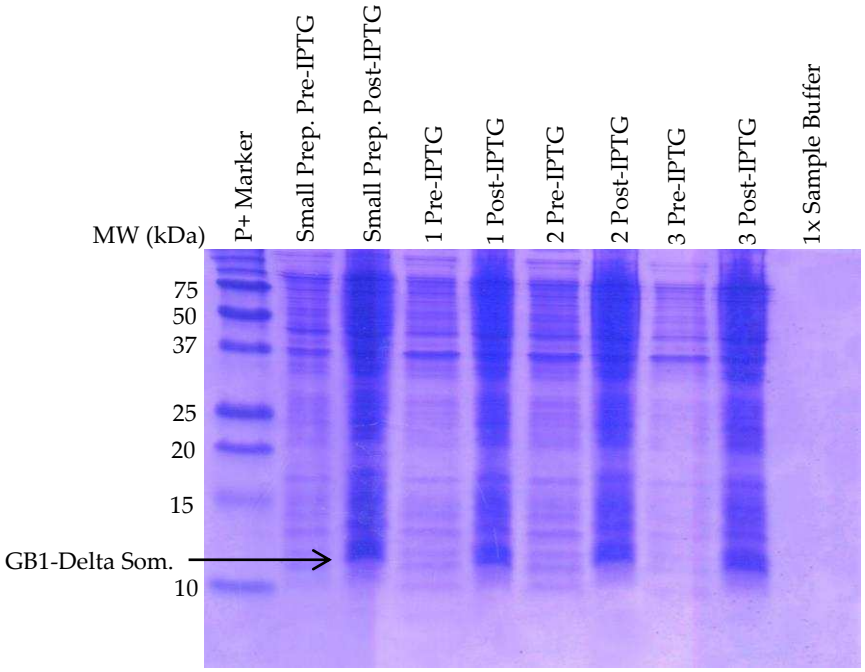

Figure 2.18 SDS-PAGE analysis of pre and post IPTG induction of GB1-Δ-somatostatin
Precision plus marker is shown on the left hand sides of the pre and post IPTG sample lanes. GB1-Δ-somatostatin is indicated by the arrow.

The pre and post IPTG SDS-PAGE's for both GB1 and GB1-Δ-somatostatin both presented with bands just above the 10 kDa marker band despite their respective molecular weights being 8 kDa and 10 kDa.

2.1.2. Purification

Nickel affinity chromatography is the only purification step utilised for the PDI ligands, the double His-tag on the N-terminal of the protein allows the constructs to bind to the nickel in the column whereas the protein impurities are washed out.

2.1.2.1. Nickel Affinity Chromatography

Again this purification process proved to be extremely effective in removing the vast majority of impurities after cell lysis. The buffer running through the column was collected in 2 ml fractions and its A_{280} was measured and plotted on a graph (Figure 2.19), allowing the tracking of the protein as it comes off the column.

The total lysis, supernatant, pellet, flow through, wash peak and elution peak fractions were all prepared in the same manner as the PDI fragments post nickel column SDS-PAGE samples. The pellet sample of both GB1 and GB1-Δ-som did not contain any of the ligand, showing total lysis of the cell. The flow through and wash peak samples did not show any bands for GB1 or GB1-Δ-som, showing that all the ligand had bound to the column and was not washed out by the wash buffer (50 mM Imidazole).

As this is the only purification step for the PDI ligands, both GB1 and GB1-Δ-som's SDS-PAGE's are shown in Figure 2.20. Again, just like with the pre and post IPTG samples, the GB1 and GB1-Δ-som fractions run to just above 10 kDa despite their respective molecular weights being 8 and 10 kDa.

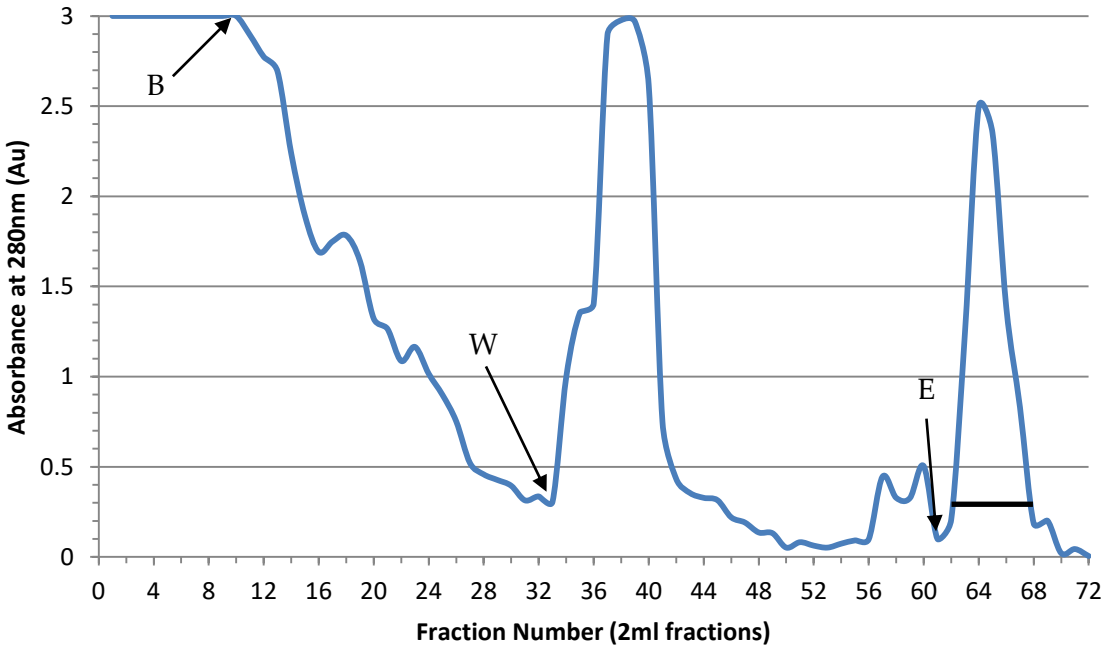

Figure 2.19 Nickel affinity chromatography of GB1-Δ-somatostatin

The absorbance at 280nm of the samples is shown, **B** is when the binding buffer is added, **W** is when the wash buffer was added and **E** is when the elution buffer was added. The black line represents the fractions that were pooled for spin concentration after dialysis.

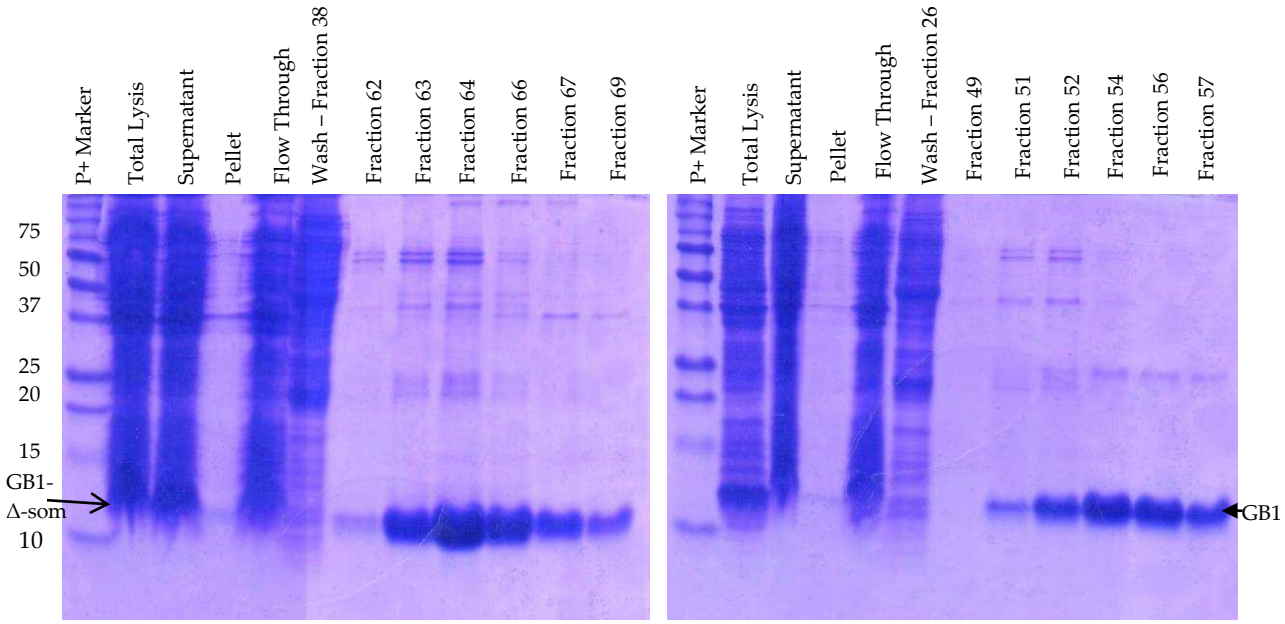

Figure 2.20 SDS-PAGE analysis of GB1 and GB1-Δ-som by nickel affinity chromatography

Precision plus marker is shown on the left hand side, with total lysis, supernatant, pellet, flow through, and the wash fraction (50 mM imidazole), the fractions after are taken across the elution peak (20 mM EDTA). GB1-Δ-somatostatin is indicated by the arrow on the left, and GB1 is indicated by the arrow on the right.

After nickel column chromatography the protein fraction samples were pooled and dialysed ready for spin concentration. Once spin concentrated the protein is ready for the NMR experiments.

2.1.2.2. Molecular weight and protein yield

Just like with the PDI fragments, mass spectrometry was utilised to elucidate the molecular weight of the proteins expressed, the results of which are shown below.

GB1 presented with a molecular weight of 7957 Da (mass spec. data shown in Figure 2.23) despite it presenting with a molecular weight of about 10 kDa on the SDS-PAGE gels that were run. Three other molecular weights of GB1 were also shown to be present in the purified sample, 7974, 8010 and 8064 Da, this makes the other peaks 17, 53 and 107 Da larger respectively GB1-Δ-somatostatin presented with a molecular weight of 10147 Da with only one other peak at 10200 Da, which means it's 53 Da higher in mass. The + 53 Da species is present in both GB1 and GB1-Δ-som.

PDI Ligand	Expected MW (Da)	Mass Spec. Data MW (Da)
GB1	7957.6	7957.0
GB1-Δ-somatostatin	10147.0	10147.0

Figure 2.21 Expected and actual molecular weight of both GB1 and GB1-Δ-som

Total quantity purified was calculated in exactly the same way as the PDI fragments in Figure 2.16, the results of which are shown in Figure 2.22. GB1-Δ-som appears to have purified a lot more effectively than just GB1 on its own.

PDI Ligand	Total Quantity Purified (mg)	Concentration of protein in 600 ml culture (mg/L)
GB1	8.17	13.62
GB1-Delta Somatostatin	19.56	32.60

Figure 2.22 Quantity of protein produced from 600ml cell culture as well as its concentration

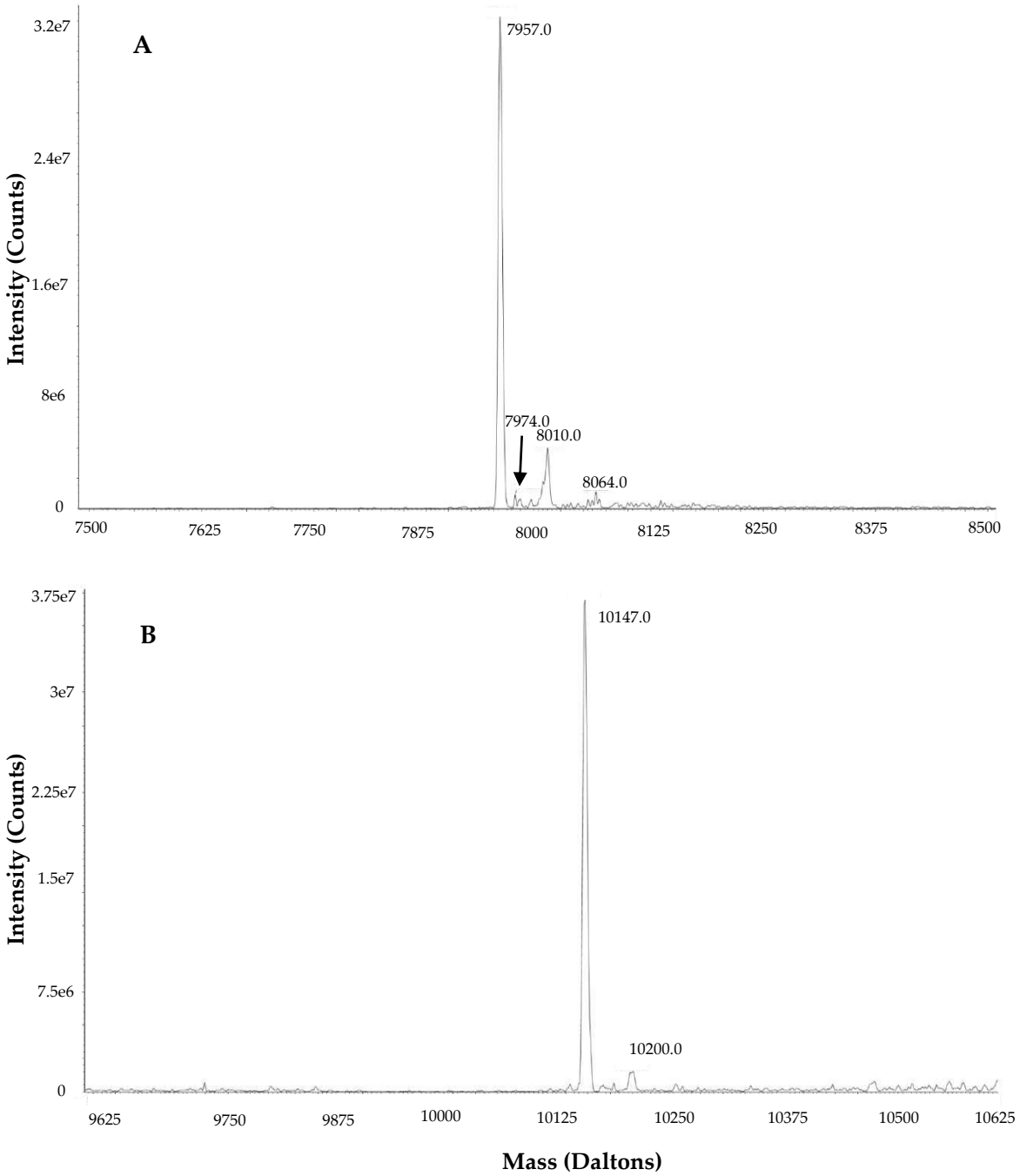

Figure 2.23 Mass spectrometry data for GB1 (A) and GB1-Δ-somatostatin (B)

GB1 shown to be 7957 Da and GB1-Δ-som to be 10147 Da. GB1 with three other peaks present and GB1-Δ-som with one other peak.

3.0 Discussion

Both the PDI fragments and PDI ligands were successfully expressed in *E. coli* BL21 (DE3) pLysS and purified using the various purification techniques demonstrated above showing various expression yields.

The first purification step, nickel column chromatography, proved to be an extremely effective way to purify the PDI fragments and ligands, due to the massive reduction in both low and high MW impurities. Although the purification protocol might still have room for optimisation due to there being no band at all of the desired protein in the wash peak sample as shown in Figures 2.6 and 2.20. This optimisation could be achieved through slightly increasing the concentration of imidazole in the wash buffer; this would be most useful for the PDI ligand purification as its purification is still to be optimised due to the presence of high MW bands being present in Figure 2.20. Ion exchange chromatography was not used for the ligands partly because the nickel column step was so successful, but mainly because of time limitations and that the protein was sufficiently pure for the experiments planned. The fact that more protein would be lost with another purification step was also a factor. Also in Figures 2.6 there was an indication that lysis of the cells was not complete due to the presence of the PDI fragments bands showing in the pellet, this is either due to human error or the protocol needs tweaking, most likely the former as this is a well-established protocol for lysing cells. Very faint bands were showing for the PDI ligand pellet indicating almost complete lysis, this showed that lysis by sonication was an effective technique for the PDI ligand pellet, shown in Figure 2.20.

It should be mentioned that both PDI ligands, GB1 and GB1-Δ-som presented with slightly higher MW's of 10 kDa when analysed using SDS-PAGE's, this was despite mass

spectrometry showing GB1 to have a MW of 7957 Da, it is unclear as to why this happened, although this was shown to be the case for each SDS-PAGE analysis performed on GB1.

Ion exchange chromatography was also very useful for further purifying the PDI fragments, as it removed the vast majority of the impurities left after the nickel column step. Due to the asymmetrical peaks forming from ion exchange chromatography for **xa'c** and **a'c** (Figures 2.9 and 2.11 respectively), it was expected for there to be multiple species of these constructs, this was proven to be correct as the mass spectrometry data showed. **b'xa'c** displayed a symmetrical peak, however other **b'xa'c** species were present as shown in Figure 2.17, indicating that a symmetrical peak doesn't necessarily mean there are no other species present.

Gel filtration chromatography was the final purification process for the PDI fragment **b'xa'c** as it's known to contain a large amount of dimer. For this reason when unlabelled **b'xa'c** was needed, it was also grown in MM. This was because in LB media, *E. coli* have a much faster growth rate and thus a much faster protein expression rate, this meant that in LB media **b'xa'c** would be expressed very quickly, leading to close proximity of folding proteins, resulting in much higher levels of dimerization (unpublished observation from previous work in the lab). MM on the other hand would most likely express **b'xa'c** at a slower rate due to the lack of free amino acids and trace elements etc, allowing the protein to fold properly.

xa'c and **a'c** presented with two peaks, the most probable reason for the two distinct peaks is **xa'c** and **a'c** in the reduced and non-reduced forms coming off the column at different times due to slight changes in their isoelectric points.

The majority of the extra peaks shown in the mass spectrometry data were higher in MW than the desired protein; these are either post-translational modifications or something within the purification process itself which is binding to these constructs. All the PDI fragments showed degradation products, however the PDI ligands did not.

The PDI fragment mass spec. data showed species that were 178 and 258 Da higher in MW than the desired proteins, these can be attributed to the post translational modification which involves the alpha-N-6-phosphogluconoylation of the proteins His-tag, this results in the species 178 Da higher in mass and only sometimes the species 258 Da higher in mass [82].This explains why the + 258 Da species was present in **b'xa'c** but not in the other PDI fragments whereas derivatives of the + 178 Da species was present in all three PDI fragments. However it is unclear why this modification did not occur for the PDI ligands. It should be noted that this modification did not alter the purification during ion exchange chromatography due to the modifications being in such low quantities.

The presence of the + 46 to + 48 Da species was present in all three PDI fragments and could possibly be attributed to oxidative modification to kyneurine (+ 4 Da), singly oxidised tryptophan (+ 16 Da) and hydroxy-N-formyl kyneurine (+ 48 Da), the + 17 Da species of **xa'c** and GB1 might also be accounted for due to this [83].

+ 53 Da species was present in both GB1 and GB1-Δ-som, although another two were present in GB1 at + 17 and + 107 Da, the extra + 107 Da peak possibly 2 x the + 53 Da post translational modification. Although at the moment it is unclear as to what the + 53 Da modification could be.

xa'c was shown to have the best expression yield of the PDI fragments at 73.54 mg/L, with **b'xa'c** a distant 2nd with just over a third of **xa'c** protein yield at 24.56 mg/L and **a'c** a close 3rd with 17.72 mg/L. **a'c** produced a surprisingly low yield in comparison to **xa'c**, this could indicate that the **x** linker of **xa'c** helps to stabilise it, preventing it from being degraded so quickly, although it could possibly be attributed to human error during the expression and purification process.

The protein yield for GB1 was surprisingly low at 13.62 mg/L whereas GB1-Δ-som yield was 32.60 mg/L, this is in comparison to the higher expression yields (20 mg/L) described in the literature [84], whereas the protein yield for GB1-Δ-som agrees with the literature of the other purified fusion proteins GST and MBP (15 to 50 mg/L) [85]. This reduction in GB1 yield is most likely due to human error during the expression and purification process.

CHAPTER 3

1.0 Redox potential of the *a′* domain

1.1 Introduction

A vast number of reactions catalysed by enzymes are reduction-oxidation reactions. This reaction involves the reduction of one compound and the oxidisation of another. Enzymes can only catalyse these reactions however in the right environment, described as its reduction potential or redox potential. Redox potential varies from compound to compound; the more positive it's potential, the more likely it is to accept electrons and become reduced, therefore showing oxidising characteristics and the more negative the redox potential the more likely it is to be oxidised and exhibit reducing properties.

Protein reduction potentials have typically been elucidated in the past via the use of tryptophan fluorescence or through the use of radiolabelling or HPLC. However these methods can only be utilised when there is just one catalytically active site present, as these

methods work by separating and quantifying the different amounts of reduced and oxidised species of the protein present.

In this chapter the redox potential of hPDI's **a'** domain is investigated through the addition of domains surrounding **a'**, NMR spectrometry is utilised with HSQC experiments to gather data on this, see Taylor, S., et al., 2013 [86]. This adds to our understanding of the overall redox potential of PDI, allowing us to develop a more complete picture of its role *in vivo*.

1.2 Redox-dependent conformational change of hPDI

PDI is a redox regulated chaperone protein which undergoes large redox dependent changes to its conformation [30], **b'xa'** being the minimal number of domains required for PDI to undergo redox regulated conformational change, with the **a'** domain being the key domain to induce conformational change once oxidised. The PDI domain region **bb'xa'** showed that the **a'** domain was situated closely to both the **b'** domain and **x** linker, to form one tightly bound structural module. Once the **a'** domain is oxidised the compact structure is lost, exposing the substrate binding site of the **b'** domain, allowing hPDI to undergo its chaperone function [30], [31].

In the reduced state all 4 main domains of PDI are on the same plane, whereas in the oxidised state, the **a'** domain twists around the **x** linker at about a 45° angle above the plane, this explains why in the reduced state, the **a** and **a'** domains are 27.6 Angstroms (Å) apart but in the oxidised state they're 40.3 Å apart (Figure 3.1). This means that in the reduced state hPDI reveals a smaller hydrophobic surface than when it's in the more open oxidised state [30], [31].

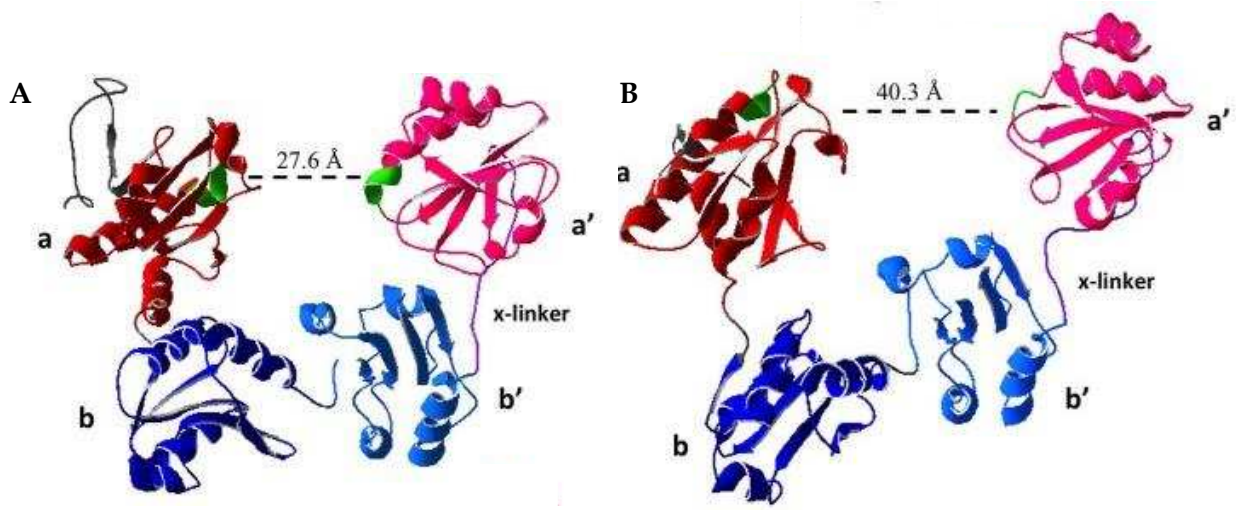

Figure 3.1 Crystal structure of (A) reduced and (B) oxidised PDI
a domain shown in red, **b** domain in blue, **b'** domain in light blue, **x** linker in purple and **a'** domain in pink. Both **a** and **a'** domains active sites highlighted in green.
Representing the distance between the active sites in Angstroms (Å) in the reduced **(A)** and oxidised **(B)** states.
Adapted from Wang, C., et al., 2013 [30].

This process is essential to regulation of hPDI's chaperone activity. The **a'** domain triggers this conformational change as the amino acid residue Trp396, adjacent to the active site, interacts with the **b'** domain when it is in the reduced state, however in the oxidised state, the residue is exposed [31]. This is indicative of its role in PDI's conformational change as it appears to play a role in sensing the change in redox state. The β2-β3 loop of the **a'** domain is also involved in conformational change as it interacts with **b'** in the reduced state and is exposed when PDI is in the oxidised state [31].

Another region which may play an important role in the sensing of changes in the redox conditions is the highly conserved, among thioredoxin-like proteins, Pro441. This residue is also located adjacent to the active site, just like Trp396, and has been shown to be an important part of substrate binding and release; this is based on studies conducted on DsbA, thioredoxin and yPDI [29], [87], [88]. PDI was first shown to be a redox regulated chaperone

in 2001 due to it binding to and unfolding the cholera toxin A1 subunit in the reduced form [89].

1.3 Redox potential of hPDI overview

PDI catalyses the formation of disulphides as well as retaining the ability to re-arrange non-native disulphides in an isomerisation reaction. For this to occur PDI's active sites redox potentials must be placed in a position so that they can both donate electrons (to Ero1) and take them (from substrates) [90].

In 1993 PDI was demonstrated to have a redox potential of -190 +/- 10 mV, in the same paper, its dithiol active sites were shown to have a redox potential of roughly -175 mV +/- 15 mV [91]. In 2010, a paper was published showing a more accurate redox potential measurement for domains **a** and **a'**, -162.7 +/- 2.9 and -169.4 +/- 2.3 mV respectively [90]. This indicated that, during disulphide exchange reactions, any difference in the amount of reactivity would most likely not be due to the difference in redox potential. In the study the CGHC active site motif was changed to CGPC, this changed the **a** and **a'** domains redox potential to -228.9 +/- 0.6 and -225.9 +/- 2.6 mV respectively, making them more reducing and therefore allowing them to be oxidised a lot faster by Ero1α. This was achieved through the use of site directed mutagenesis and mass spectrometry; this helped to show how the reduction potential of hPDI active sites limited the re-oxidation ability of Ero1α. This study demonstrated that changing the reduction potential of PDI's active sites regulates the efficiency of their oxidation using Ero1α, which led to the conclusion that the increased activity is most likely due to its improved ability to donate its electrons to Ero1α active site [90].

1.4 $^{15}N/^{1}H$ HSQC Experiments

HSQC experiments were used in this study as they are quick to run and produce high quality data. HSQC's allow you to see a single peak for each amino acid residue, except proline as it does not contain an amide group. These peaks shift in position due to environmental changes such as pH, temperature or the presence of a reductant or oxidant.

An improved method to elucidate redox potentials via the use of $^{15}N/^{1}H$ HSQC's was used in this study, first demonstrated by Taylor S.L., et al, 2013 [86], this method was used due to it being quick and convenient, as well as it suiting the size of the proteins, as the MW limit for this method is in excess of 60 kDa whereas the proteins used only go up to 32 kDa. It uses multiple resonances to elucidate the redox potential, meaning a degree of data redundancy can be implemented as weak, overlapping or low signal to noise ratios data can be discarded from the analysis leading to improved accuracy of the redox potential. I refer the reader to the paper Taylor S.L. et al, 2013 [86] for further clarification if required.

It should be noted that these redox potential calculations are carried out on an *in vitro* system and therefore are not open to the different altering factors encountered in an *in vivo* measurement, and so may differ slightly.

1.5 Redox Couples

1.5.1 GSH/GSSG

The main redox couple used throughout this thesis was reduced and oxidised glutathione (GSH and GSSG respectively). Glutathione (structure shown in Figure 3.2) is the model redox couple for these experiments as it is found within the ER in the optimum ratio for disulphide bond formation [92]. The ratio of GSH to GSSG was reported to be between 1:1

and 1:3 in the secretion pathway and microsomal vesicles, this is based on an *in vitro* study that showed the oxidative folding of proteins in redox buffers with a similar ratio of GSH:GSSG [93], [94].

GSH is a tripeptide (L-γ-glutamyl-L-cysteinyl-glycine) and is synthesised from the precursor amino acids glutamate, cysteine and glycine in the cytosol in concentrations up to 10 mM. Glutathione remains in the reduced form (GSH) due to the cytosolic glutathione reductase catalysed reaction with NADPH [95]. All this makes GSH/GSSG the natural model for redox couple reaction experiments.

Rost and Rapport [96] were the first to give the redox potential of GSH/GSSG as -240 mV [96], this is the redox potential used for the calculations in this chapter.

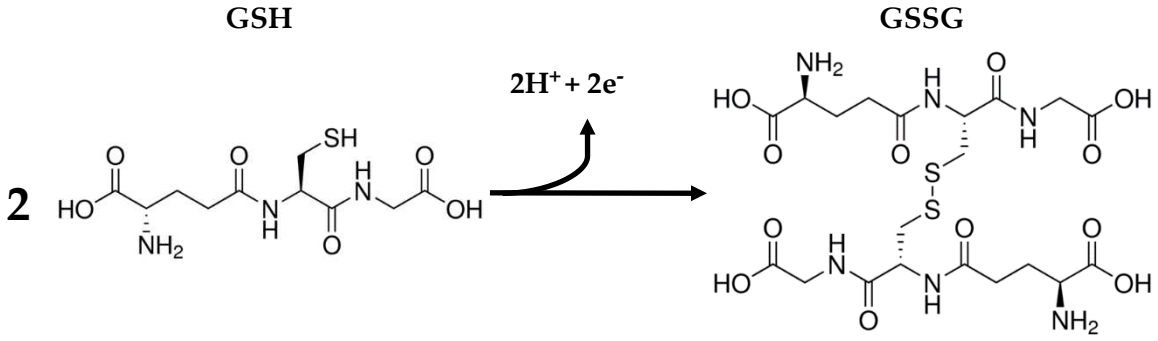

Figure 3.2 Showing reduced glutathione (left) and oxidised glutathione (right) Skeletal structure of GSH and GSSG adapted from Sigma-Aldrich

In recent years the hypothesis that GSSG was the main route through which PDI was oxidised was called in to question by the discovery of Ero1 [97], [98]. It was shown that yeast cells carrying a mutant Ero1 had their normal level of oxidised PDI severely reduced when Ero1 was not functioning. It was also shown that the oxidation of Ero1 substrates is largely independent of the redox buffer glutathione [99].

1.5.2 rDTT/oxDTT

Dithiothreitol (DTT, $HSCH_2(CH(OH))_2CH_2SH$) was also used at times due to its extreme reducing abilities with a redox potential of -332 mV at pH 7 [100]. However DTT did not work very well as a redox couple due to its oxidising form not being oxidising enough, this is because the oxidised form is too stable for the reverse reaction of Figure 3.3 to be kinetically favourable.

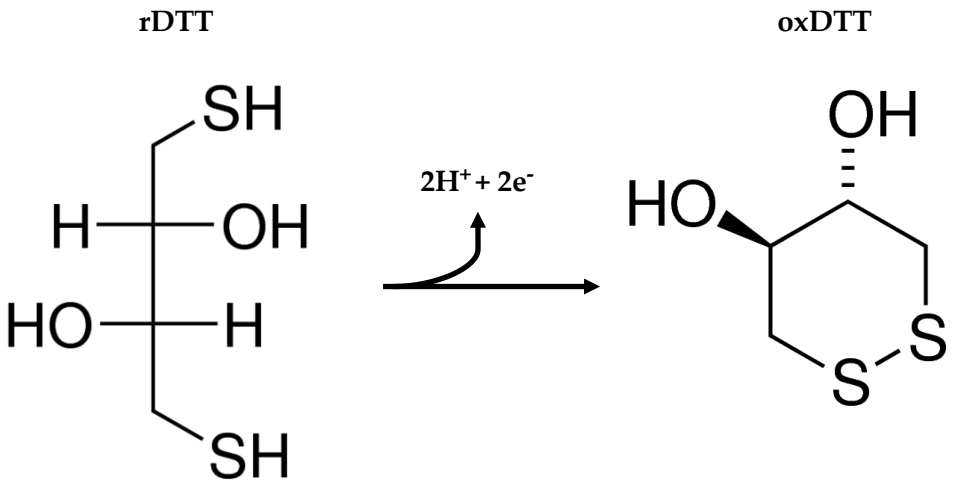

Figure 3.3 Showing reduced DTT (left) and oxidised DTT (right)
Skeletal structure of rDTT and oxDTT adapted from Sigma-Aldrich

2.0 Results

The redox potential was determined using various ratios of GSH and GSSG, the total concentration equalling 5 mM. This was to oxidise and reduce the purified protein to varying degrees; equilibrium for these reactions was reached within 5 min of setting up each sample. Peaks in the HSQC spectra were identified which shifted with the oxidation status. The NMR data gathered from these peaks was presented as peak height or peak volume, either parameter could be used to calculate the redox potential; however the peak volume tended to give better fits with the Hill equation and so was used. Analysis v2.2 [73] was used to determine the peak heights and volumes for all the oxidised and reduced peaks.

The data collected was then used to calculate the fraction reduced of each of the peaks and fitted using Kaleidograph v4.1 (Synergy Software) to the Hill equation.

The K_{eq} value was calculated from Figure 3.4 A at the point at which the Fraction reduced (F_{red}) equals 0.5. This is the point at which the ratio of GSH:GSSG changes the least and therefore should provide the most accurate redox potential. K_{eq} is then put into the Nernst equation (Figure 3.4 B) to calculate the redox potential, where the standard reduction

A. Fraction Reduced

$$F_{red} = ([GSH]^2 / [GSSG] / (K_{eq} + [GSH]^2 / [GSSG])$$

B. Nernst Equation

$$E'_0 = E'_{0(GSH)} - (RT / n\mathrm{F})\ln(K_{eq})$$

Figure 3.4 Fraction reduced and Nernst equations used to calculate redox potential Adapted from Taylor S.L., et al, 2013 [86].

potential of GSH ($E'_{0(GSH)}$) = -0.24 V, R is the molar gas constant, T = 298 K, n = 2 , F is the Faraday constant. K_{eq} must be used in molar concentration. Errors were calculated using the Levenberg-Marquardt R value for the fit of the Hill equation.

xa'c and **b'xa'c** were assigned using assignments determined previously (unpublished data) by Dr Denisa Doko [81].

2.1 xa'c

xa'c proved to be the easiest PDI construct to use throughout this thesis. It expressed highly as well as being easy to analyse through NMR spectrometry due to its stable conformation. As the **a'** domain has previously been reported to be difficult to work with as it has a low expression yield (approximately 1 mg/L) and exhibits very poor NMR spectra. The addition of the **x** linker and the **c** region helped to stabilise the construct.

HSQC

A fully assigned reduced spectrum (using 5 mM GSH), shown below in Figure 3.5 was used to calculate the fraction reduced of the other spectra, as the fully reduced was used as the maximum. This was the same principle used throughout the redox calculations.

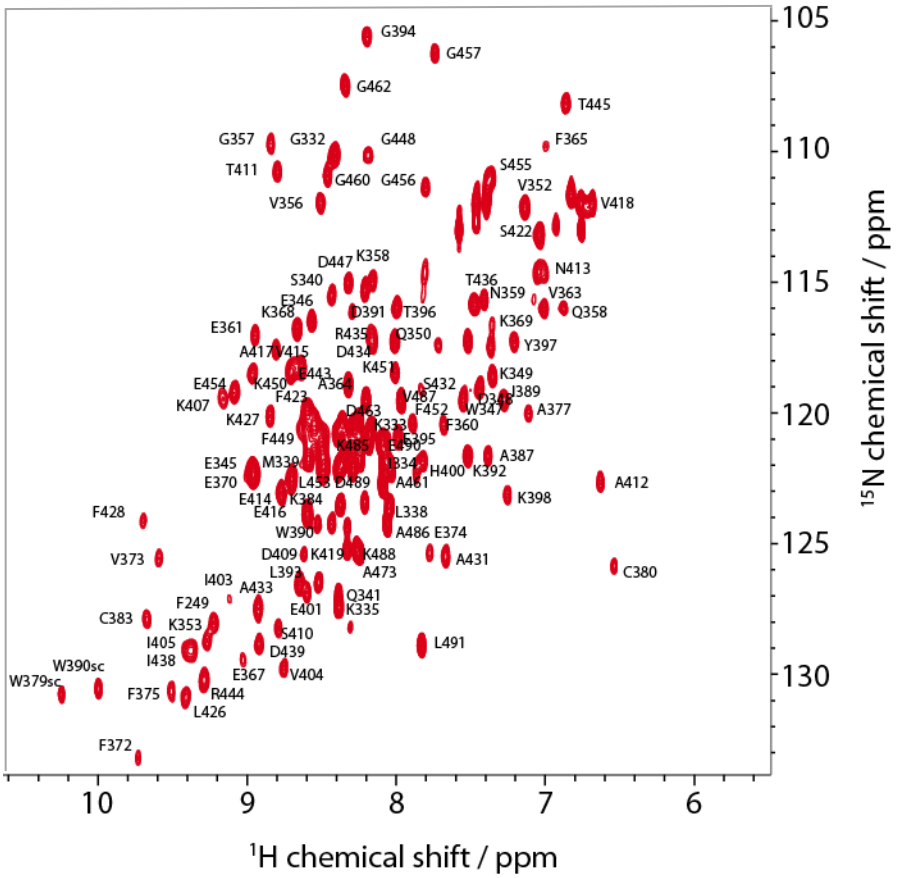

Figure 3.5 NMR ^{15}N HSQC spectra of xa'c

NMR ^{15}N HSQC spectra of xa'c in the fully reduced state with 5 mM GSH. Fully assigned using previously determined assignments from Denisa Doko's unpublished data [81].

HSQC redox calculations

The peaks for **xa'c** identified which move in the different oxidation states were G462, T411, T445, Q350 and A387. The fully reduced and fully oxidised HSQC's are shown in Figure 3.6 below with the selected amino acid residues highlighted.

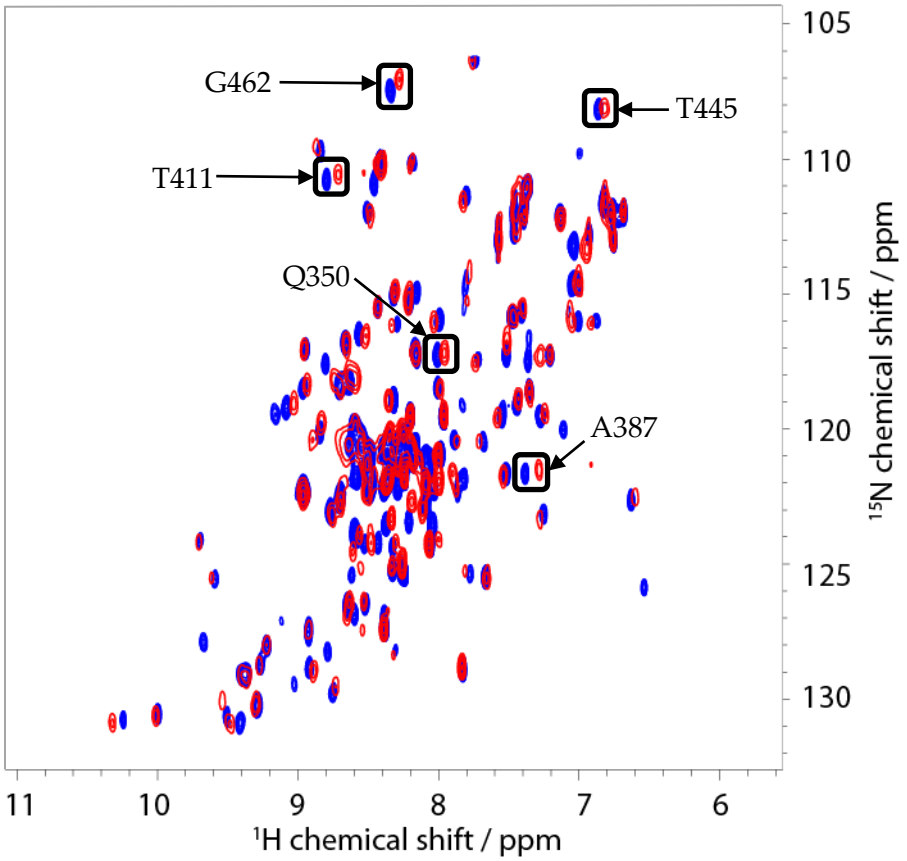

Figure 3.6 Two NMR ^{15}N HSQC spectra's of fully reduced and fully oxidised xa'c
Fully oxidised (with 5 mM GSSG) spectra are shown in red and fully reduced (with 5 mM GSH) spectra shown in blue. The amino acid residues G462, T411, T445, Q350 and A387 are shown. Assignments identified using previously determined assignments from Denisa Doko's unpublished data [81].

Fraction Reduced

The plot for each amino acid residues fraction reduced shown in Figure 3.7 for **xa'c**, this is used as an example for the other redox calculations. Figure 3.7 was used to calculate the average fraction reduced, with the average calculated from the sum of the 5 residues at each GSH:GSSG ratio. This is the same principle used throughout the redox calculations.

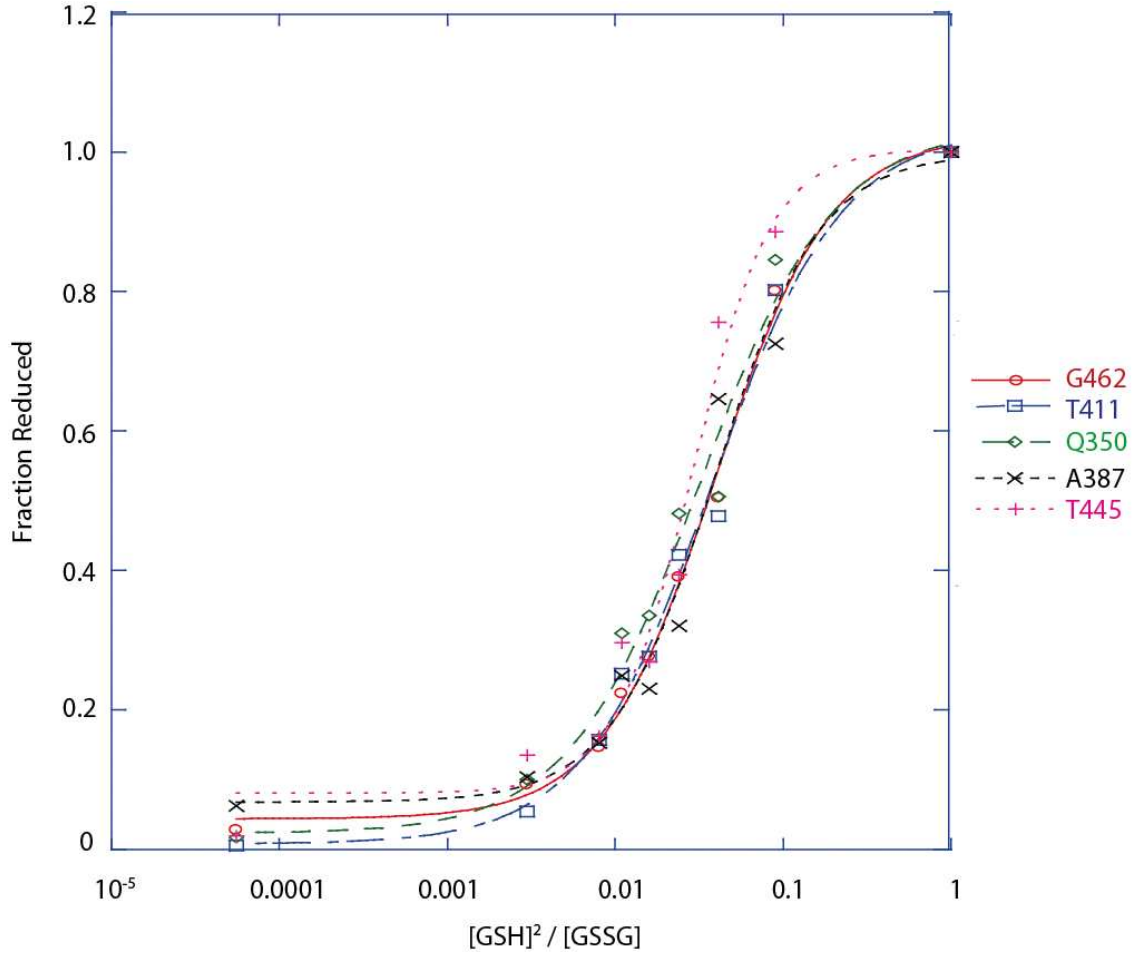

Figure 3.7 xa'c fraction reduced, using Kaleidograph v4.1 (Synergy Software) to fit the Hill equation

All data sets for amino acid residues G462, T411, T445, Q350 and A387. Ratio of GSH:GSSG shown on the x axis and fraction reduced on the y axis.

Average Fraction Reduced

xa'c exhibited very consistent NMR data, as the loss of peak intensity for the reduced peaks due to oxidation was easily trackable. The redox potential is calculated from the point at which the curve crosses the y axis at 0.5 (Figure 3.8). This y value was used as F_{red} in the Fraction reduced equation (Figure 3.4 A) to calculate the value of K_{eq}. This allows you to calculate the redox potential using the Nernst equation. The redox potential was calculated the same way for each PDI construct. From this graph the redox potential was calculated and found to be -196.23 mV +/- 0.42.

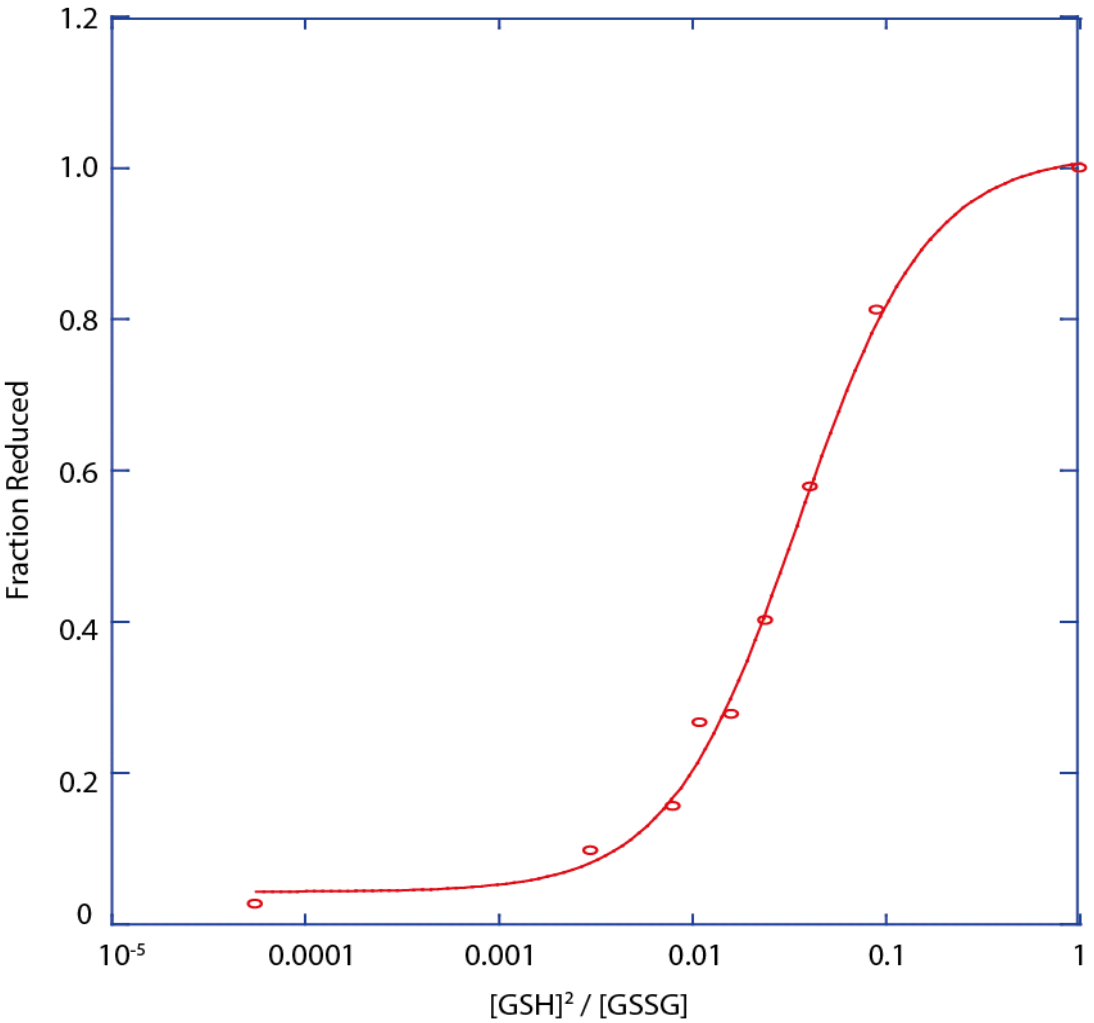

Figure 3.8 xa'c average fraction reduced, using Kaleidograph v4.1 (Synergy Software) to fit the Hill equation

Average of data sets for Figure 3.7, with the ratio of GSH:GSSG on the x axis and average fraction reduced on the y axis. **xa'c** with a redox potential of -196.23 mV +/- 0.42

2.2 b'xa'c

This construct was a lot more difficult to work with, the addition of the **b'** domain seemed to increase line broadening for all the peak resonances massively decreasing the quality of the spectra. It also rapidly aggregated in solution when it was fully oxidised with 5 mM GSSG, and did not become fully reduced in the presence of 5 mM GSH as shown in Figure 3.9, so 1.5 mM of DTT was used instead to fully reduce it, due to its reduction potential being -332 mV, in contrast to GSH's -240 mV. This improved the resolution of the spectrum (shown in Figure 3.10) however the spectrum was still broad compared to **xa'c**. The number of residues identified to shift on oxidation and used for the redox calculation was 11 in total.

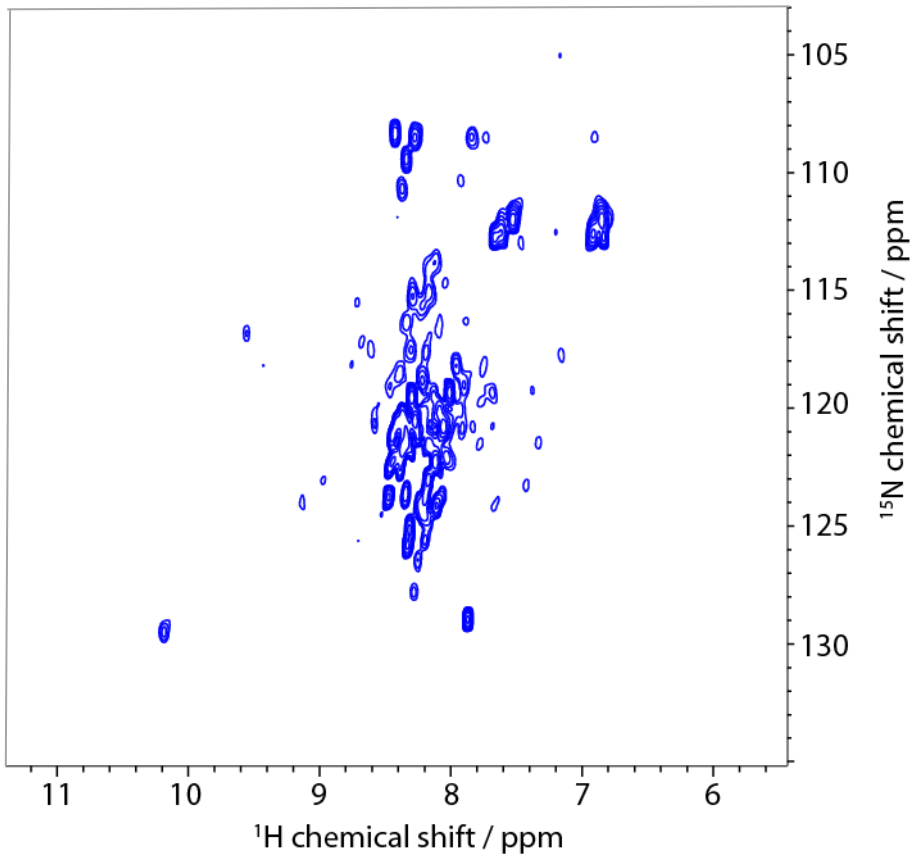

Figure 3.9 NMR ^{15}N HSQC spectra of bxa'c
NMR ^{15}N HSQC spectra of **b'xa'c** in the partially reduced state using 5 mM GSH.

Figure 3.10 showing the partially assigned spectrum of **b'xa'c**. The spectrum is only partially assigned as it was not possible to assign past this point with any accuracy due to the still poor resolution.

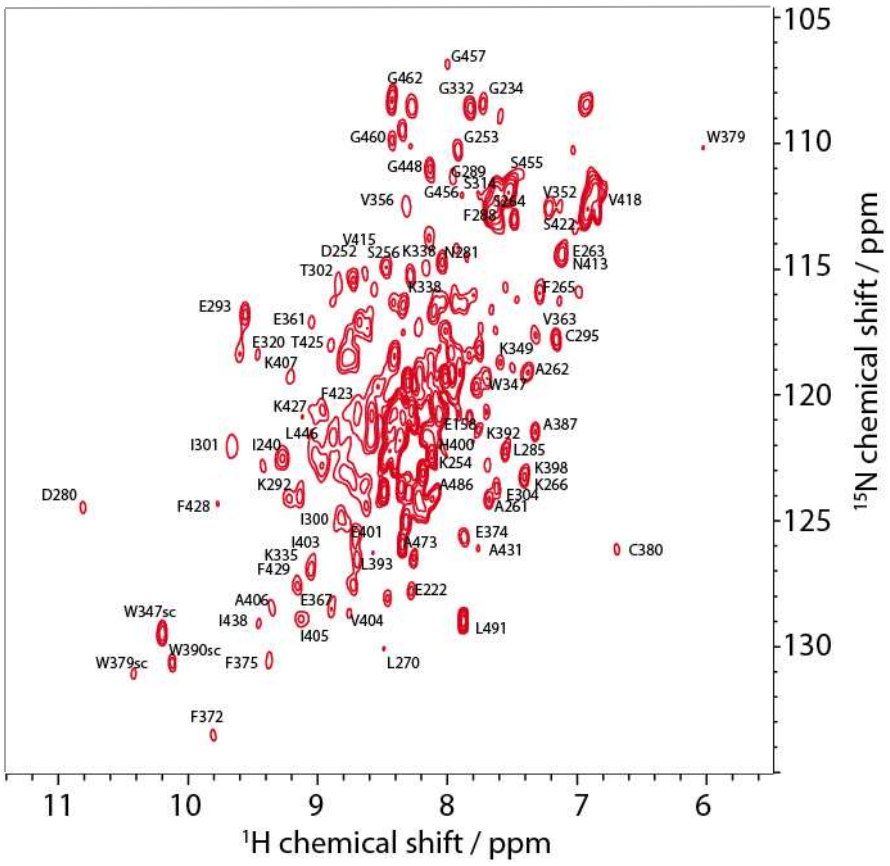

Figure 3.10 NMR ^{15}N HSQC spectra of bxa'c

NMR ^{15}N HSQC spectra of b'xa'c in the fully reduced state with 1.5 mM DTT. Partially assigned using previously determined assignments from Denisa Doko's unpublished data [81].

The residues identified were E293, I240, K292, W390, N413, F265, C295, A262, A387, L285, K398 and E304 shown below in Figure 3.11. The fully reduced spectra with 1.5 mM DTT (Figure 2.6) was used as the fully reduced to calculate the fraction reduced.

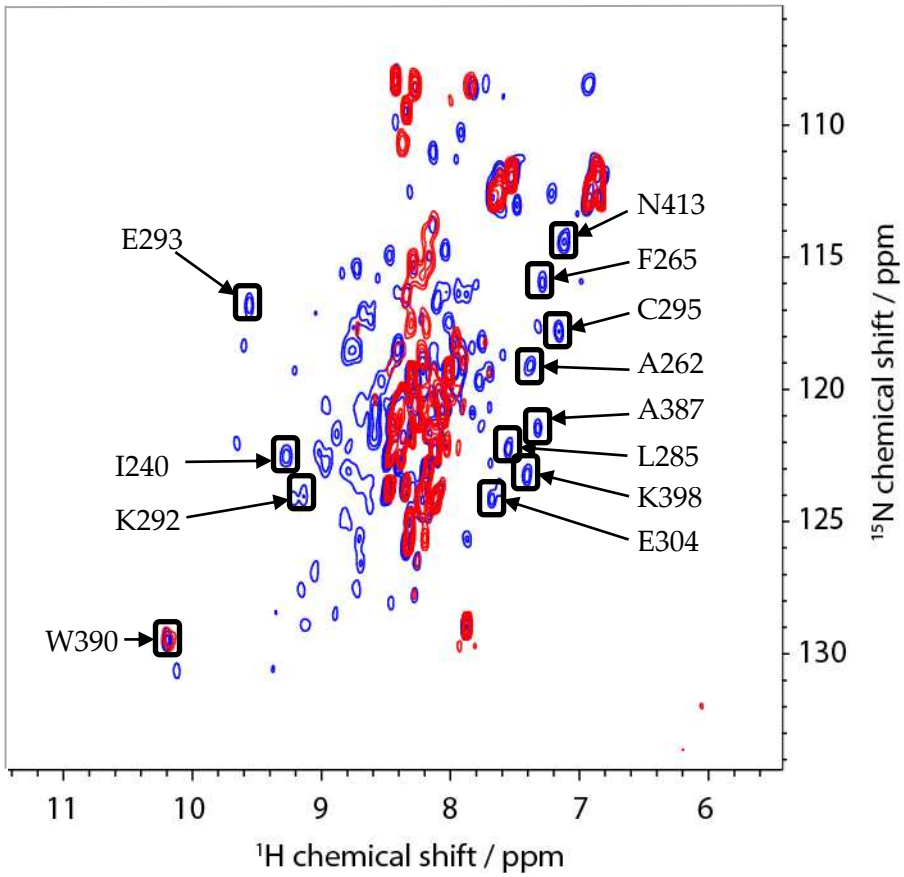

Figure 3.11 Two NMR ^{15}N HSQC spectra's of fully reduced and fully oxidised b'xa'c Fully oxidised (with 5 mM GSSG) spectra are shown in red and fully reduced (with 1.5 mM DTT) spectra shown in blue. The amino acid residues W390, K292, I240, E293, N413, F265, C295, A262, A387, L285, K398 and E304 are shown. Assignments identified using previously determined assignments from Denisa Doko's unpublished data [81].

Fraction reduced

From 0.5 of the y axis from Figure 3.12 it was possible to calculate the redox potential to be -213.71 mV +/- 0.16. This means that the addition of the **b'** domain on to **xa'c** decreases the redox potential from -196.23 to -213.71 mV, meaning it's more reducing, this is a total decrease of 17.48 mV.

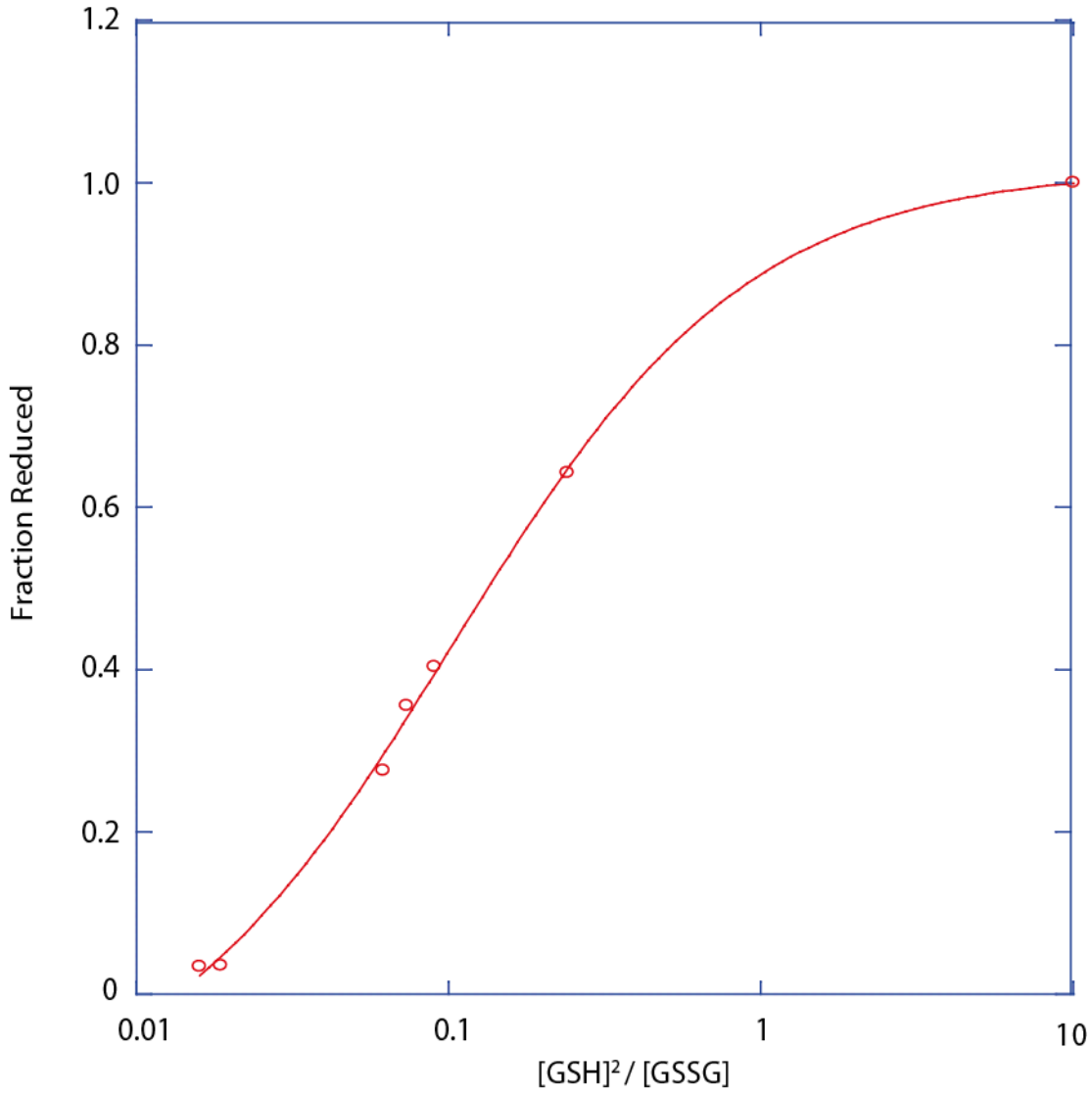

Figure 3.12 bxa'c average fraction reduced, using Kaleidograph v4.1 (Synergy Software) to fit the Hill equation

The ratio of GSH:GSSG on the x axis and average fraction reduced on the y axis. **b'xa'c** with a redox potential of -213.71 mV +/- 0.16

2.3 a'c

It has been previously reported that the **a'** domain is notoriously difficult to characterise through NMR, the addition of the **c**-region stabilised the construct and allowed for a higher yield in purification as well as improved resolution in the NMR spectra with the unstructured **c** region appearing as peaks between 8 and 8.5 ppm, typical for an unstructured region. However **a'c** proved to be very problematic when attempting to calculate its redox potential. The PDI fragment was not reduced enough by 5 mM GSH (as shown in Figure 3.13), so the GSH/GSSG redox couple wouldn't work. Reduced and oxidised DTT was then used, which also proved to have its own difficulties, as it was able to improve the quality of the spectra collected when it was fully reduced (as shown below in Figure 3.14) but oxDTT was unable to oxidise it enough to track any change. Also the data collected showed poor reproducibility and hence errors seen on fitting the data were very high.

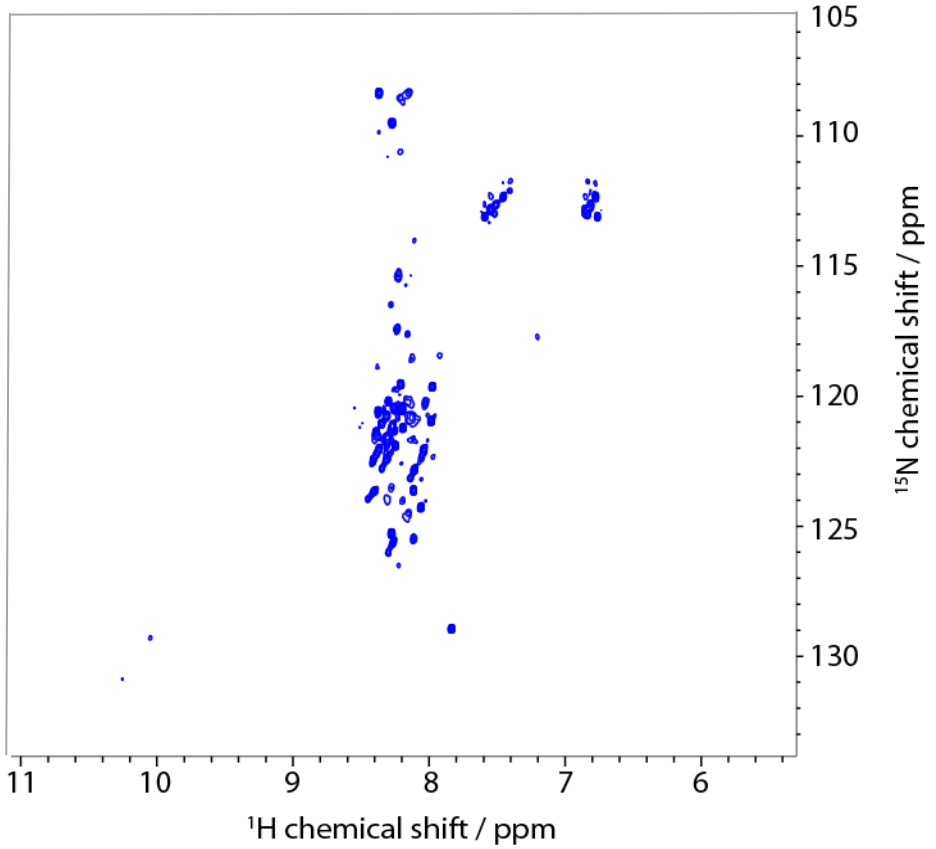

Figure 3.13 NMR ^{15}N HSQC spectra of a'c

NMR ^{15}N HSQC spectra of **a'c** in the partially reduced state with 5 mM GSH.

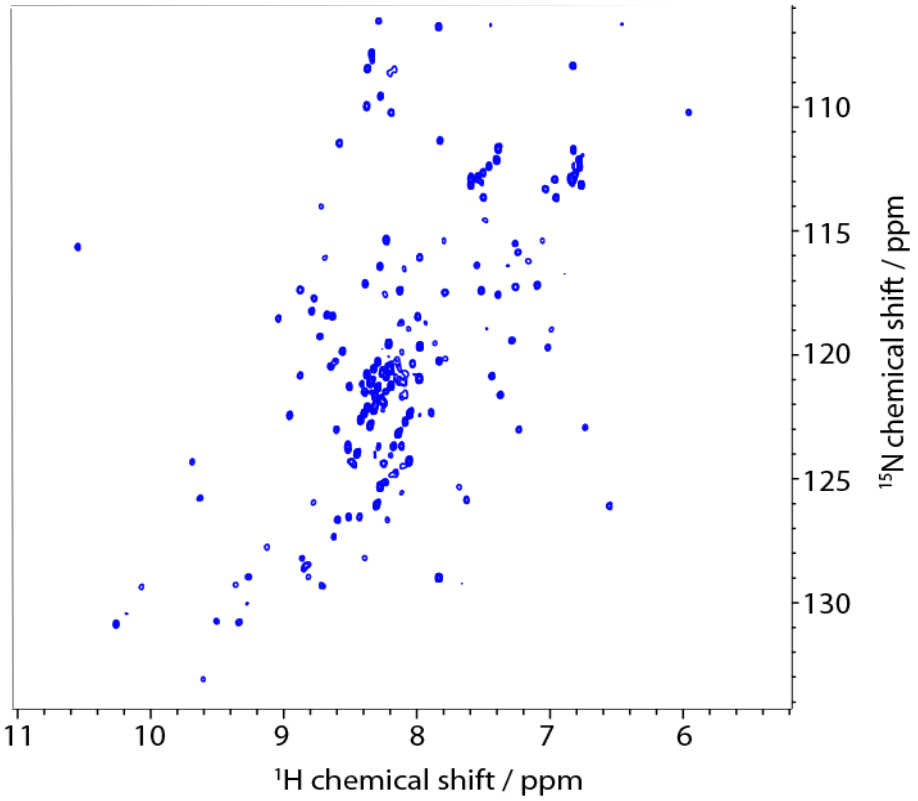

Figure 3.14 NMR ^{15}N HSQC spectra of a'c

NMR ^{15}N HSQC spectra of **a'c** in the fully reduced state with 1.5 mM DTT.

	xa′c	b′xa′c
Number of resonances	5	11
K_{eq} (M)	0.033	0.129
E'_0 (mV)	-196.23 +/- 0.42	-213.71 +/- 0.16

Figure 3.15 K_{eq} and the reduction potentials (E'_0) determined for the PDI fragments xa′c and bxa′c with error margins

3.0 Discussion

Protein disulphide isomerase is a multidomain protein functioning as a redox regulated chaperone protein. It undergoes large redox dependent changes to its conformation to allow it to perform both oxidative folding and reductive unfolding of its protein substrates. As PDI is able to undergo these conformational changes, it is able to bind to an extremely broad range of substrates [61], [101]. The conformational changes hPDI undergoes are essential to the regulation of its chaperone activity. As PDI needs to act as both an oxidase as well as an isomerase protein; the active sites of PDI need to balance in between the redox potentials that are required, so that they can be reduced or oxidised when required [90].

The redox potentials of **xa'c** and **b'xa'c** were found to be -196.23 +/- 0.42 mV and -213.71 +/- 0.16 mV respectively, showing that the redox potential shifts to be more negative when the **b'** domain is added to the **xa'c** fragment. This means that with the addition of the **b'** domain, the fragment becomes a lot more reducing and therefore allowing the fragment to be re-oxidised a lot more easily. This also indicates some form of communication between the **b'** and **a'** domains.

xa'c

xa'c proved to have a stable conformation throughout the NMR experiments, and was predicted to have a redox potential more positive than -240 mV (GSH's redox potential) due to 5 mM of GSH being able to fully reduce the protein. This was proven to be the case as **xa'c** was shown to have a redox potential of -196.23 mV. As it has been previously reported that the **a'** domains redox potential is -169.4 +/- 2.3 mV [90], the addition of the **x** linker and the **c** region not only stabilise the **a'** domain structurally but also reduce its redox potential by 26.83 mV to -196.23 +/- 0.61 mV. K_{eq} for **a** and **a'** domains are 2.6×10^{-3} and 4.4×10^{-3} M

respectively in the full PDI protein [90], whereas on their own they are $7x10^{-4}$ and $1.9x10^{-3}$ M respectively [102], this is in contrast to the equilibrium constant (K_{eq}) of 0.033 M calculated for **xa'c.**

b'xa'c

The redox potential of **b'xa'c** was thought to more negative than **xa'c**, this is due to one of the first results gathered for **b'xa'c**, the 5 mM GSH sample (Figure 3.9). As GSH was unable to fully reduce **b'xa'c** we came to the conclusion that **b'xa'c** must have a lower reduction potential than **xa'c**. This was proven as DTT was able to fully reduce it (Figure 3.10) even though it presented with broad peaks suggesting conformational instability. **b'xa'c** conformational instability could be partly due to the flexibility of the **x** linker, the N-terminal region of the **x** linker has been reported to stabilise the **b'** domain [103], on the other hand the C-terminal region of the **x** linker only loosely binds to the **a'** domain and does not contribute to the stability of **a'** structure. This could account for why **b'xa'c** appears to undergo a lot of conformational change in different redox states [101].

Decrease in redox potential from **xa'c** to **b'xa'c** was a difference of 17.48 mV, meaning the difference in reduction potential can be put down to the addition of the **b'** domain. This means **b'xa'c** is a stronger reductant (redox potential more negative), meaning the fragments isomerase activity would be increased but its oxidase activity would be decreased.

The aggregation that occurred in many of the fully oxidised **b'xa'c** NMR samples could be due to the change in conformation of the fragment making the hydrophobic binding site of **b'** more exposed and therefore resulting in aggregation due to hydrophobic interactions. This was the only PDI fragment used in this work where aggregation was an issue.

Capping of the **b′** domain using an I272A mutant has been used previously to improve conformational stability, however this would affect the redox potential so the wild type was used instead [61].

a′c

The redox potential for **a′c** appeared to be unobtainable, the addition of 5 mM GSH didn't seem to reduce the protein to even the same level as **b′xa′c**, indicating that the reduction potential for **a′c** will be even more reducing than both **xa′c** and **b′xa′c**. This indicates that the addition of the **x** linker has a big effect on **a′c**, even more so than the addition of **b′x.**

b′xa′c had a redox potential of -213.71 mV, this was reaching the limits of what the GSH/GSSG redox couple could achieve, as it can only go down to -240 mV, that's why DTT was used (-332 mV). As DTT was so reducing it had to be used in such small quantities that the bands for error were very high. In hindsight, it would have been better to try and acquire a redox couple with a reduction potential in between DTT and GSH, such as β-mercaptoethanol (-260 mV) or lipoic acid (-288 mV).

It was initially suspected that **a′c** had unfolded due to Figure 3.13 showing no peaks either side of the unstructured **c** region in the presence of 5 mM GSH, but through the addition of 1.5 mM DTT this was shown not to be the case (Figure 3.14). This suggests that **a′c** exhibits conformational exchange when in the oxidised form.

CHAPTER 4

1.0 Ligand Binding

1.1 Introduction

hPDI's ligand binding behaviour, despite being a highly important aspect for the function of the protein and having a long history of research based on this topic, is still not fully understood. This chapter aims to help further clarify the ligand binding behaviour of hPDI using the PDI ligand Δ-somatostatin.

The most recent research in this area by Yagi-Utsumi M., et al. in 2015 [104] has been able to elucidate the three dimensional structure of PDI in thermophilic fungus (*Humicola insolens*) in relation to its ligand binding mode. Through the use of NMR and X-ray crystallography it was shown that the model substrate α-synuclein (αSN) binds to PDI via the hydrophobic αSN segment Val37-Val40 (Val-Leu-Tyr-Val) only in the oxidised form. It was also reported by the same paper that through comparison of the crystal structure of the fragment **b'xa'** with previously reported crystal structures, the **a'** domain partially covers the **b'** binding domain (Figure 4.1), causing steric hindrance fore substrate binding when **b'xa'** is in the reduced state. The αSN contact site largely overlaps with that of the same **b'** surface known to be involved in interactions with Δ-somatostatin [104].

The binding site characterised in the PDI of *Humicola insolens* is located towards the N-terminal of the **b'** domain [104], whereas in hPDI, the **b'** domains binding site is bigger and the residues involved are located across a **b'** β sheet as well as in the C-terminal half of the protein [60], [105].

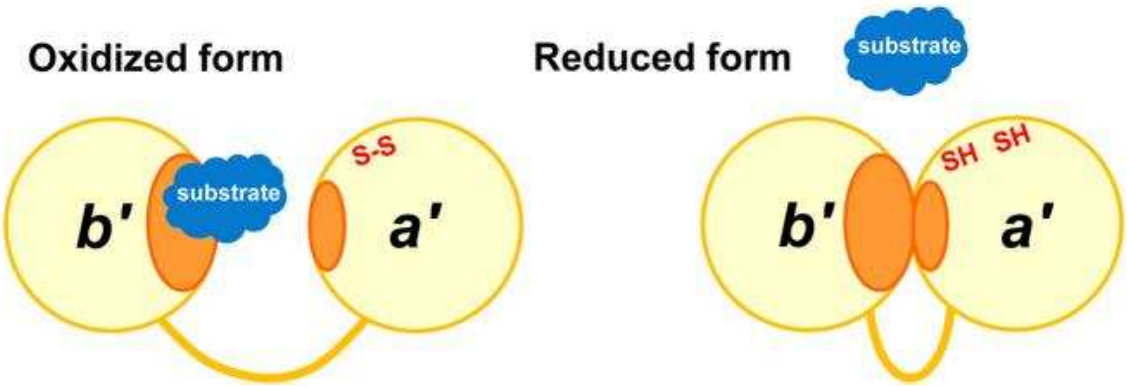

Figure 4.1 Model of redox dependent ligand binding
Substrate shown in blue with hydrophobic domains shown in orange. Showing open conformation of PDI in the oxidised form with the hydrophobic segment of the substrate binding to the hydrophobic domain of **b'**, whereas with the reduction of **a'**, the **b'** and **a'** domains interact forming a closed conformation, leading to release of the substrate with disulphide formation.
Adapted from Yagi-Utsumi M., et al., 2015 [104]

Other research in this area has further characterised the binding behaviour of hPDI via the use of the model ligand Δ-somatostatin, this research was also conducted from both the view of the ligand and the protein [106]. Δ-som does not contain valine or leucine residues, which was part of the key binding segment for αSN to bind to *Humicola insolens* PDI, implying that the fungal PDI has a distinctive substrate recognition mechanism in comparison to hPDI [104], [106].

Richards, K.L., et al., 2015 [106] demonstrated the importance of Δ-som's three phenylalanine residues (mainly Phe11) in the interaction between Δ-som and hPDI. All three phenylalanine residues in Δ-som are involved in its recognition by **b'x** of hPDI, removal of

phenylalanine causes Δ-som not to be recognised by **b'x** whereas removal of one or two of them leads to a much lower binding affinity.

The ligand binding site of hPDI has been extensively mapped through the use of NMR [60], [61], [107], it has also been shown that the **b'** binding domain is capable of binding to peptides in the size range of 10 to 15 residues long independently of disulphide bonds but through hydrophobic interactions [103], and that the binding of larger peptides and non-native proteins however requires additional binding contributions from both the **a** and **a'** domains [108].

Previous studies have shown that GB1 fusion proteins can be directly used in NMR studies involving lipids such as micelles, bicelles or liposomes, as GB1 on its own does not significantly interact with the lipids, so any chemical shift seen with the GB1 fusion protein can be attributed to the fusion [109]. In this chapter ligand binding behaviour of hPDI is further characterised from the view of the ligand Δ-somatostatin. GB1 is also investigated to determine whether it interacts with **b'xa'c** to determine whether GB1 fused to Δ-som can be used in future ligand binding experiments or whether the ligand has to be cleaved off GB1 first. This means that the cleaving of GB1 from the ligand is potentially unnecessary and can be avoided. Additionally the cleavage is not always complete or could even lead to the digest of the target ligand itself. Also another purification step would be required to remove the cleaved GB1 from the sample leading to a smaller overall yield as some ligand will be lost with each purification step. This extra purification step is not only time consuming but also costly.

To achieve this, ^{15}N labelled GB1-Δ-som as well as unlabelled **b'xa'c,** were expressed and purified. Bonding of **b'xa'c** to GB1-Δ-som was analysed on both reducing and oxidising conditions. Peak shifts in $^{15}N/^{1}H$ HSQC spectra were identified and measured. This method has been extensively documented to determine chemical shift perturbations via NMR [110], [111]. A control of GB1 without fusion was also used to see if there was any interaction between GB1 alone and **b'xa'c**.

1.2 GB1-Δ-somatostatin

Expressing Δ-somatostatin (structure shown in Figure 4.2) on its own in *E. coli* would lead to high levels of degradation. Therefore the fusion protein GB1 was employed to prevent this. This fusion protein is the B1 domain of the *Streptococcus* protein (GB1). It folds into a 3D structure and is fused to Δ-som to increase expression yield and stability [112].

The GB1-Δ-som fusion has a His-tag at its N-terminus to enable purification via nickel affinity chromatography, and although it has been reported to lower the expression by some [113], it has also been reported to increase protein yield and purity [84], [113],

as well as enhancing the peptide stability six fold [84].

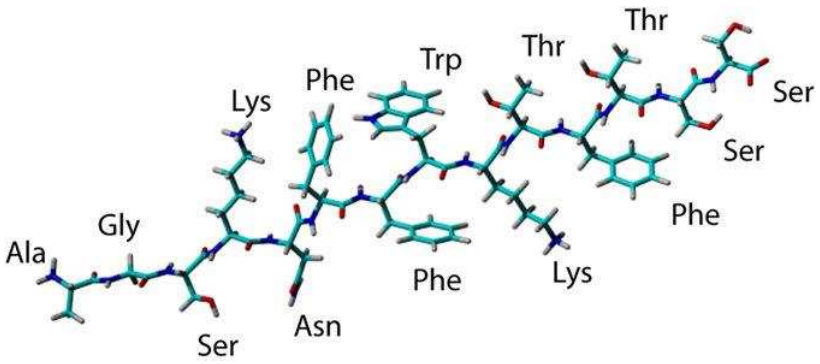

Figure 4.2 Stick model of Δ-somatostatin showing all amino acids
Adapted from Richards K.L., et al., 2015 [106].

2.0 Results

GB1 and GB1-Δ-som were compared directly by the chemical shifts of GB1 being measured. Both GB1 and GB1-Δ-som have their chemical shifts measured in the presence of **b'xa'c** in either the fully reduced (with 1.5 mM DTT) or fully oxidised (with 5 mM GSSG) states. **b'xa'c** without reductant or oxidant is used as a control. GB1, GB1-Δ-som and **b'xa'c** were all at 0.15 mM.

This is to show how the fusion of Δ-som to GB1 affects GB1's conformation, as well as whether GB1 interacts with **b'xa'c** to see if GB1-Δ-som can be used in future experiments to avoid the purification step of the cleavage of Δ-som from GB1 as this would speed up the purification process as well as allowing for a higher yield of Δ-som as the final product.

Minimal chemical shift mapping was used to measure the chemical shift change of the $^{15}N/^{1}H$ backbone amide peak seen in the HSQC spectra for GB1 on the addition of the fusion sequence, or for GB1 and GB1-Δ-som in the presence of **b'xa'c**. The spectral width of the ^{15}N dimension for the amide cross-peaks was 8 times larger than that in the ^{1}H dimensions, so the chemical shift change in the ^{15}N dimension was divided by 8 to ensure equal weighting in the ^{1}H and ^{15}N dimensions. In minimal chemical shift mapping, the chemical shift change to the nearest peak is measured [105]. This method avoids the need to assign the peaks in the second spectrum and gives a minimum value for the magnitude of the chemical change assuming that all peaks are still present in the spectrum.

There was not enough time to run ^{15}N edited TOCSY experiments to unambiguously assign GB1 as well as the new cross-peaks in GB1-Δ-som. Assignments for GB1 were made from previous data that was found to be in good agreement to our own (Serber, Z., et al., 2006

[114] and Sun, Z.Y., et al., 2005 [115]). The backbone amide cross-peaks for Δ-som were labelled as P1 – P20 as shown in Figure 4.3 B. The identity of these peaks to residue number was unknown.

2.1 GB1 and GB1-Δ-somatostatin

The assigned HSQC spectrum for GB1 is shown in Figure 4.3 A, and this spectrum is shown overlaid with an HSQC spectrum for GB1-Δ-som in Figure 4.3 B. Chemical shift changes were measured for all GB1 cross-peaks, and this chemical shift change across the sequence of the protein is shown in Figure 4.3 C. Residues 8 – 12 and 40 – 44 and 56 of GB1 showed large shifts, with residue 56 (the C-terminal residue) shifting the most due to it no longer being at the C-terminal residue in the Δ-som fusion protein.

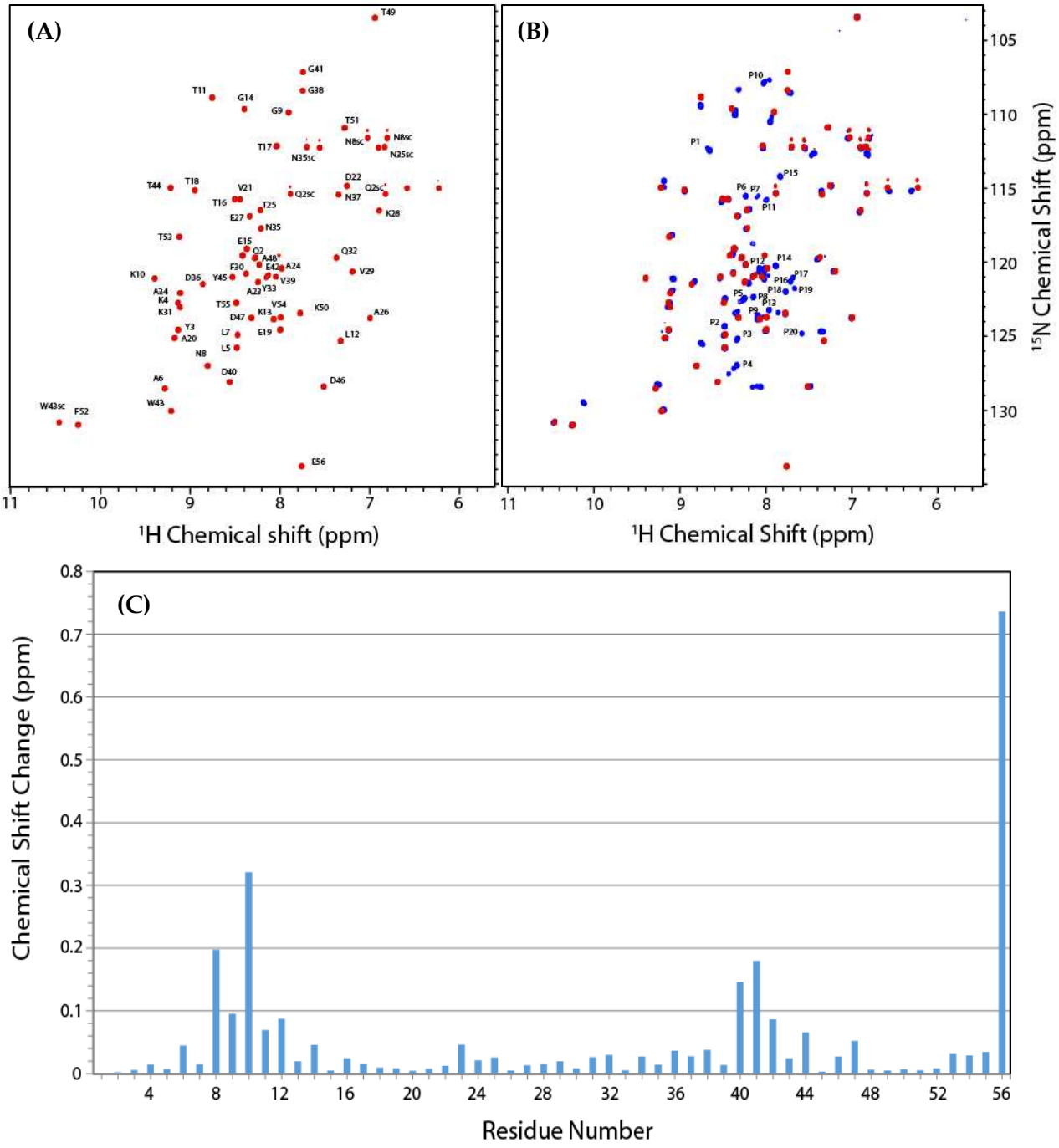

Figure 4.3 HSQC spectra and chemical shift map of GB1 and GB1-Δ-somatostatin.
(A) Assigned HSQC of GB1, **(B)** GB1 HSQC with GB1-Δ-som HSQC overlaid in blue, with Δ-som cross-peaks marked as P1, P2 etc. **(C)** chemical shift map showing the chemical shifts that occur upon fusion of the Δ-som sequence to the C-terminus.

2.2 GB1 and GB1-Δ-somatostatin with b′xa′c

Chemical shift changes seen for GB1 in the absence and presence of **b′xa′c** are shown in Figure 4.5 A. Only very minor shift changes were seen suggesting little or no interaction. An almost identical result was obtained when reduced **b′xa′c** was added to GB1 (Figure 4.5 C). Chemical shift changes of greater magnitude are seen when **b′xa′c** is added to GB1-Δ-som (Figure 4.5 B), both within the GB1 and the Δ-som part of the fusion. The spectra for GB1-Δ-som and GB1-Δ-som with **b′xa′c** is given in Figure 4.4 as an example (spectra for chemical shift map Figure 4.5 B). In addition to peaks shifting, 8 of the Δ-som peaks were seen to disappear (P7, P8, P9, P11, P15, P16, P18 and P19). A very similar result was seen when reduced **b′xa′c** was added to GB1-Δ-som (Figure 4.5 D), although in this experiment, E56 was seen to shift considerably less as judged by the closest peak mapping technique.

Much larger chemical shifts for GB1 and GB1-Δ-som were seen when oxidised **b′xa′c** was added (Figure 4.5 E and F respectively). Interestingly, larger chemical shifts were seen for the GB1 portion on the fusion compared to the Δ-som section (Figure 4.5 F), however, this could be a consequence of the nearest peak analysis which will tend to underestimate changes in the crowded central region of the spectrum where the majority of the unstructured Δ-som peak were seen (Figure 4.3 B). A different pattern of behaviours (peaks shifting and disappearing) is seen when oxidised **b′xa′c** is compared to "as purified" or reduced **b′xa′c** (compare Figure 4.5 panels B and D with panel F). This finding suggests a potential difference in the **b′xa′c** interaction when the oxidation state of the **a′** domain is changed.

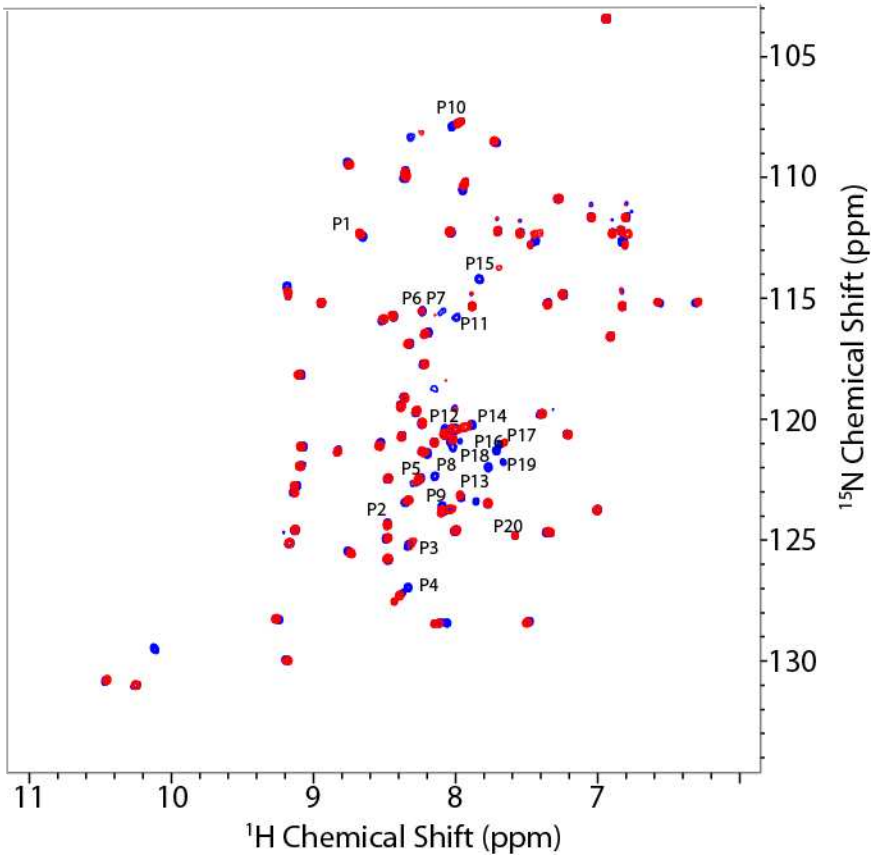

Figure 4.4 GB1-Δ-som HSQC in blue, and GB1-Δ-som with **b'xa'c** HSQC overlaid in red. Δ-som labelled as P1 – P20

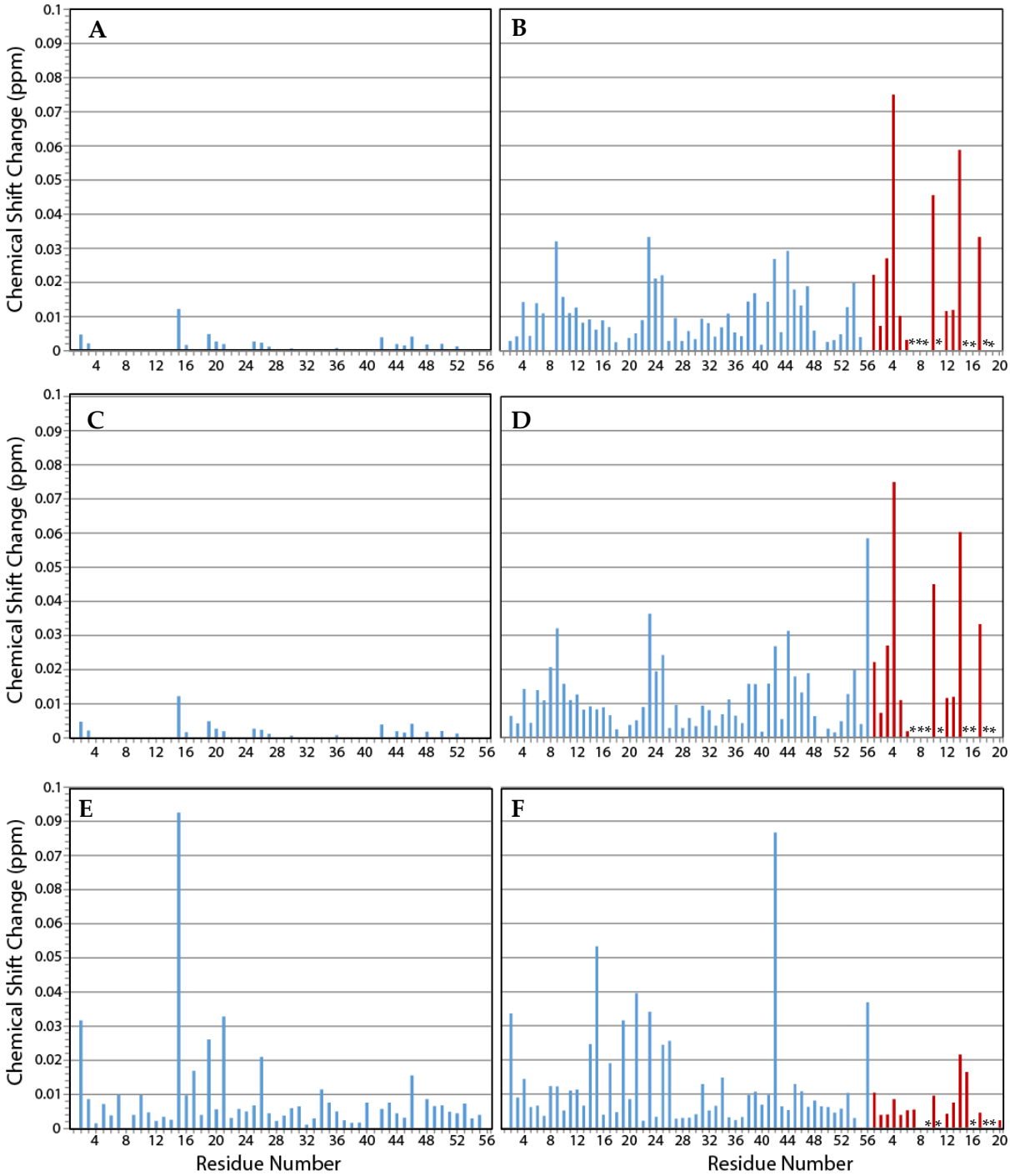

Figure 4.5 Chemical shift maps of GB1 (A, C, E) and GB1-Δ-somatostatin (B, D, F)
Blue bars show the residues of GB1 (1-56) and the red bars show the residues for Δ-som (1-20) Asterisks indicate residues whose peaks have become undetectable due to line broadening upon addition of **b'xa'c**. **(A)** shows GB1 chemical shift changes that occur upon addition of **b'xa'c** without reductant or oxidant, and **(B)** shows the same but with GB1-Δ-som instead of GB1. **(C)** shows GB1 chemical shift changes that occur when reduced **b'xa'c** (1.5 mM DTT) is added and **(D)** shows the same but with GB1-Δ-som. **(E)** shows GB1 chemical shift changes that arise when oxidised **b'xa'c** (5 mM GSSG) is added to GB1 and **(F)** shows the same but with GB1-Δ-som. Chemical shift changes were measured to the nearest peak.

3.0 Discussion

3.1 GB1 and GB1-Δ-somatostatin

GB1 presented with chemical shifts spread throughout its structure (Figure 4.3 C). The residues localised at the C-terminus shifted the most as shown in Figure 4.6, this was because of the close proximity of the fusion sequence. There is only a small possibility that the fusion binds to GB1, as there would be much bigger chemical shifts if this had been the case. Residue E56 shifted the most (Figure 4.3 C) due to the fusion; this was because E56 was no longer the C-terminus, which had a large effect on its environment.

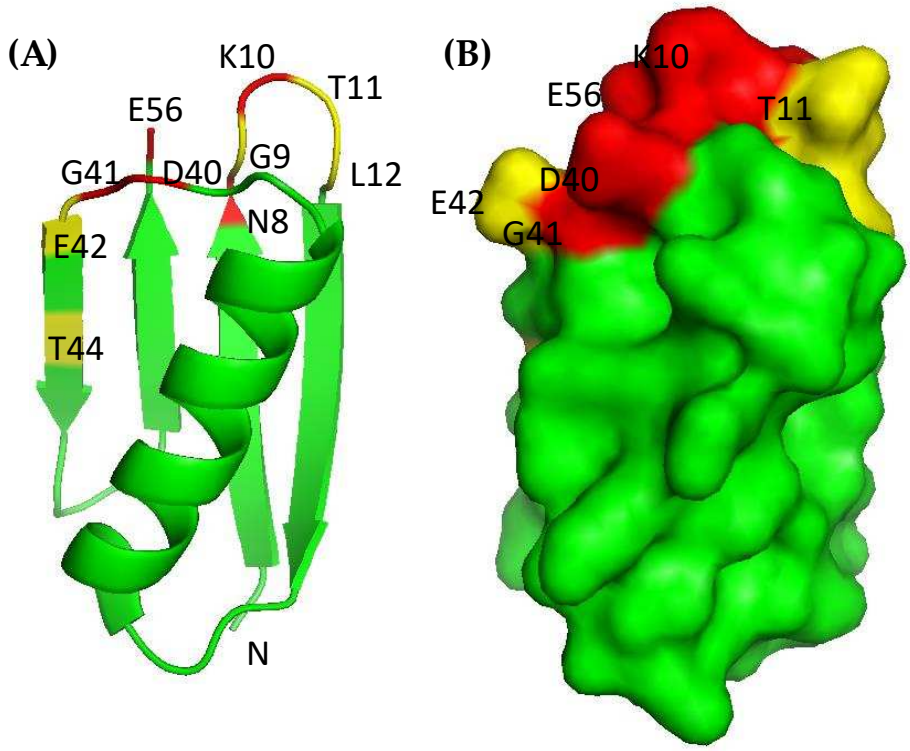

Figure 4.6 (A) GB1 (pdb structure 2QMT) shown as a backbone cartoon and **(B)** as a surface representation with sidechains in the same orientation and scale. Residues with $^{15}N/^{1}H$ backbone amide resonances found not to shift on addition of the C-terminal Δ-som fusion sequence are shown in green, those with a chemical shift change >0.06 but <0.12 ppm are shown in yellow, whereas those with a chemical shift change >0.12 ppm are shown in red. Chemical shift perturbation is seen to be localised and at the end of the molecule including the C-terminal residue (E56) as well as the loops between β-strands 1 and 2, and α-helix 1 and β-strand 3.

3.2 GB1 and GB1-Δ-somatostatin with b′xa′c

As the chemical shift changes seen for GB1 with "as purified" **b′xa′c** and reduced **b′xa′c** are so similar (Figure 4.5 A and C), but different from the result with oxidised **b′xa′c** (Figure 4.5 E), it suggests that **b′xa′c** is purified largely in the reduced form. The same pattern can be seen for GB1-Δ-som with "as purified" and reduced **b′xa′c** (Figure 4.5 B and D) compared to oxidised **b′xa′c** (Figure 4.5 E).

It should be noted that the maximum value on the y axis scale in Figure 4.3 C is 0.8 whereas the y axis of Figure 4.5 A – F it is 0.1, this shows that there are much greater chemical shifts in GB1 when Δ-som is fused to it than when GB1 and GB1-Δ-som interact with **b′xa′c**.

As the chemical shift perturbations are so small in GB1 with reduced **b′xa′c** (Figure 4.5 C), we can conclude that GB1 does not significantly interact with **b′xa′c** when it is in the reduced form and in the presence of a reductant (1.5 mM DTT), the same can be said for when GB1 and **b′xa′c** are not in the presence of a reductant (Figure 4.5 A). This suggests that the chemical shift perturbations seen for GB1-Δ-som in the presence of reduced **b′xa′c** can be attributed to the Δ-som sequence. This includes those changes in the GB1 portion of the fusion as well as those in the Δ-som sequence.

GB1 in the presence of oxidised **b′xa′c** (5 mM GSSG) (Figure 4.5 E) showed a lot more chemical shift changes in comparison to reduced **b′xa′c** (Figure 4.5 C), especially in residues Q2, E15, E19 and V21. These residues however are not hydrophobic, and so are unlikely to interact with the hydrophobic binding site on the **b′** domain. This suggests that the oxidised environment is having an effect on the GB1 spectrum or that oxidised **b′xa′c** may interact directly with GB1, however this is very unlikely as the residues that

shift are not hydrophobic and PDI has a very low affinity for folded proteins. Therefore it's most likely that the shifts are just artefactual. Unfortunately a spectrum of GB1 was not collected in the presence of 5 mM GSSG alone which would have determined whether the chemical shift changes seen in Figure 4.5 E are due directly to the presence of GSSG. In comparison to the chemical shift changes shown in Figure 4.3 C these are relatively small, but when comparing these chemical shifts to GB1-Δ-som (Figures 4.5 B, D and F) the shifts are significant; the chemical shifts can't be attributed to the addition of Δ-som.

The Δ-som peaks that disappeared in Figures 4.5 B, D and F indicate significant interactions between Δ-som and **b'xa'c**. Therefore we're able to conclude that Δ-som does interact with **b'xa'c**.

Δ-som is thought to interact largely via its hydrophobic residues, phenylalanine and tryptophan, as previous studies have reported these residues to be important for binding [106]. This suggests that four of the disappeared residues in Δ-som (see Figures 4.5 B, D and F) are most likely the three phenylalanines and tryptophan residue.

Future Work

1.0 Protein expression and purification

Purification process for PDI fragments is a well-documented protocol and has been optimised fully; however nickel affinity chromatography purification of GB1 and GB1-Δ-som is still to be fully optimised. The concentration of imidazole in the wash buffer could be used to see if some of the lower and higher MW bands on the SDS-PAGE analysis become fainter or disappear. SDS-PAGE analysis of **xa′c** and **a′c** carried out on a non-reducing gel to elucidate if the two peaks from ion exchange chromatography are reduced and non-reduced.

2.0 Redox potential

The redox potential of **a′c** still needs to be calculated. This would most likely be achieved using a different redox couple other than glutathione or DTT. The redox couples of β-mercaptoethanol (-260 mV) or lipoic acid (-288 mV) are possible alternatives.

3.0 Ligand binding

Confirm backbone assignments for GB1 using a ^{15}N TOCSY experiment to help verify sidechain type. Fully assign the HSQC spectrum for GB1-Δ-som using ^{15}N edited TOCSY and NOESY experiments to make sequential assignments. This work would allow the chemical shift changes seen in the Δ-som sequence of the fusion protein to be identified to a particular residue.

It would also be good to determine whether it was oxidised **b′xa′c** affecting GB1 or the oxidising environment itself. To achieve this GB1 would be placed in an oxidising environment without **b′xa′c** or Δ-som and its chemical shift change measured.

Other work could elucidate the Kd value of GB1-Δ-som to reduced or oxidised **b′xa′c**. A titration experiment using a range of **b′xa′c** concentrations would be used for this.

Appendix

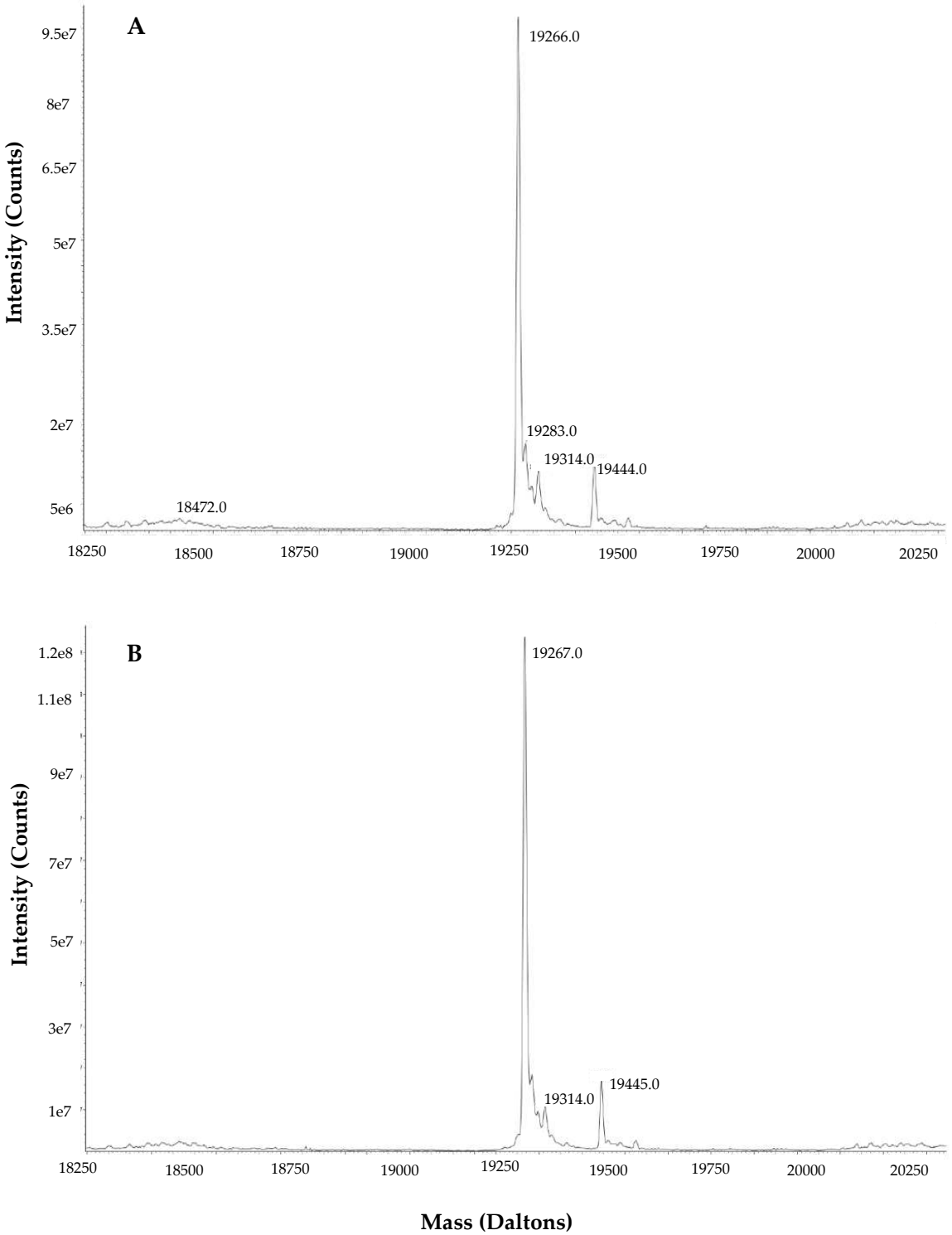

Figure 1 Mass spectrometry data for xa'c in both the (A) non-reduced and (B) reduced forms

The molecular weight of **xa'c** in daltons, in its reduced form is 19267 Da and in its non-reduced form is 19266 Da. Four additional peaks are shown for the non-reduced and two for the reduced.

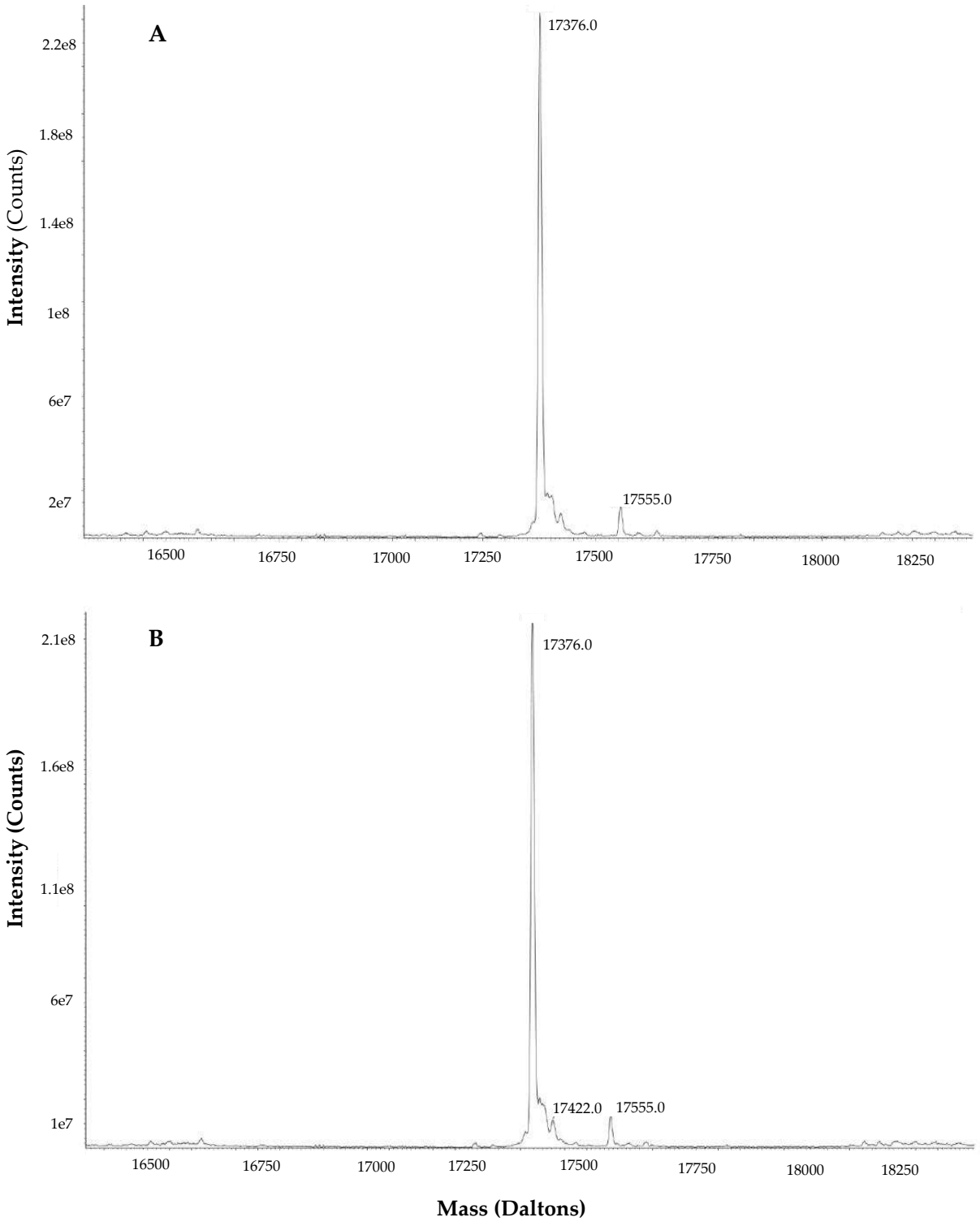

Figure 2 Mass spectrometry data for a'c in (A) non-reduced and (B) reduced forms
The molecular weight of **a'c** in daltons, in its reduced form is 17376 Da and in its non-reduced form is 17376 Da. Two additional peaks are shown for the non-reduced and one for the reduced.

References

[1] R. Sitia and I. Braakman, "Quality control in the endoplasmic reticulum protein factory," *Nature*, vol. 426, no. 6968, pp. 891–894, Dec. 2003.

[2] C. B. Anfinsen, "Principles that Govern the Folding of Protein Chains," *Science (80-.).*, vol. 181, no. 4096, pp. 223–230, 1973.

[3] J. Kemmink, N. J. Darby, K. Dijkstra, R. M. Scheek, and T. E. Creighton, "Nuclear magnetic resonance characterization of the N-terminal thioredoxin-like domain of protein disulfide isomerase.," *Protein Sci.*, vol. 4, no. 12, pp. 2587–93, Dec. 1995.

[4] N. Marcus, D. Shaffer, P. Farrar, and M. Green, "Tissue distribution of three members of the murine protein disulfide isomerase (PDI) family.," *Biochim. Biophys. Acta*, vol. 1309, no. 3, pp. 253–60, Dec. 1996.

[5] P. Venetianer and F. B. Straub, "The enzymic reactivation of reduced ribonuclease.," *Biochim. Biophys. Acta*, vol. 67, pp. 166–8, Jan. 1963.

[6] R. F. Goldberger, C. J. Epstein, and C. B. Anfinsen, "Acceleration of reactivation of reduced bovine pancreatic ribonuclease by a microsomal system from rat liver.," *J. Biol. Chem.*, vol. 238, pp. 628–35, Feb. 1963.

[7] M. van Lith, A.-R. Karala, D. Bown, J. A. Gatehouse, L. W. Ruddock, P. T. K. Saunders, and A. M. Benham, "A developmentally regulated chaperone complex for the endoplasmic reticulum of male haploid germ cells.," *Mol. Biol. Cell*, vol. 18, no. 8, pp. 2795–804, Aug. 2007.

[8] S. Persson, M. Rosenquist, B. Knoblach, R. Khosravi-Far, M. Sommarin, and M. Michalak, "Diversity of the protein disulfide isomerase family: identification of breast tumor induced Hag2 and Hag3 as novel members of the protein family.," *Mol. Phylogenet. Evol.*, vol. 36, no. 3, pp. 734–40, Sep. 2005.

[9] H. I. Alanen, R. A. Williamson, M. J. Howard, F. S. Hatahet, K. E. H. Salo, A. Kauppila, S. Kellokumpu, and L. W. Ruddock, "ERp27, a new non-catalytic endoplasmic reticulum-located human protein disulfide isomerase family member, interacts with ERp57.," *J. Biol. Chem.*, vol. 281, no. 44, pp. 33727–38, Nov. 2006.

[10] K. Vuori, T. Pihlajaniemi, M. Marttila, and K. I. Kivirikko, "Characterization of the human prolyl 4-hydroxylase tetramer and its multifunctional protein disulfide-isomerase subunit synthesized in a baculovirus expression system.," *Proc. Natl. Acad. Sci. U. S. A.*, vol. 89, no. 16, pp. 7467–70, Aug. 1992.

[11] D. C. John, M. E. Grant, and N. J. Bulleid, "Cell-free synthesis and assembly of prolyl 4-hydroxylase: the role of the beta-subunit (PDI) in preventing misfolding and aggregation of the alpha-subunit.," *EMBO J.*, vol. 12, no. 4, pp. 1587–95, Apr. 1993.

[12] J. R. Wetterau, K. A. Combs, S. N. Spinner, and B. J. Joiner, "Protein disulfide isomerase is a component of the microsomal triglyceride transfer protein complex.," *J. Biol. Chem.*, vol. 265, no. 17, pp. 9800–7, Jun. 1990.

[13] R. Wilson, "Protein disulfide Isomerase Acts as a Molecular Chaperone during the Assembly of Procollagen," *J. Biol. Chem.*, vol. 273, no. 16, pp. 9637–9643, Apr. 1998.

[14] J. Koivu, R. Myllylä, T. Helaakoski, T. Pihlajaniemi, K. Tasanen, and K. I. Kivirikko, "A single polypeptide acts both as the beta subunit of prolyl 4-hydroxylase and as a protein disulfide-isomerase.," *J. Biol. Chem.*, vol. 262, no. 14, pp. 6447–9, May 1987.

[15] J. Wahlman, G. N. DeMartino, W. R. Skach, N. J. Bulleid, J. L. Brodsky, and A. E. Johnson, "Real-time fluorescence detection of ERAD substrate retrotranslocation in a mammalian in vitro system.," *Cell*, vol. 129, no. 5, pp. 943–55, Jun. 2007.

[16] S. Lee, B. Park, K. Kang, and K. Ahn, "Redox-regulated export of the major histocompatibility complex class I-peptide complexes from the endoplasmic reticulum.," *Mol. Biol. Cell*, vol. 20, no. 14, pp. 3285–94, Jul. 2009.

[17] X.-M. Fu, P. Wang, and B. T. Zhu, "Characterization of the estradiol-binding site structure of human protein disulfide isomerase (PDI).," *PLoS One*, vol. 6, no. 11, p. e27185, Jan. 2011.

[18] J. D. Malhotra and R. J. Kaufman, "The endoplasmic reticulum and the unfolded protein response.," *Semin. Cell Dev. Biol.*, vol. 18, no. 6, pp. 716–31, Dec. 2007.

[19] S. Akagi, A. Yamamoto, T. Yoshimori, R. Masaki, R. Ogawa, and Y. Tashiro, "Localization of protein disulfide isomerase on plasma membranes of rat exocrine pancreatic cells.," *J. Histochem. Cytochem.*, vol. 36, no. 8, pp. 1069–74, Aug. 1988.

[20] E. Fenouillet, R. Barbouche, J. Courageot, and R. Miquelis, "The catalytic activity of protein disulfide isomerase is involved in human immunodeficiency virus envelope-mediated membrane fusion after CD4 cell binding.," *J. Infect. Dis.*, vol. 183, no. 5, pp. 744–52, Mar. 2001.

[21] R. Barbouche, R. Miquelis, I. M. Jones, and E. Fenouillet, "Protein-disulfide isomerase-mediated reduction of two disulfide bonds of HIV envelope glycoprotein 120 occurs post-CXCR4 binding and is required for fusion.," *J. Biol. Chem.*, vol. 278, no. 5, pp. 3131–6, Jan. 2003.

[22] D. W. Essex and M. Li, "Protein disulphide isomerase mediates platelet aggregation and secretion.," *Br. J. Haematol.*, vol. 104, no. 3, pp. 448–54, Mar. 1999.

[23] V. R. Wiersma, M. Michalak, T. M. Abdullah, E. Bremer, and P. Eggleton, "Mechanisms of Translocation of ER Chaperones to the Cell Surface and Immunomodulatory Roles in Cancer and Autoimmunity.," *Front. Oncol.*, vol. 5, p. 7, 2015.

[24] Y. Chen, Y. Zhang, Y. Yin, G. Gao, S. Li, Y. Jiang, X. Gu, and J. Luo, "SPD--a web-based secreted protein database.," *Nucleic Acids Res.*, vol. 33, no. Database issue, pp. D169–73, Jan. 2005.

[25] R. B. Freedman, T. R. Hirst, and M. F. Tuite, "Protein disulphide isomerase: building bridges in protein folding.," *Trends Biochem. Sci.*, vol. 19, no. 8, pp. 331–6, Aug. 1994.

[26] J. Kemmink, N. J. Darby, K. Dijkstra, M. Nilges, and T. E. Creighton, "The folding catalyst protein disulfide isomerase is constructed of active and inactive thioredoxin modules.," *Curr. Biol.*, vol. 7, no. 4, pp. 239–45, Apr. 1997.

[27] H. I. Alanen, K. E. H. Salo, M. Pekkala, H. M. Siekkinen, A. Pirneskoski, and L. W. Ruddock, "Defining the domain boundaries of the human protein disulfide isomerases.," *Antioxid. Redox Signal.*, vol. 5, no. 4, pp. 367–74, Aug. 2003.

[28] R. B. Freedman, P. J. Gane, H. C. Hawkins, R. Hlodan, S. H. McLaughlin, and J. W. Parry, "Experimental and theoretical analyses of the domain architecture of mammalian protein disulphide-isomerase.," *Biol. Chem.*, vol. 379, no. 3, pp. 321–8, Mar. 1998.

[29] G. Tian, S. Xiang, R. Noiva, W. J. Lennarz, and H. Schindelin, "The Crystal Structure of Yeast Protein Disulfide Isomerase Suggests Cooperativity between Its Active Sites," *Cell*, vol. 124, no. 1, pp. 61–73, Jan. 2006.

[30] C. Wang, W. Li, J. Ren, J. Fang, H. Ke, W. Gong, W. Feng, and C.-C. Wang, "Structural insights into the redox-regulated dynamic conformations of human protein disulfide isomerase.," *Antioxid. Redox Signal.*, vol. 19, no. 1, pp. 36–45, Jul. 2013.

[31] C. Wang, J. Yu, L. Huo, L. Wang, W. Feng, and C. Wang, "Human protein-disulfide isomerase is a redox-regulated chaperone activated by oxidation of domain a'.," *J. Biol. Chem.*, vol. 287, no. 2, pp. 1139–49, Jan. 2012.

[32] P. Klappa, L. W. Ruddock, N. J. Darby, and R. B. Freedman, "The b' domain provides the principal peptide-binding site of protein disulfide isomerase but all domains contribute to binding of misfolded proteins.," *EMBO J.*, vol. 17, no. 4, pp. 927–35, Feb. 1998.

[33] L. Wang, L. Wang, S. Vavassori, S. Li, H. Ke, T. Anelli, M. Degano, R. Ronzoni, R. Sitia, F. Sun, and C.-C. Wang, "Crystal structure of human ERp44 shows a dynamic functional modulation by its carboxy-terminal tail.," *EMBO Rep.*, vol. 9, no. 7, pp. 642–7, Jul. 2008.

[34] F.-X. Kober, W. Koelmel, J. Kuper, J. Drechsler, C. Mais, H. M. Hermanns, and H. Schindelin, "The crystal structure of the protein-disulfide isomerase family member ERp27 provides insights into its substrate binding capabilities.," *J. Biol. Chem.*, vol. 288, no. 3, pp. 2029–39, Jan. 2013.

[35] G. Kozlov, P. Määttänen, D. Y. Thomas, and K. Gehring, "A structural overview of the PDI family of proteins.," *FEBS J.*, vol. 277, no. 19, pp. 3924–36, Oct. 2010.

[36] C. I. Andreu, U. Woehlbier, M. Torres, and C. Hetz, "Protein disulfide isomerases in neurodegeneration: From disease mechanisms to biomedical applications," *FEBS Lett.*, vol. 586, no. 18, pp. 2826–2834, 2012.

[37] B. Wilkinson and H. F. Gilbert, "Protein disulfide isomerase," *Biochim. Biophys. Acta - Proteins Proteomics*, vol. 1699, no. 1, pp. 35–44, 2004.

[38] D. M. Ferrari and H.-D. So= Ling, "The protein disulphide-isomerase family : unravelling a string of folds," *Biochem. J*, vol. 339, pp. 1–10, 1999.

[39] K. Araki and K. Nagata, "Functional in vitro analysis of the ERO1 protein and protein-disulfide isomerase pathway.," *J. Biol. Chem.*, vol. 286, no. 37, pp. 32705–12, Sep. 2011.

[40] K. Araki, S. Iemura, Y. Kamiya, D. Ron, K. Kato, T. Natsume, and K. Nagata, "Ero1-α and PDIs constitute a hierarchical electron transfer network of endoplasmic reticulum oxidoreductases.," *J. Cell Biol.*, vol. 202, no. 6, pp. 861–74, Sep. 2013.

[41] A. K. Lappi, M. F. Lensink, H. I. Alanen, K. E. H. Salo, M. Lobell, A. H. Juffer, and L. W. Ruddock, "A conserved arginine plays a role in the catalytic cycle of the protein disulphide isomerases.," *J. Mol. Biol.*, vol. 335, no. 1, pp. 283–95, Jan. 2004.

[42] A.-R. Karala, A.-K. Lappi, and L. W. Ruddock, "Modulation of an Active-Site Cysteine pKa Allows PDI to Act as a Catalyst of both Disulfide Bond Formation and Isomerization," *J. Mol. Biol.*, vol. 396, no. 4, pp. 883–892, 2010.

[43] L. W. Ruddock, "Low-molecular-weight oxidants involved in disulfide bond formation.," *Antioxid. Redox Signal.*, vol. 16, no. 10, pp. 1129–38, May 2012.

[44] T. J. Tavender and N. J. Bulleid, "Molecular mechanisms regulating oxidative activity of the Ero1 family in the endoplasmic reticulum.," *Antioxid. Redox Signal.*, vol. 13, no. 8, pp. 1177–87, Oct. 2010.

[45] M. Pagani, M. Fabbri, C. Benedetti, A. Fassio, S. Pilati, N. J. Bulleid, A. Cabibbo, and R. Sitia, "Endoplasmic reticulum oxidoreductin 1-lbeta (ERO1-Lbeta), a human gene induced in the course of the unfolded protein response.," *J. Biol. Chem.*, vol. 275, no. 31, pp. 23685–92, Aug. 2000.

[46] S. Masui, S. Vavassori, C. Fagioli, R. Sitia, and K. Inaba, "Molecular bases of cyclic and specific disulfide interchange between human ERO1alpha protein and protein-disulfide isomerase (PDI).," *J. Biol. Chem.*, vol. 286, no. 18, pp. 16261–71, May 2011.

[47] V. D. Nguyen, M. J. Saaranen, A.-R. Karala, A.-K. Lappi, L. Wang, I. B. Raykhel, H. I. Alanen, K. E. H. Salo, C. Wang, and L. W. Ruddock, "Two Endoplasmic Reticulum PDI Peroxidases Increase the Efficiency of the Use of Peroxide during Disulfide Bond Formation," *J. Mol. Biol.*, vol. 406, no. 3, pp. 503–515, 2011.

[48] L. Wang, L. Zhu, and C. Wang, "The endoplasmic reticulum sulfhydryl oxidase Ero1β drives efficient oxidative protein folding with loose regulation.," *Biochem. J.*, vol. 434, no. 1, pp. 113–21, Feb. 2011.

[49] L. Wang, L. Zhang, Y. Niu, R. Sitia, and C.-C. Wang, "Glutathione peroxidase 7 utilizes hydrogen peroxide generated by Ero1α to promote oxidative protein folding.," *Antioxid. Redox Signal.*, vol. 20, no. 4, pp. 545–56, Feb. 2014.

[50] T. Kakihana, K. Araki, S. Vavassori, S. Iemura, M. Cortini, C. Fagioli, T. Natsume, R. Sitia, and K. Nagata, "Dynamic regulation of Ero1α and peroxiredoxin 4 localization

in the secretory pathway.," *J. Biol. Chem.*, vol. 288, no. 41, pp. 29586–94, Oct. 2013.

[51] C. C. Wang and C. L. Tsou, "Protein disulfide isomerase is both an enzyme and a chaperone.," *FASEB J.*, vol. 7, no. 15, pp. 1515–7, Dec. 1993.

[52] H. Quan, G. Fan, and C. C. Wang, "Independence of the chaperone activity of protein disulfide isomerase from its thioredoxin-like active site.," *J. Biol. Chem.*, vol. 270, no. 29, pp. 17078–80, Jul. 1995.

[53] Y. Yao, Y. Zhou, and C. Wang, "Both the isomerase and chaperone activities of protein disulfide isomerase are required for the reactivation of reduced and denatured acidic phospholipase A2.," *EMBO J.*, vol. 16, no. 3, pp. 651–8, Feb. 1997.

[54] J. L. Song and C. C. Wang, "Chaperone-like activity of protein disulfide-isomerase in the refolding of rhodanese.," *Eur. J. Biochem.*, vol. 231, no. 2, pp. 312–6, Jul. 1995.

[55] H. Cai, C. C. Wang, and C. L. Tsou, "Chaperone-like activity of protein disulfide isomerase in the refolding of a protein with no disulfide bonds.," *J. Biol. Chem.*, vol. 269, no. 40, pp. 24550–2, Oct. 1994.

[56] P. Klappa, R. B. Freedman, and R. Zimmermann, "Protein disulphide isomerase and a lumenal cyclophilin-type peptidyl prolyl cis-trans isomerase are in transient contact with secretory proteins during late stages of translocation.," *Eur. J. Biochem.*, vol. 232, no. 3, pp. 755–64, Sep. 1995.

[57] J. D. Oliver, F. J. van der Wal, N. J. Bulleid, and S. High, "Interaction of the thiol-dependent reductase ERp57 with nascent glycoproteins.," *Science*, vol. 275, no. 5296, pp. 86–8, Jan. 1997.

[58] X. X. Sun, Y. Dai, H. P. Liu, S. M. Chen, and C. C. Wang, "Contributions of protein disulfide isomerase domains to its chaperone activity.," *Biochim. Biophys. Acta*, vol. 1481, no. 1, pp. 45–54, Aug. 2000.

[59] S. Yang, X. Wang, L. Cui, X. Ding, L. Niu, F. Yang, C. Wang, C.-C. Wang, and J. Lou, "Compact conformations of human protein disulfide isomerase.," *PLoS One*, vol. 9, no. 8, p. e103472, Jan. 2014.

[60] L. J. Byrne, A. Sidhu, A. K. Wallis, L. W. Ruddock, R. B. Freedman, M. J. Howard, and R. A. Williamson, "Mapping of the ligand-binding site on the b' domain of human PDI: interaction with peptide ligands and the x-linker region.," *Biochem. J.*, vol. 423, no. 2, pp. 209–17, Oct. 2009.

[61] V. D. Nguyen, K. Wallis, M. J. Howard, A. M. Haapalainen, K. E. H. Salo, M. J. Saaranen, A. Sidhu, R. K. Wierenga, R. B. Freedman, L. W. Ruddock, and R. A. Williamson, "Alternative Conformations of the x Region of Human Protein Disulphide-Isomerase Modulate Exposure of the Substrate Binding b' Domain," *J. Mol. Biol.*, vol. 383, no. 5, pp. 1144–1155, 2008.

[62] A. G. Irvine, A. K. Wallis, N. Sanghera, M. L. Rowe, L. W. Ruddock, M. J. Howard, R. A. Williamson, C. A. Blindauer, and R. B. Freedman, "Protein disulfide-isomerase

interacts with a substrate protein at all stages along its folding pathway.," *PLoS One*, vol. 9, no. 1, p. e82511, 2014.

[63] S. H. McLaughlin and N. J. Bulleid, "Thiol-independent interaction of protein disulphide isomerase with type X collagen during intra-cellular folding and assembly.," *Biochem. J.*, vol. 331 (Pt 3, pp. 793–800, May 1998.

[64] W. Scheper and J. J. M. Hoozemans, "The unfolded protein response in neurodegenerative diseases: a neuropathological perspective.," *Acta Neuropathol.*, vol. 130, no. 3, pp. 315–31, Sep. 2015.

[65] J. F. Díaz-Villanueva, R. Díaz-Molina, and V. García-González, "Protein Folding and Mechanisms of Proteostasis.," *Int. J. Mol. Sci.*, vol. 16, no. 8, pp. 17193–230, 2015.

[66] B. Bhandary, A. Marahatta, H.-R. Kim, and H.-J. Chae, "An involvement of oxidative stress in endoplasmic reticulum stress and its associated diseases.," *Int. J. Mol. Sci.*, vol. 14, no. 1, pp. 434–56, 2012.

[67] R. A. Roth, "Bacitracin: An inhibitor of the insulin degrading activity of glutathione-insulin transhydrogenase," *Biochem. Biophys. Res. Commun.*, vol. 98, no. 2, pp. 431–438, Jan. 1981.

[68] N. Dickerhof, T. Kleffmann, R. Jack, and S. McCormick, "Bacitracin inhibits the reductive activity of protein disulfide isomerase by disulfide bond formation with free cysteines in the substrate-binding domain.," *FEBS J.*, vol. 278, no. 12, pp. 2034–43, Jun. 2011.

[69] S. Xu, A. N. Butkevich, R. Yamada, Y. Zhou, B. Debnath, R. Duncan, E. Zandi, N. A. Petasis, and N. Neamati, "Discovery of an orally active small-molecule irreversible inhibitor of protein disulfide isomerase for ovarian cancer treatment.," *Proc. Natl. Acad. Sci. U. S. A.*, vol. 109, no. 40, pp. 16348–53, Oct. 2012.

[70] T. Horibe, H. Nagai, K. Sakakibara, Y. Hagiwara, and M. Kikuchi, "Ribostamycin inhibits the chaperone activity of protein disulfide isomerase.," *Biochem. Biophys. Res. Commun.*, vol. 289, no. 5, pp. 967–72, Dec. 2001.

[71] R. Jasuja, F. H. Passam, D. R. Kennedy, S. H. Kim, L. van Hessem, L. Lin, S. R. Bowley, S. S. Joshi, J. R. Dilks, B. Furie, B. C. Furie, and R. Flaumenhaft, "Protein disulfide isomerase inhibitors constitute a new class of antithrombotic agents.," *J. Clin. Invest.*, vol. 122, no. 6, pp. 2104–13, Jun. 2012.

[72] F. Baneyx, "Recombinant protein expression in Escherichia coli," *Curr. Opin. Biotechnol.*, vol. 10, no. 5, pp. 411–421, 1999.

[73] W. F. Vranken, W. Boucher, T. J. Stevens, R. H. Fogh, A. Pajon, M. Llinas, E. L. Ulrich, J. L. Markley, J. Ionides, and E. D. Laue, "The CCPN data model for NMR spectroscopy: development of a software pipeline.," *Proteins*, vol. 59, no. 4, pp. 687–96, Jun. 2005.

[74] Novagen, "pET system manual 11th edition," p. TB055 p1–63, 2006.

[75] Y.-P. Weng, F.-C. Hsu, W.-S. Yang, and H.-P. Chen, "Optimization of the overexpression of glutamate mutase S component under the control of T7 system by using lactose and IPTG as the inducers," *Enzyme Microb. Technol.*, vol. 38, no. 3, pp. 465–469, 2006.

[76] R. Daber, S. Stayrook, A. Rosenberg, and M. Lewis, "Structural Analysis of Lac Repressor Bound to Allosteric Effectors," *J. Mol. Biol.*, vol. 370, no. 4, pp. 609–619, 2007.

[77] J. W. Dubendorff and F. W. Studier, "Controlling basal expression in an inducible T7 expression system by blocking the target T7 promoter with lac repressor.," *J. Mol. Biol.*, vol. 219, no. 1, pp. 45–59, May 1991.

[78] F. W. Studier, "Use of bacteriophage T7 lysozyme to improve an inducible T7 expression system," *J. Mol. Biol.*, vol. 219, no. 1, pp. 37–44, May 1991.

[79] J. Ratelade, M.-C. Miot, E. Johnson, J.-M. Betton, P. Mazodier, and N. Benaroudj, "Production of recombinant proteins in the lon-deficient BL21(DE3) strain of Escherichia coli in the absence of the DnaK chaperone.," *Appl. Environ. Microbiol.*, vol. 75, no. 11, pp. 3803–7, Jun. 2009.

[80] S. H. Pan and B. A. Malcolm, "Reduced background expression and improved plasmid stability with pET vectors in BL21 (DE3).," *Biotechniques*, vol. 29, no. 6, pp. 1234–8, Dec. 2000.

[81] D. Denisa and University of Kent, "Biophysical characterization and NMR analysis of the PDI fragment b'xa'c," 2012.

[82] K. F. Geoghegan, H. B. F. Dixon, P. J. Rosner, L. R. Hoth, A. J. Lanzetti, K. A. Borzilleri, E. S. Marr, L. H. Pezzullo, L. B. Martin, P. K. LeMotte, A. S. McColl, A. V. Kamath, and J. G. Stroh, "Spontaneous α-N-6-Phosphogluconoylation of a 'His Tag' inEscherichia coli:The Cause of Extra Mass of 258 or 178 Da in Fusion Proteins," *Anal. Biochem.*, vol. 267, no. 1, pp. 169–184, Feb. 1999.

[83] I. Perdivara, L. J. Deterding, M. Przybylski, and K. B. Tomer, "Mass spectrometric identification of oxidative modifications of tryptophan residues in proteins: chemical artifact or post-translational modification?," *J. Am. Soc. Mass Spectrom.*, vol. 21, no. 7, pp. 1114–7, Jul. 2010.

[84] Y. Cheng and D. J. Patel, "An efficient system for small protein expression and refolding," *Biochem. Biophys. Res. Commun.*, vol. 317, no. 2, pp. 401–405, 2004.

[85] W. G. Zhou P1, Lugovskoy AA, "A solubility-enhancement tag (SET) for NMR studies of poorly behaving proteins.," *J Biomol NMR.*, vol. 20(1), pp. 11–4, 2001.

[86] S. L. Taylor, H. Crawley-Snowdon, J. L. Wagstaff, M. L. Rowe, M. Shepherd, R. A. Williamson, and M. J. Howard, "Measuring protein reduction potentials using 15N HSQC NMR spectroscopy.," *Chem. Commun. (Camb).*, vol. 49, no. 18, pp. 1847–9, Mar. 2013.

[87] H. Kadokura, H. Tian, T. Zander, J. C. A. Bardwell, and J. Beckwith, "Snapshots of DsbA in action: detection of proteins in the process of oxidative folding.," *Science*, vol. 303, no. 5657, pp. 534–7, Jan. 2004.

[88] K. Maeda, P. Hägglund, C. Finnie, B. Svensson, and A. Henriksen, "Structural Basis for Target Protein Recognition by the Protein Disulfide Reductase Thioredoxin," *Structure*, vol. 14, no. 11, pp. 1701–1710, 2006.

[89] B. Tsai, C. Rodighiero, W. I. Lencer, and T. A. Rapoport, "Protein Disulfide Isomerase Acts as a Redox-Dependent Chaperone to Unfold Cholera Toxin," *Cell*, vol. 104, no. 6, pp. 937–948, 2001.

[90] J. E. Chambers, T. J. Tavender, O. B. V Oka, S. Warwood, D. Knight, and N. J. Bulleid, "The reduction potential of the active site disulfides of human protein disulfide isomerase limits oxidation of the enzyme by Ero1α.," *J. Biol. Chem.*, vol. 285, no. 38, pp. 29200–7, Sep. 2010.

[91] J. Lundström and A. Holmgren, "Determination of the reduction-oxidation potential of the thioredoxin-like domains of protein disulfide-isomerase from the equilibrium with glutathione and thioredoxin.," *Biochemistry*, vol. 32, no. 26, pp. 6649–55, Jul. 1993.

[92] M. M. Lyles and H. F. Gilbert, "Catalysis of the oxidative folding of ribonuclease A by protein disulfide isomerase: dependence of the rate on the composition of the redox buffer.," *Biochemistry*, vol. 30, no. 3, pp. 613–9, Jan. 1991.

[93] R. Bass, L. W. Ruddock, P. Klappa, and R. B. Freedman, "A Major Fraction of Endoplasmic Reticulum-located Glutathione Is Present as Mixed Disulfides with Protein," *J. Biol. Chem.*, vol. 279, no. 7, pp. 5257–5262, Feb. 2004.

[94] C. Hwang, A. J. Sinskey, and H. F. Lodish, "Oxidized redox state of glutathione in the endoplasmic reticulum.," *Science*, vol. 257, no. 5076, pp. 1496–502, Sep. 1992.

[95] S. Chakravarthi, C. E. Jessop, and N. J. Bulleid, "The role of glutathione in disulphide bond formation and endoplasmic-reticulum-generated oxidative stress.," *EMBO Rep.*, vol. 7, no. 3, pp. 271–5, Mar. 2006.

[96] J. Rost and S. Rapport, "Reduction-potential of Glutathione," *Nature*, vol. 201, no. 4915, pp. 185–185, Jan. 1964.

[97] M. G. Pollard, K. J. Travers, and J. S. Weissman, "Ero1p: A Novel and Ubiquitous Protein with an Essential Role in Oxidative Protein Folding in the Endoplasmic Reticulum," *Mol. Cell*, vol. 1, no. 2, pp. 171–182, 1998.

[98] A. R. Frand and C. A. Kaiser, "The ERO1 Gene of Yeast Is Required for Oxidation of Protein Dithiols in the Endoplasmic Reticulum," *Mol. Cell*, vol. 1, no. 2, pp. 161–170, 1998.

[99] B. P. Tu, S. C. Ho-Schleyer, K. J. Travers, and J. S. Weissman, "Biochemical basis of oxidative protein folding in the endoplasmic reticulum.," *Science*, vol. 290, no. 5496, pp. 1571–4, Nov. 2000.

[100] W. W. Cleland, "Dithiothreitol, a new protective reagent for SH groups.," *Biochemistry*, vol. 3, pp. 480–2, Apr. 1964.

[101] C. Wang, S. Chen, X. Wang, L. Wang, A. K. Wallis, R. B. Freedman, and C. Wang, "Plasticity of human protein disulfide isomerase: evidence for mobility around the X-linker region and its functional significance.," *J. Biol. Chem.*, vol. 285, no. 35, pp. 26788–97, Aug. 2010.

[102] N. J. Darby and T. E. Creighton, "Characterization of the active site cysteine residues of the thioredoxin-like domains of protein disulfide isomerase.," *Biochemistry*, vol. 34, no. 51, pp. 16770–80, Dec. 1995.

[103] A. Pirneskoski, P. Klappa, M. Lobell, R. A. Williamson, L. Byrne, H. I. Alanen, K. E. H. Salo, K. I. Kivirikko, R. B. Freedman, and L. W. Ruddock, "Molecular characterization of the principal substrate binding site of the ubiquitous folding catalyst protein disulfide isomerase.," *J. Biol. Chem.*, vol. 279, no. 11, pp. 10374–81, Mar. 2004.

[104] M. Yagi-Utsumi, T. Satoh, and K. Kato, "Structural basis of redox-dependent substrate binding of protein disulfide isomerase.," *Sci. Rep.*, vol. 5, p. 13909, 2015.

[105] R. Curtis-Marof, D. Doko, M. L. Rowe, K. L. Richards, R. A. Williamson, and M. J. Howard, "19F NMR spectroscopy monitors ligand binding to recombinantly fluorine-labelled b'x from human protein disulphide isomerase (hPDI).," *Org. Biomol. Chem.*, vol. 12, no. 23, pp. 3808–12, Jun. 2014.

[106] K. L. Richards, M. L. Rowe, P. B. Hudson, R. A. Williamson, M. J. Howard, R. B. Freedman, T. R. Hirst, M. F. Tuite, and P. Klappa, "Combined ligand-observe 19F and protein-observe 15N,1H-HSQC NMR suggests phenylalanine as the key Δ-somatostatin residue recognized by human protein disulfide isomerase," *Sci. Rep.*, vol. 6, p. 19518, Jan. 2016.

[107] A. Y. Denisov, P. Määttänen, C. Dabrowski, G. Kozlov, D. Y. Thomas, and K. Gehring, "Solution structure of the bb' domains of human protein disulfide isomerase.," *FEBS J.*, vol. 276, no. 5, pp. 1440–9, Mar. 2009.

[108] N. J. Darby, E. Penka, and R. Vincentelli, "The multi-domain structure of protein disulfide isomerase is essential for high catalytic efficiency," *J. Mol. Biol.*, vol. 276, no. 1, pp. 239–247, 1998.

[109] L. A. M. Sommer, M. A. Meier, and S. A. Dames, "A fast and simple method for probing the interaction of peptides and proteins with lipids and membrane-mimetics using GB1 fusion proteins and NMR spectroscopy.," *Protein Sci.*, vol. 21, no. 10, pp. 1566–70, Oct. 2012.

[110] M. P. Williamson, "Using chemical shift perturbation to characterise ligand binding," *Prog. Nucl. Magn. Reson. Spectrosc.*, vol. 73, pp. 1–16, 2013.

[111] L. Fielding, "NMR methods for the determination of protein-ligand dissociation constants.," *Curr. Top. Med. Chem.*, vol. 3, no. 1, pp. 39–53, 2003.

[112] W.-J. Bao, Y.-G. Gao, Y.-G. Chang, T.-Y. Zhang, X.-J. Lin, X.-Z. Yan, and H.-Y. Hu, "Highly efficient expression and purification system of small-size protein domains in Escherichia coli for biochemical characterization," *Protein Expr. Purif.*, vol. 47, no. 2, pp. 599–606, 2006.

[113] M. Hammarström, N. Hellgren, S. van Den Berg, H. Berglund, and T. Härd, "Rapid screening for improved solubility of small human proteins produced as fusion proteins in Escherichia coli.," *Protein Sci.*, vol. 11, no. 2, pp. 313–21, Feb. 2002.

[114] Z. Serber, P. Selenko, R. Hänsel, S. Reckel, F. Löhr, J. E. Ferrell, G. Wagner, and V. Dötsch, "Investigating macromolecules inside cultured and injected cells by in-cell NMR spectroscopy.," *Nat. Protoc.*, vol. 1, no. 6, pp. 2701–9, 2006.

[115] Z.-Y. J. Sun, D. P. Frueh, P. Selenko, J. C. Hoch, and G. Wagner, "Fast assignment of 15N-HSQC peaks using high-resolution 3D HNcocaNH experiments with non-uniform sampling.," *J. Biomol. NMR*, vol. 33, no. 1, pp. 43–50, Sep. 2005.

[116] S. Parakh and J. D. Atkin, "Novel roles for protein disulphide isomerase in disease states: a double edged sword?," *Front. cell Dev. Biol.*, vol. 3, p. 30, 2015.

[117] L. Wang, S. Li, A. Sidhu, L. Zhu, Y. Liang, R. B. Freedman, and C. Wang, "Reconstitution of human Ero1-Lalpha/protein-disulfide isomerase oxidative folding pathway in vitro. Position-dependent differences in role between the a and a' domains of protein-disulfide isomerase.," *J. Biol. Chem.*, vol. 284, no. 1, pp. 199–206, Jan. 2009.